IMPACT OF DIFFERENT VEHICLE MODELS ON THREAT ASSESSMENT IN CRITICAL CURVE SITUATIONS

Mohammad Ali
Volvo Car Corporation
Jonas Sjöberg
Chalmers University of Technology
Sweden
Paper Number 09-0076

ABSTRACT

Curve speed warning systems (CSW) utilize information about the road and warn drivers if they are about to enter a curve too fast. Recent research shows that CSW is successful in warning for upcoming curves. However no statistically significant change in driver behaviour due to CSW has been shown. In addition, a common requirement cited by drivers is that the amount of false alarms needs to be reduced.

This paper evaluates how the level of detail in the modelled vehicle dynamics influences the threat assessment in a situation with an oncoming curve. The point mass model that is commonly used by CSW is compared with more detailed models. Maximum velocity the vehicle can have while still following a curve is investigated and compared for the point mass model, the single track model and the double track model. It is shown that as the level of detail in the modelled dynamics increase, the maximum velocity profile is significantly reduced. This implies that in order to make a reliable threat assessment that can reduce the amount of false alarms and even be used as a base for an autonomous intervention, a more complex vehicle model than the point mass model is required.

INTRODUCTION

The number of fatalities in vehicles leaving the road due to loss of control has been greatly reduced since car manufacturers started to equip vehicles with electronic stability systems, [1]. Despite this, unintended roadway departures still account for the highest share of traffic related fatalities, [2][3]. Roadway departures are thus still a highly significant problem.

Currently a new type of active safety systems that also addresses roadway departures is emerging. Curve speed warning systems (CSW) utilize sensor data about the road and warn drivers if they are about to enter a curve too fast. In [3], it is shown that CSW is successful in warning for upcoming curves. CSW might therefore give a significant contribution to further reduction of roadway departures, provided that drivers take the warnings seriously.

However, in the study presented in [3], no statistically significant change in driver behaviour due to CSW could be shown. Even though the concept of CSW was generally thought to increase safety, a common requirement cited by drivers is that the amount of false alarms needs to be reduced. In fact, drivers often commented that when they received a CSW alert, they would make their own evaluation of the situation rather than simply slowing down in response to the alert.

Drivers only experience the system through its interface and it is therefore crucial that false alerts are avoided so that drivers are confident with the system. How to define a false alert can of course be disputed, however alerts which common drivers consider as unnecessary will contribute negatively to their confidence in the system.

In this paper we focus on the threat assessment part of CSW i.e. the part where it is evaluated whether an alert or intervention is required. Current CSW systems attempt to keep drivers within the range of lateral accelerations associated with normal curve taking [3]. In general it can be stated that the threat assessment related with such an approach is suitable for issuing early warnings or calculating reference velocity in curves for e.g. an adaptive cruise control. The starting point of this work is however that drivers need to see a clear connection between an alert from the system and an actual threat in order for the system to gain credibility. In fact, the long term aim is to have a threat assessment that is reliable enough to motivate an intervention rather than just alerting the driver.

In particular, the purpose of this paper is to evaluate how the level of detail in the modelled vehicle dynamics influences the threat assessment in a situation with an oncoming curve. The point mass model that is used by the threat assessment of CSW (see e.g. [3]) is here compared with other, well established vehicle models that are more detailed. The vehicle is modelled using a point mass model, a single track model and a four wheel model. As comparison measure, the maximum

velocity the vehicle can have while still following a particular curve is investigated and compared for the different models. Even though the comparison is quite simple, it shows that the level of detail in the modelled dynamics has a significant impact on the result.

This implies that in order to make a reliable threat assessment that can reduce the amount of false alarms and even be used as a base for an autonomous intervention, a more complex vehicle model than the point mass model is required.

SIMULATION STRATEGY

In this section, the chosen approach for calculating the maximum velocity profile is explained using the point mass vehicle model as an example. In order to compare the different vehicle models, a scenario where a vehicle approaches a specific curve is considered. The curve is represented as a clothoid which means that the curvature increases linearly along the travelled path and can be expressed

$$c(s) = c_0 + c_1 s \qquad \textbf{(1)}$$

where c_0 is the curvature at the starting point, c_1 the increase rate of the curvature along the curve and s is the travelled distance along the curve. The construction of real roads corresponds well with equation (1), [4][5]. Clothoids are often used as transitions between straight road segments and segments with constant curvature. In particular, the curve used in all simulations in this paper is a 120m long clothoid that has a radius of 50m at the apex i.e. the end of the clothoid. This curve is quite short and typically suitable as a transition curve followed by a segment with constant curvature on a road with 50 km/h as posted velocity [5].

For a point mass model, the maximum velocity profile through the curve is easily obtained using the principles described in [6]. The equations of motion for a point mass can be stated

$$m\ddot{s} = F_x$$

$$m\dot{s}^2 = \frac{F_y}{c(s)} \qquad \textbf{(2)}$$

with m as the vehicles mass, F_x the force in the tangential direction of the path and F_y as the force normal to the direction of travel.

A common assumption regarding available friction force is that it is limited by a friction ellipse [7]. In its simplest form the friction ellipse can be expressed as a circle according to

$$F_x^2 + F_y^2 \le (\mu F_z)^2 \qquad \textbf{(3)}$$

where μ is the friction coefficient and F_z is the normal load. Since this is a comparative study, the friction coefficient will be given the same value μ=1 in all simulations which corresponds to assuming that the vehicle travels on dry asphalt.

With F_x and F_y as control inputs, assuming controllability conditions to be fulfilled and the dynamics to be well defined, it is stated in [6] that for the vehicle to exactly follow the path in minimum time, it has been formally proven that the following control law holds

$$F_y = mc\dot{s}^2$$

$$F_x = \pm\sqrt{(\mu F_z)^2 - F_y^2} \qquad \textbf{(4)}$$

The control law has been reformulated to fit the notation of this paper. An interpretation of the control law is that as much lateral force as needed to follow the reference curvature should be utilized and the rest of the available force should be used for either full acceleration or full deceleration.

By combining (3) and (2), it can be derived that there exists a critical velocity for which a vehicle can no longer follow the specified curvature

$$\dot{s}_{critical} = \sqrt{\frac{\mu F_z c}{m}} \qquad \textbf{(5)}$$

which is the maximum allowable velocity at each point of the path [6]. For the considered curve, the curvature has only one minimum at the end of the clothoid. As a consequence of (5), the optimal velocity profile then also has a minimum at the same point. By setting the critical velocity at the apex as boundary condition and applying the control law (4), the optimal velocity profile can be obtained by starting a simulation at the end of the clothoid where the vehicle travels in the reversed direction.

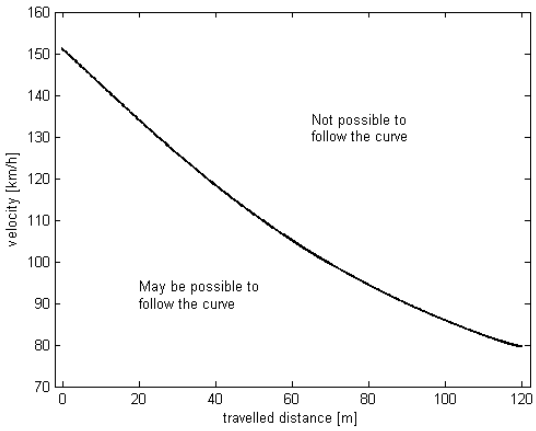

Figure 1. Maximum velocity profile computed using a point mass model.

The result of such a simulation can be seen in Figure 1. The computed velocity profile implies that an optimal driver can enter the curve with a velocity of about 150 km/h and pass the end of the clothoid in about 80 km/h.

Principle of optimality

When the level of detail in the modelled vehicle dynamics is increased it is not straightforward to reverse the direction of motion without first taking care of the inverted dynamics. The vehicle's behaviour during acceleration will be different from the behaviour during deceleration. Consequently the method used above for the point mass is not used here to obtain the optimal velocity profile when more detailed models are considered. Instead the principle of optimality is used which can be stated:

"An optimal policy has the property that whatever the previous state and decision (i.e. control), the remaining decision must constitute an optimal policy with regard to the state resulting from the previous decision." [8]

In other words, the optimal velocity profile can be divided into smaller segments which are themselves optimal. If one can find the optimal solution for the small segments, one can put them together to get the optimal solution for the whole path [8].

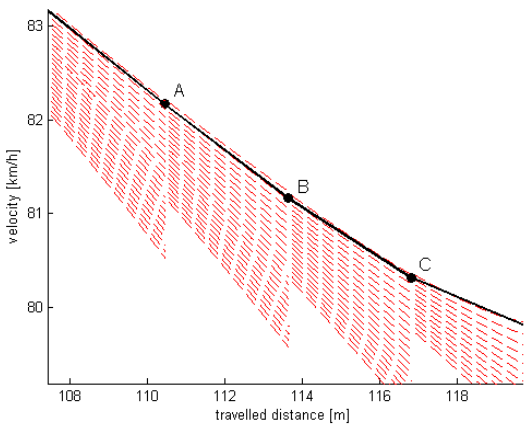

Figure 2. The principle of optimality is used to obtain the optimal velocity profile. The black solid line represents the optimal profile while the red dashed lines represent simulations conducted in order to find the maximum velocity for each segment.

The following bullets together with Figure 2 explain how the principle of optimality is utilized in this study:

- The curve is uniformly divided into several small segments. In Figure 2 this is illustrated by the dividing points A, B and C.
- The optimal velocity at the point C in Figure 2 is assumed to be known and denoted v_c.
- A simulation of the vehicle's motion between the points B and C is conducted where the lateral force needed in order to follow the curve is applied and the rest of the available force is utilized to brake in accordance with the control law (4).
- The vehicle's initial velocity at point B is gradually increased with a predefined resolution as the simulation is iteratively repeated.
- When available brake force is no longer sufficient to reduce the vehicle's velocity below v_c, at point C, the iterations stop.
- The highest velocity the vehicle can have at point B while still reaching point C without exceeding v_c, is then considered to be v_b.
- Once v_b has been acquired, the procedure can be repeated between the points A and B to obtain v_a and analogously for the remaining segments until solutions has been acquired for the whole curve.
- The points A, B and C was here used to give an illustration of the procedure, in reality the procedure is initiated at the end of the clothoid and the maximum velocity at that point is calculated using (5).

The optimal velocity obtained using the principle of optimality is of course an approximation, since the set of possible solutions as well as the curve is discretized. As the resolution is increased, the accuracy of the obtained solution will however improve and if infinite resolution could be achieved, the difference from the true optimum would tend to zero.

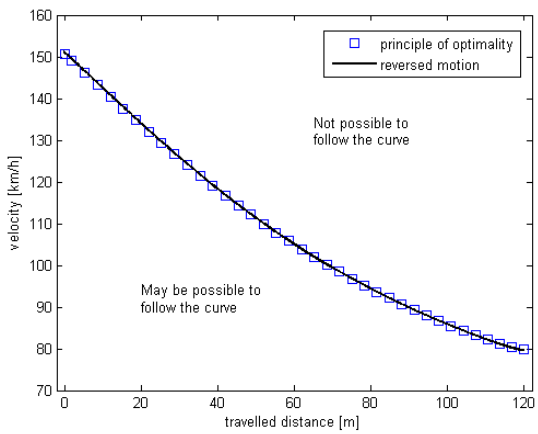

Figure 3. Time optimal velocity profile obtained through reversing the vehicles motion is compared with the solution acquired with the principle of optimality.

In Figure 3, a validation of the chosen resolution is made by comparing the optimal path of a point mass computed by reversing the vehicle's motion and the one computed using the principle of optimality. Even though the solutions are not identical, the difference is satisfactorily small. The principle of optimality will therefore be used in the following sections to obtain optimal velocity profiles for more detailed vehicle models.

SINGLE TRACK VEHICLE MODEL

In a point mass representation of the vehicle, the wheelbase and track width are collapsed to zero, hence all forces are applied on the centre of mass. In this section, a single track model is considered, which means that the car's length and orientation is also taken into account. Applied forces are distributed between the front and rear axle and might therefore also cause the vehicle to rotate around its own axis rather than just moving the mass centre. Without loss of generality each axle is here considered as a tire and with notation defined in Figure 4 the equations of motion can then be expressed, [9]

$$\dot{\psi} = \frac{1}{J_z}(F_{fy} l_f - F_{ry} l_r)$$

$$\dot{v}_x = \frac{1}{m}(F_{fx} + F_{rx}) + v_y \dot{\psi}$$

$$\dot{v}_y = \frac{1}{m}(F_{fy} + F_{ry}) - v_x \dot{\psi} \qquad \textbf{(6)}$$

Note however that the forces in (6), are denoted F and expressed in the vehicle frame which is different from the forces denoted f in Figure 4 which are expressed in the tire's coordinate system. The forces can easily be expressed in the vehicle frame by feeding the forces in Figure 4 through the following coordinate transformation

$$F_{fx} = f_{fx}\cos(\delta) - f_{fy}\sin(\delta)$$

$$F_{fy} = f_{fx}\sin(\delta) + f_{fy}\cos(\delta)$$

$$F_{rx} = f_{rx}$$

$$F_{ry} = f_{ry} \qquad \textbf{(7)}$$

The acceleration limits are in this case given by two friction ellipses, one at each tire. An illustration is given in Figure 5, it can be seen that combinations of the forces at each tire can achieve a total force anywhere in the dashed ellipse which represents the total friction limit.

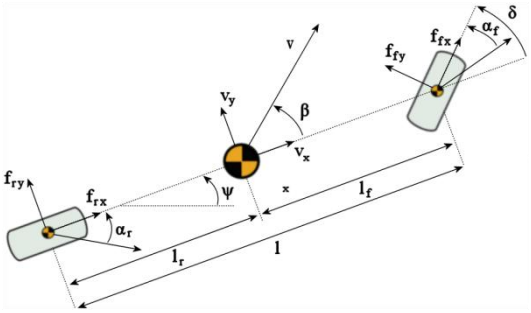

Figure 4. Notation for the single track model.

In conventional vehicles, lateral force is however in general generated by turning the front wheel and brake force by applying braking torque on the wheels. By turning the front wheel, the lateral force at the front can thus be directly controlled while the lateral force at the rear is completely determined by the state of the vehicle and only indirectly influenced by the front wheel angle. In addition, a driver can only control brake torque through a brake pedal which distributes brake torque between the front and rear axle with a fix ratio. Under the assumption that no active systems like e.g. the antilock brake system intervenes, one can therefore say that the torque distribution and hence longitudinal force distribution between the front and back wheel is fixed. These limitations imply that arbitrary combinations of the forces at the front and the rear wheel may not be achieved by a driver and it is not certain that the force applied on the vehicle can always be anywhere in the friction ellipse.

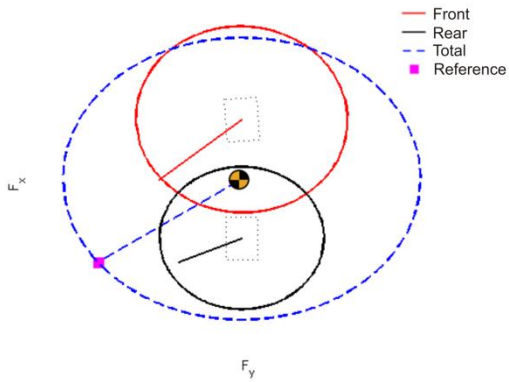

Figure 5. Tire forces with constraints. The lines represent forces while the ellipses surrounding them are bounding constraints.

In order to adopt a control strategy corresponding to (4), a cascade control with an inner control loop that delivers the required force is introduced. The inner control loop is required since the mapping from applied wheel angle and brake torque to acquired force is dynamic. The adopted control strategy is illustrated by the block diagram in Figure 6 where

- The block $\mathbf{C_1}$, compares the vehicle's state with the desired path and decides which lateral and longitudinal forces that needs to be applied on the vehicle in the same fashion as in (4). In Figure 5, the output of $\mathbf{C_1}$ i.e. the required force is represented by the square that is located at the limit of the dashed ellipse.
- The block $\mathbf{C_2}$, which is much faster than $\mathbf{C_1}$, compares the generated force i.e. the dashed line in Figure 5, with the required force and decides which wheel angle and brake torque that is required in order to achieve the force demanded by $\mathbf{C_1}$.
- The wheel torque, which is one of the outputs of $\mathbf{C_2}$ is a "total" torque, T_{tot}. The torque, T_{tot} is distributed between the front and back wheel according to

$$T_f = 0.7T_{tot} \qquad T_r = 0.3T_{tot} \qquad \textbf{(8)}$$

The larger portion of the torque is applied at the front since the normal load is greater there for the vehicle considered in this study.

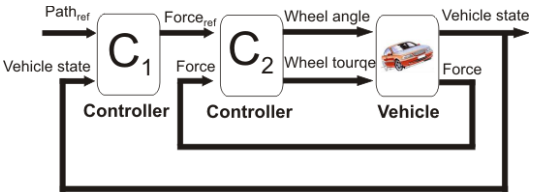

Figure 6. Block diagram describing the control strategy.

In addition to introducing the cascade control we also need to model the mapping from wheel angle and wheel torque to the forces acting on the vehicle. Two different approaches is tested here, one linear tire model (with saturation) and one nonlinear tire model. The tire models are explained in the following subsections.

Linear Tires

The longitudinal force at each tire is calculated as a function of the longitudinal slip. In order to keep track of the longitudinal slip, the rotational velocity is introduced as an additional state for each tire. The state model is therefore extended with

$$\dot{\omega}_i = (T_i - f_{xi})\frac{1}{J_\omega} \qquad i=f,r \qquad \textbf{(9)}$$

where J_ω denotes wheel inertia, T_i denotes wheel torque, ω_i denotes rotational velocity of the wheel and f_{xi} denotes longitudinal force expressed in the tires coordinate system. Given the rotational velocity at each wheel, one can calculate the longitudinal slip κ as

$$\kappa_i = -(1 - \frac{\omega_i r}{v_x}) \qquad i=f,r \qquad \textbf{(10)}$$

where r denotes the effective wheel radius [10].

A simple way of representing the relation between the longitudinal slip and longitudinal force at a wheel is by the linear relation

$$f_{xi} = K_{xi}\kappa_i \qquad i=f,r \qquad \textbf{(11)}$$

with K_{xi} as longitudinal stiffness.

Also the lateral force can be approximated using a linear relation. The mapping from lateral slip to lateral force is then

$$f_{yi} = K_{yi}\alpha_i \qquad i=f,r \qquad \textbf{(12)}$$

with K_{yi} as cornering stiffness and α_i as the tire slip angle as defined in Figure 4, this linear representation is commonly used in electronic stability systems, see e.g. [11] and [12].

For the front wheel the slip angle is easily derived by considering Figure 4 as

$$\alpha_f = \frac{v_y + l_f\dot{\psi}}{v_x} - \delta \qquad \textbf{(13)}$$

and for the rear wheel it is calculated as

$$\alpha_r = \frac{v_y - l_r\dot{\psi}}{v_x} \qquad \textbf{(14)}$$

The stiffness parameters K_{xi} and K_{yi} are acquired by linearizing the tire characteristics around κ_i=0 and α_i=0, [7].

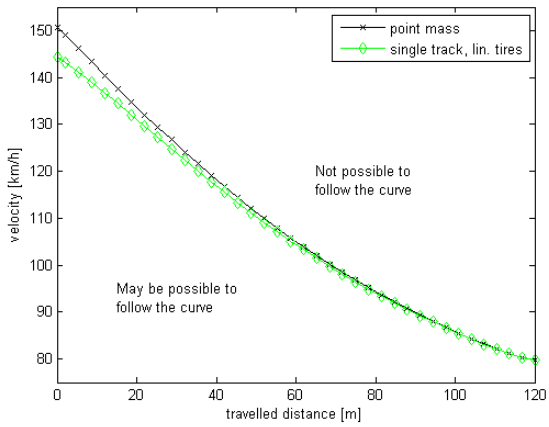

Figure 7. Time optimal velocity profile.

Figure 7 shows a comparison between the result obtained with the point mass model and the result obtained using the single track model with linear tires. Since the same boundary value is used for both models and most of the available force is utilized laterally to follow the path, the velocity

profiles are quite similar to each other at the end of the clothoid. However, earlier in the curve when more of the available force can be used longitudinally the difference is higher.

Nonlinear Tires

The primary external influence on the vehicle's behaviour is provided by the tire forces and it is therefore important to have a realistic nonlinear tire model when investigating vehicle motion near the limits of manoeuvring capability, [10].

In Figure 8, lateral force characteristics are illustrated for different values of the friction coefficient. It can be seen that for small slip angles, a linear approximation of the tire works well. In normal driving conditions this is where the tire operates and the linear approximation is therefore useful. As the operating point gets closer to the limit of adhesion, the nonlinearity however becomes more evident and eventually, the tire force saturates and then starts to decrease.

Also for the longitudinal force, the nonlinearity becomes more evident as the slip value is increased. This can be seen in Figure 9 which shows longitudinal force characteristics.

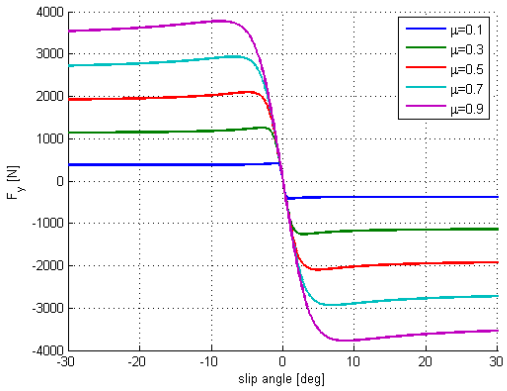

Figure 8. Lateral tire force.

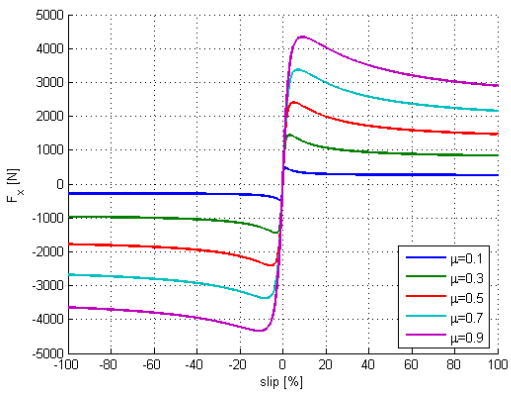

Figure 9. Longitudinal tire force.

There is a strong coupling between the longitudinal and lateral tire force. The illustrations in Figure 8 and Figure 9 are only valid in either pure cornering or pure braking. If both lateral and longitudinal force is produced at the same time, they will influence each other. Figure 10 shows lateral force as a function of lateral slip for different values of the longitudinal slip. It can be seen that if longitudinal force is utilized, the acquired lateral force is reduced. Figure 11 also shows that the analogue relation holds for longitudinal force.

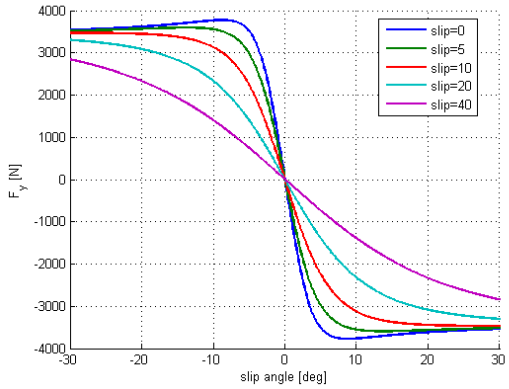

Figure 10. Lateral tire force during combined slip for μ=0.9.

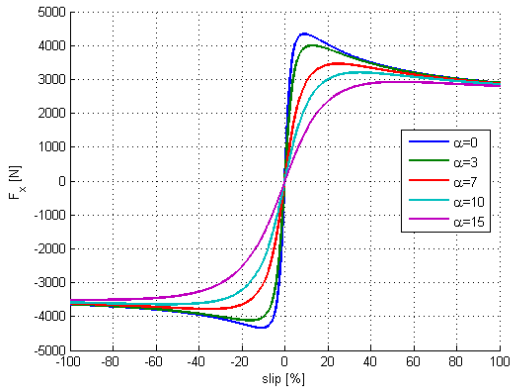

Figure 11. Longitudinal tire force during combined slip for μ=0.9.

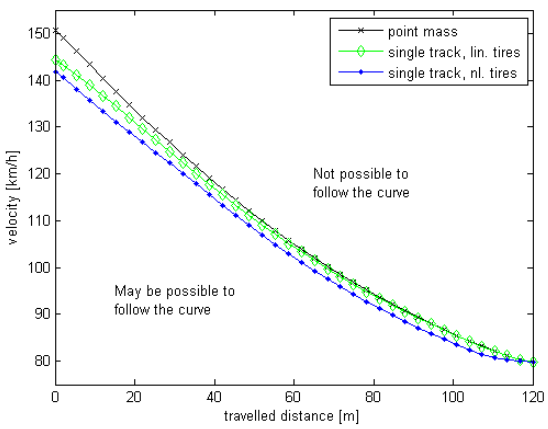

Figure 12. Time optimal velocity profile

One common way to model tire characteristics is by the empirical magic tire formula. The formula is a curve fitting which takes into account the nonlinear nature of a tire in a good way. The coupling between longitudinal and lateral force can be taken into consideration using the combined slip form of the formula

$$f_x = f_{x0}(\kappa, F_z) G_{x\alpha}(\alpha, \kappa, F_z)$$

$$f_y = f_{y0}(\alpha, F_z) G_{x\kappa}(\alpha, \kappa, F_z) \qquad \textbf{(15)}$$

where f_x and f_y are lateral and longitudinal forces, f_{x0} and f_{y0} are the forces calculated for pure braking or cornering and $G_{x\kappa}$ and $G_{x\alpha}$ are weight factors that take care of the combined slip effect. A comprehensive treatment of the magic tire formula is given in [13].

Figure 12 shows the obtained profile when the magic tire formula is used to model the tires. The same boundary condition is used in this case as for the previous models. It can be seen that there is a noticeable difference in slope between the profiles for the linear and the nonlinear tire model in the end of the clothoid. The difference is however less evident earlier in the curve. This is due to that in the case with the nonlinear tire model, a higher share of the available force is used in the lateral direction. As a consequence of the coupling between longitudinal and lateral force, the braking has to "stop" earlier along the path so that enough lateral force to follow the curve can be produced.

Longitudinal Load Transfer

In Figure 5, the friction ellipse constraining the tire force at the front wheel is larger than the ellipse at the rear. This is due to that the modelled vehicle, as mentioned earlier, has a larger portion of its weight in the front. Available and acquired tire force is thus dependant on the normal load on the tire.

If the height of the vehicle is taken into consideration, the normal load at each tire is no longer considered to be constant. When longitudinal force is applied, a moment around the vehicle's y-axis is generated. Depending on whether the vehicle is accelerating or decelerating, this moment is balanced by an increase in normal load at either the front or the rear tire. The longitudinal load transfer can be calculated

$$\Delta F_z = \frac{(F_{fx} + F_{rx})h}{l} \qquad \textbf{(16)}$$

with h as the height of the vehicle's mass centre. A derivation of equation (16) is provided in [14].

Obviously since the normal load has a direct influence on acquired force, it affects the manoeuvrability of the vehicle. It is therefore interesting to evaluate what effect the longitudinal load transfer has on the optimal velocity profile. In Figure 13, the velocity profile for a single track model with nonlinear tires and longitudinal load transfer has been added. Figure 13 reveals that the load transfer has a slightly positive influence on the time optimal velocity profile. When brake force is applied, the normal load at the front tire is increased. Since applied brake torque is in our case higher at the front, this results in a higher total longitudinal force. However as the vehicle moves further along the curve and the curvature increases, the difference disappears since the limiting factor becomes available lateral force.

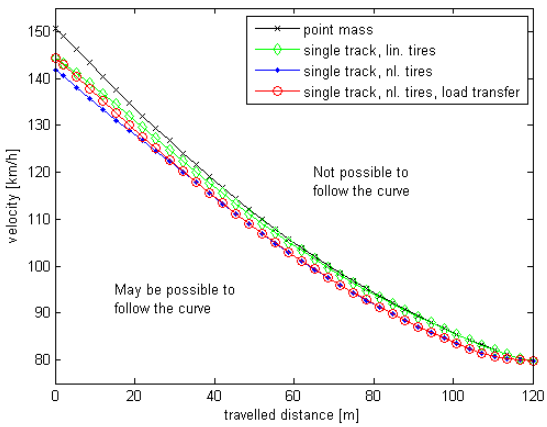

Figure 13. Time optimal velocity profile.

DOUBLE TRACK VEHICLE MODEL

In this section, we also take into account that the vehicle has a width. The equations of motion are then

$$\dot{\psi} = \frac{1}{J_z}\Big[(-F_{1x} + F_{2x} - F_{3x} + F_{4x})\frac{w}{2}$$

$$+ (F_{1y} + F_{2x})l_f - (F_{3y} + F_{4y})l_r \Big]$$

$$\dot{v}_x = \frac{1}{m}(F_{1x} + F_{2x} + F_{3x} + F_{4x}) + v_y\dot{\psi}$$

$$\dot{v}_y = \frac{1}{m}(F_{1y} + F_{2y} + F_{3y} + F_{4y}) - v_x\dot{\psi}$$

$$\dot{\omega}_i = (T_i - f_{ix}r)\frac{1}{J_\omega} \qquad i = 1,2,3,4 \qquad \textbf{(17)}$$

where J_ω is the wheel inertia and the rest of the notation is defined in Figure 14. As above, forces are denoted f when expressed in the tires coordinate system and F in the vehicle frame.

When the vehicle's height was taken into consideration for the single track model, we saw that the vehicle's vertical load varies when longitudinal force is applied. Similarly, taking the

vehicle's width into account reveals a lateral load transfer. The lateral load transfer can be calculated

$$\Delta F_{fz_{lat}} = \frac{\dot{\psi} v_x m}{w}\left[\frac{h_{rf} l_r}{l} + R_{sf}(h - h_{rc})\right]$$

$$\Delta F_{rz_{lat}} = \frac{\dot{\psi} v_x m}{w}\left[\frac{h_{rr} l_f}{l} + R_{sr}(h - h_{rc})\right] \quad \textbf{(18)}$$

where R_{sf} and R_{sr} is the roll stiffness distribution at the front and rear axles and the rest of the notation is defined in Figure 14.

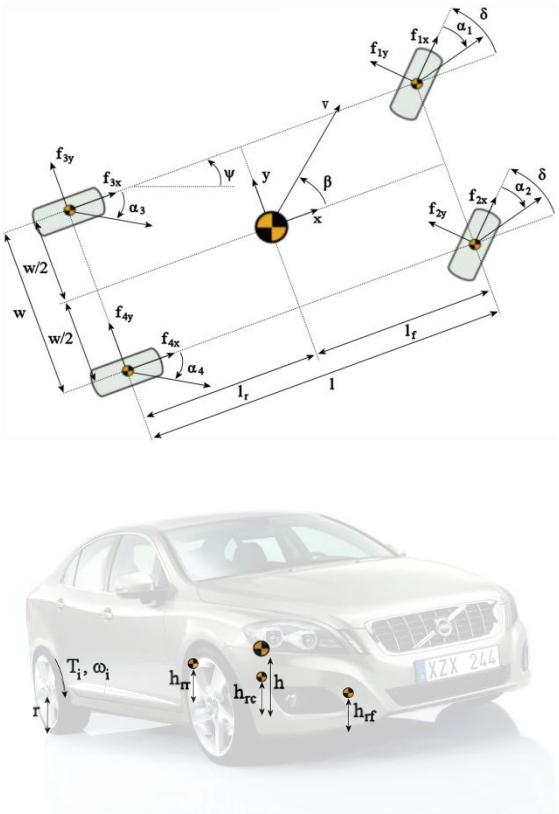

Figure 14. Notation for the double track model.

The equations presented earlier to calculate e.g. the slip quantities for the single track model can easily be extended to fit the double track model. An extensive treatment of the double track model is however omitted here and the reader is referred to [14] where a complete derivation is provided together with the assumptions it is based on.

With different vertical load at each tire, the forces generated at the contact patch of the tires will also be different even if they have the same slip values. The longitudinal forces will then contribute to the yaw moment imposed on the vehicle, especially in cornering when the lateral load transfer is large. The additional yaw moment might cause instability in the vehicle's behaviour if it is too large and it is therefore worth examining the impact of this phenomenon on the maximum velocity profile.

In Figure 15, the optimal velocity profile for the double track model has been added. The nonlinear tire model with both longitudinal and lateral load transfer has been used. It is clear that the velocity profile is lower for the double track model. In addition to the yaw moment caused by the difference in longitudinal forces, uneven distribution of the vertical load between the right and the left side also reduces the total amount of lateral force available. A lower velocity is therefore required at each point of the path in order for the lateral force to be sufficient to keep the vehicle following the curve.

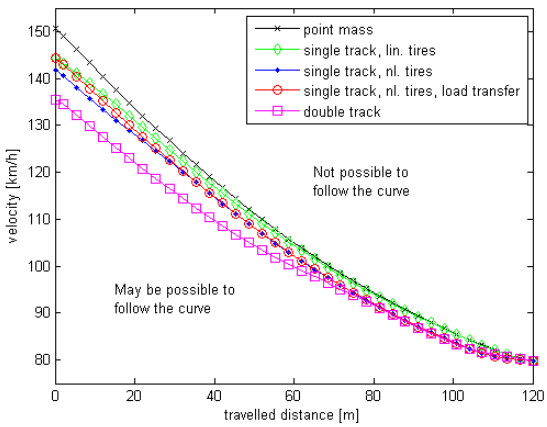

Figure 15. Time optimal velocity profile.

DISCUSSION & FUTURE WORK

In this paper, maximum velocity profiles for a vehicle travelling through a specific curve were computed using a set of well known vehicle models. It was found that the resulting velocity profile differs significantly between the simplest and the most detailed model. This is especially remarkable since the curve considered in this study is only 120m long and suited for 50km/h as posted velocity. The curve is thus relatively short and greater differences can be expected for longer curves.

Information about the maximum velocity a vehicle can have while still following the road can be used in an active safety system to either warn drivers or assist them by issuing autonomous interventions. If the car travels faster than the maximum velocity at any point along the curve, it is impossible for the vehicle to stay on the road and an autonomous intervention can then be motivated. This approach is conservative and guarantees that false alerts or interventions are never issued. As can be seen by the result, the acquired thresholds however becomes very high and in practice such a conservative system will seldom intervene.

Drivers are however never completely optimal, hence a vehicle travelling slower than the computed maximum velocity is not necessarily

safe. In CSW the issue of high thresholds is worked around by introducing a safety factor which basically shifts the velocity profile downwards. The problem with that approach is that, the mapping between the velocity profile and an actual threat is then lost. This is acceptable for a system that warns for upcoming curves but cannot be used as a base for autonomous interventions.

The velocity profiles computed in this paper only considers how fast it is possible for a vehicle to travel through the curve and does not say anything about how difficult it is. A common assumption is that it is difficult for normal drivers to manoeuvre a vehicle operating in the nonlinear region of the tires [11]. This assumption is the base of current state of the art in electronic stability systems and might also be beneficial to incorporate in a threat assessment for upcoming curves. We are therefore currently investigating a threat assessment algorithm based on this assumption.

CONCLUSIONS

It has been shown that the level of detail in the modelled vehicle dynamics has a significant impact on the maximum velocity profile for a vehicle negotiating a curve. The theoretically achievable velocity is however still very high and additional limitations of a driver's ability therefore need to be taken into consideration in order to achieve thresholds that have a higher practical benefit.

REFERENCES

[1] S. Ferguson, "The Effectiveness of Electronic Stability Control in Reducing Real World Crashes: A Literature Review", Traffic Injury Prevention, 8:4, 329-338, 2007

[2] W. Najm, B. Sen, J. Smith, B. Campbell, "Analysis of Light Vehicle Crashes and Pre-Crash Scenarios Based on the 2000 General Estimates System", Final Report, US Department of Transportation

[3] D. LeBlanc, J. Sayer, C. Winkler, R. Ervin, S. Bogard, J. Devonshire, M. Mefford, M. Hagan, Z. Bareket, R. Goodsell, T. Gordon, "Road Departure Crash Warning System Field Operational Test: Methodology and Results", Technical Report, University of Michigan Transportation Research Institute, 2006

[4] A. Eidehall, "Tracking and threat assessment for automotive collision avoidance ", Linköping University, PhD Thesis 1066, 2007

[5] Vägverket, "Vägar och gators utformning", Swedish Road Authority, Tech. Rep. 2004:80, 5 2004.

[6] E. Velenis, P. Tsiotras, "Optimal Velocity Generation for given Acceleration Limits; The Half-Car Model Case", Proceedings of the IEEE International Symposium on Industrial Electronics, 2005

[7] T.D. Gillespie, "Fundamentals of Vehicle Dynamics", Society of Automotive Engineers, 1992

[8] D.S. Naidu , "Optimal Control Systems", CRC Press, 2003

[9] M. Klomp, M Lidberg, "Safety Margin Estimation in Steady State Maneuvers", In Proceedings of the 8th International Symposium on Advanced Vehicle Control, 2006

[10] P. Falcone, F. Borrelli, J. Asgari, H. E. Tseng, D. Hvorat, "Predictive Active Steering Control for Autonomous Vehicle Systems", IEEE Transactions on control systems technology, 2007

[11] A. Van Zanten, "Bosch ESP Systems; 5 Years Of Experience", SAE, 2000

[12] H.E. Tseng, B. Ashrafi, D. Madau, T. Brown and D. Recker, "The Development of Vehicle Stability Control at Ford", IEEE/ASME Transactions on Mechatronics, vol 4, 1999

[13] H. Pacejka, "Tyre and Vehicle Dynamics", 2nd ed, Elsevier Ltd, 2006

[14] D. Casanova, "On Minimum Time Vehicle Manoeuvring: The Theoretical Optimal Lap", Ph.D Thesis, Cranfield University, 2000

A PROBABILISTIC WARNING SYSTEM FOR SAFE CURVE NEGOTIATION

Guillaume Rey
David Clair
Michel Fogli
Laboratoire de Mécanique et Ingénierie (LaMI)
France
Frédéric Bernardin
Laboratoire Régional des Ponts et Chaussées (LRPC)
France
Paper Number 09-0141

ABSTRACT

While empirical evidence shows the main effects of the driving style (principally speed choices) on safety, this study aims to quantify the influent parameters and their interactions upon the roadway departure risk. A previous work [1] using a sensitivity analysis concludes that speed, lateral position on the pavement, total embedded mass and mass center position are the relevant parameters. They constitute what is called initial conditions in the following. Probabilistic methods for the risk assessment are proposed to deal with uncertainties arising from the road infrastructure, the vehicle characteristics and the driver behaviour. Those methods originally developed in the field of structural reliability reveal promising interest in the road safety question as they allow the direct computation of a risk index, not provided by a deterministic modeling. This approach involves both measurements on real traffic by static video sensors and simulations from a specifically developed model. A set of 400 experimental trajectories is used to define mean trajectories among different classes of drivers for one turn, and simulated ones are necessary for the reliability index calculation. The result of this study is a surface response of the roadway departure probability against initial speed and lateral position on the pavement. This work will lead to the development of a warning system within the French national project SARI. Envisaged alert procedures are warning light flashes inviting the driver to modify his trajectory if the risk index calculated at the entrance of the curve indicates a dangerous situation. Difficulty for short-term implementation comes from the statistical characterization of the initial conditions (i.e. mean value and standard deviation), especially for mass and mass centre position measurement device on standard vehicles.

INTRODUCTION

The 2006 French road safety figures confirm that a large majority (75%) of casualties occurs on secondary roads, which only cover 52% of the traffic. Among these accidents, the most frequent type is Single Vehicle Roadway Departure (SVRD) during cornering. The aim of the present study, conducted through the French national project SARI, is to develop a SVRD warning system that could equip dangerous turns.

SVRD prevention system are currently an active field of research [2-6] since it is a natural evolution of the Electronic Stability Program (ESP) and the lane departure prevention systems that are at the state of commercialization. Compared to these studies, the originality of the method presented here relies on two major points. First, SRVD prevention systems are generally based on forward looking camera, thus requiring specific equipment embedded in the car. This is an obstacle for a mass implementation of the system. On the contrary, the risk assessment process proposed here is thought to work with in-pavement integrated measurement devices for acquiring initial conditions at the curve entrance. Second, the specific vehicle dynamics model developed ensures that the simulated trajectories are physically realizable in comparison with trajectories geometrically defined. This also allows to introduce the inherent hazard contained in the driver's action, the road infrastructure and the vehicle by modeling the real physical parameters by random variables. Hence the statistical characterization of these variables is facilitated, compared to other studies [7] where non-physical parameters are used to perturb the system.

Expected results of this study is a roadway departure risk evaluation based on a flexible list of criteria, thus more general than Curve Speed Warning or Time to Line Crossing usually used in this context. Risk indicator evolution is here studied as a function of speed and initial lateral position at the entrance of the curve.

Approach

This study is based on structural reliability methods [8] that directly provide the computation of a risk

index. This calculation is based on simulated trajectories that reflect the possible trajectories that could be realized by the driver. These simulations are performed using a vehicle dynamics model in which uncertainties are introduced via random variables. These random variables have been chosen in a previous study [1] using a sensitivity analysis [9,10]. They represent the uncertainties arising from the driver, the vehicle and the road infrastructure. The risk evaluation process from the vehicle arrival to the alarm triggering decision is made up of three steps:

- Several position and speed measurements points placed before the curve provide information on the driver behaviour at the turn entrance. Vehicle characteristics are set to the adequate values into the dynamic model. This data set constitutes what is called next "initial conditions".
- A reference trajectory is associated to these initial conditions. This trajectory reflects the behaviour of a standard driver. The definition of this trajectory using real traffic measurements is the object of the second part of this study.
- Finally, risk assessment consists in quantifying the chances that the simulated trajectories violate the safety criteria.

VEHICLE DYNAMICS MODELING

In this first part, the vehicle dynamics model specifically developed for this application is briefly detailed, then safety criteria are chosen to distinguish between a safe and a dangerous trajectory, and finally some random variables are introduced in the model to take into account the inherent variability of the triptych *driver-vehicle-road infrastructure*.

Deterministic modeling

The basis of the vehicle dynamics model is the 3 degrees of freedom *yaw-slip-roll* model [11,12] chosen for its fast computation and satisfying accuracy. Positioning is made using the orientation angle θ and the slip angle α (see Figure 1). The driver imposes the vehicle path through the steering angle β and the vehicle speed V. The roll angle is parameterized by the angle φ.

Compared to the classical *yaw-slip-roll* model, improvements are made concerning three points:

Tire forces - Governing the tire/ground interaction, the evolution of the lateral force F_{Yi} against the influent parameters requires a careful modeling. The tire slip angle δ_i non-linear effect is modeled using the *magic formula* [13]. The normal

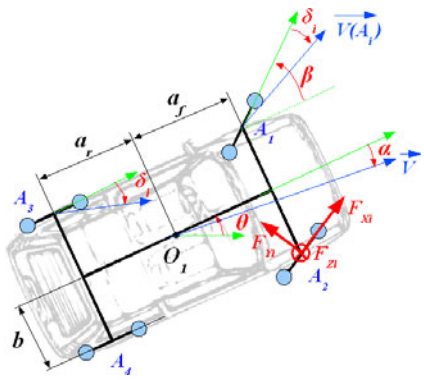

Figure 1. Scheme of the vehicle model.

force F_{Zi} influences the cornering stiffness according to the *similarity method* [14]. The last considered effect concerns the interaction between the longitudinal force F_{Xi} and the lateral force F_{Yi}, where a factor $\phi_{xi} \leq 1$ ensures that the in plane resultant force remains into the friction circle, defined by the friction coefficient μ.

Suspensions - Springs, dampers and a front anti-roll bar are considered for the calculation of the roll angle φ. Pitch and heave are neglected. For a better agreement with a complete simulator [15] in hard cornering situations, initial toe angles and roll steer phenomenon [12] are taken into account.

Time dependent input - To handle with realistic cases, variable driver commands and road infrastructure characteristics need to be simulated. Hence braking situation while cornering, as well as measured banking and slope angles can be implemented in the model.

The equation of motion is now expressed using the state vector $\boldsymbol{x_s} = (\alpha, \dot{\theta}, \dot{\varphi}, \varphi, V)^T$, the command vector $\boldsymbol{u} = (\beta, F_{X1}, \ldots, F_{X4})^T$ and the external loads. It is of the form:

$$\begin{cases} \dot{\boldsymbol{x}}_s(t) = A^{-1}(\boldsymbol{x}_s(t))F(\boldsymbol{x}_s(t), \boldsymbol{u}(t)), t > 0 \\ \boldsymbol{x}_s(0) = \boldsymbol{x}_{s0} \end{cases} \quad (1)$$

where the matrix A and the function F are calculated with the laws of motion. Trajectories can be computed once given the initial conditions $\boldsymbol{x_{s0}}$ and driver commands $\boldsymbol{u}$. The resolution of the model is made using the second order Runge-Kutta method.

Safety criteria

Safety criteria are used to classify the safe and unsafe trajectories. Two criteria are generally used

when dealing with road safety, and especially lane departure and rollover prevention. Curve Speed Warning (CSW) defines a reference speed for which the slip limit is reached for the upcoming curve. Time to Line Crossing (TLC) computes the remaining time before the lane boundary is reached, under different assumptions on the future trajectory (e.g. straight line or circular trajectory). Although showing promising results on field testing [2] in deterministic studies, basic criteria are preferred here to simplify the interpretation of these first results. Anyway, the criteria list may be modified later without any concern on the proposed methodology.

The safety criteria used in this paper are based on the lateral position d (algebraic distance from the middle of the lane) and the lateral acceleration a_y. These two control variables are functions of the state vector $\boldsymbol{x}_s$:

$$d(t) = \eta_1(\boldsymbol{x}_s(t)) \tag{2}$$

$$a_y(t) = \eta_2(\boldsymbol{x}_s(t)) \tag{3}$$

Thresholds $\overline{d}$ and $\overline{a_y}$ on the control variables define the safety criteria (i.e. the trajectory is considered as dangerous if one criterion is violated). These criteria are defined by:

$$\overline{d} - \sup_{t\in[0,T]} |d(t)| > 0 \tag{4}$$

$$\overline{a_y} - \sup_{t\in[0,T]} |a_y(t)| > 0 \tag{5}$$

where T is the total observation time. For this application, $\overline{d}$ equals the half difference between the lane width and the vehicle width and $\overline{a_y}$ is chosen equal to 3 m.s^{-2} so that a margin is kept with respect to the vehicle handling limits.

Stochastic modeling

Among all the model parameters (linked to the triptych *driver-vehicle-road infrastructure*) some present a marked random variability. Therefore it is crucial for the credibility of the approach to take into account this reality via a suited stochastic modeling. In order to reduce the calculation time and improve the model robustness, the number of random variables introduced in the model has to be optimized. This study has been made previously [1] using a global sensitivity analysis based on Sobol' indices [10]. It has been concluded that the choice of the total embedded mass M, the centre of mass position a_r, the initial lateral position D_0 and an additive speed perturbation V_0 as random parameters guarantees an efficient representativity of the uncertainties propagation through the mechanical model. These parameters are gathered in the vector $\boldsymbol{x} = (M, a_r, D_0, V_0)^T$, and this vector is modelled as a $\Re^4$-valued random variable denoted $\boldsymbol{X} = (X_1, \ldots, X_4)^T$, for which the following hypotheses are made:

(H1) its components $X_1, \ldots, X_4$ are mutually independent ;

(H2) each of its components follows a truncated Gaussian distribution, which characteristics are given in Table 1 ;

(H3) the support of the truncated Gaussian distribution is chosen of the form mean ±3 standard deviations.

Since in equation (1) the functions A and F and the initial condition $\boldsymbol{x}_{s0}$ depend on $\boldsymbol{x}$, when this deterministic vector is considered as a random vector $\boldsymbol{X}$, A, F and $\boldsymbol{x}_{s0}$ become random, and consequently the state vector function $\boldsymbol{x}_s(t)$ becomes a random process $\boldsymbol{X}_s(t)$ governed by the equation :

$$\begin{cases} \dot{\boldsymbol{X}}_s(t) = A^{-1}(\boldsymbol{X}_s(t))F(\boldsymbol{X}_s(t), \boldsymbol{u}(t)), t > 0 \\ \boldsymbol{X}_s(0) = \boldsymbol{X}_{s0} \end{cases} \tag{6}$$

in which the driver command $\boldsymbol{u}$ is kept deterministic and $\boldsymbol{X}_{s0}$ is a $\Re^5$-valued random variable depending on $\boldsymbol{X}$.

In this random context, the control variables d and a_y given by equations (2) and (3) are random processes D and A_y such that, $\forall t \in \Re_+$:

$$D(t) = \eta_1(\boldsymbol{X}_s(t)) \tag{7}$$

$$A_y(t) = \eta_2(\boldsymbol{X}_s(t)) \tag{8}$$

The aim of this study is to quantify the risk for the safety criteria to be violated. For that, once the initial conditions of the arriving vehicles are measured, a reference trajectory (which defines the driver commands) must be associated to begin the risk evaluation process. This is the object of the next section.

x	Parameter	X	Unit	Mean	Standard deviation	Truncation interval
M	Total embedded mass	X_1	kg	1610	16	[1562;1658]
a_r	Rear axle location	X_2	m	1.532	0.01	[1.502;1.562]
D_0	Position perturbation	X_3	m	0	0.2	[-0.6;0.6]
V_0	Velocity perturbation	X_4	km.h^{-1}	0	0.1	[-0.3;0.3]

Table 1. Statistical characteristics of the random variables.

REFERENCE TRAJECTORY

The reference trajectory is defined here as the trajectory that a mean driver would have realized if he has entered the curve with the given initial conditions $\boldsymbol{X}$. Therefore a theoretical definition of this trajectory is hardly realizable as it depends on a lot of factors (driving style, visibility conditions, …). Even if studies defining a driver model are topical [16-19], choice has been made to deduce the reference trajectory from real traffic measurements in order to get more realistic results.

Traffic measurement

This work has been carried out by Goyat and al. [20] in an other task of the SARI project, which consisted in the development of a portable trajectory measurement device. The measurement is based on cameras and telemeter. Images are then processed to estimate the vehicle position and velocity (Figure 2).

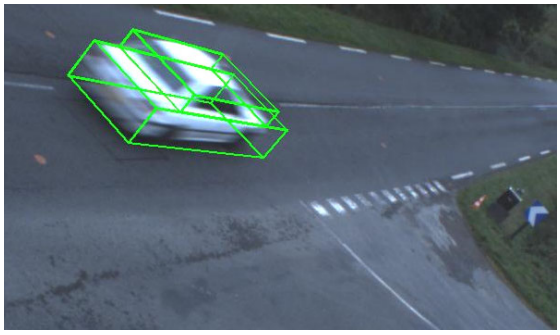

Figure 2. Image processing for position estimation.

This system has been deployed for measurements during two days on a French secondary road, and led to the construction of a 400 trajectory database. The figures 3 and 4 show the tendency of the drivers' behaviours during the curve. It can be noticed that at the entry of the right curve (on the right of the figure), drivers are mostly at the outside of the lane. It can be explained by the fact that the studied curve is preceded by a slight bend on the left and it appears that drivers tend to cut this curve. This is an example of the effects that are hardly predictable in driver models. The exit of the curve is followed by a straight line, and trajectories use the entire width of the lane with a mode nearly in the middle.

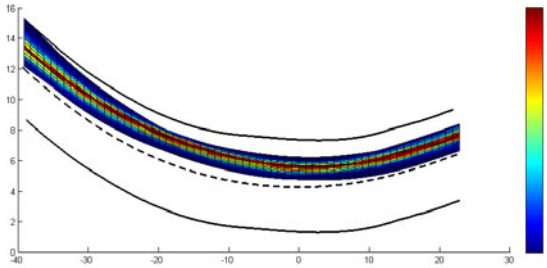

Figure 3. Density field of vehicle passage, over the 400 experimental trajectories (not to scale).

Figure 4 shows the cumulative repartition of the trajectory percentage as a function of the speed measured at the entrance, in the middle or at the exit of the curve. At the entrance of the curve, the V85 indicator (speed for which 85% of the traffic is driving slower) is 66km/h. It is far below the effective speed limit for this turn (90 km/h). So this curve negotiation requires from the driver a quick estimation of the speed that he estimates comfortable and safe, what can lead to dangerous situations. This makes this turn to be an interesting application for this study.

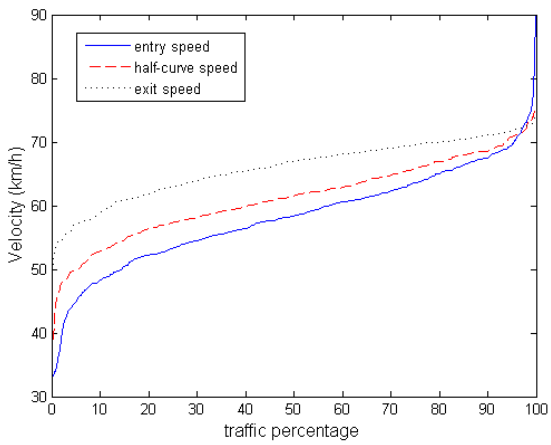

Figure 4. Measured velocity in traffic, for different position in the curve.

Driver classes

The 400 experimental trajectories are separated in different classes of driving style, so that a reference trajectory per class can be identified. As the choice of the reference trajectory must be done upon the initial conditions values, the classes definition must be made on variables measurable at the entrance of the curve. Owing to the measurement device used, these variables are restricted to the initial lateral position y_e and the initial speed v_e.

The first step of this analysis is to look for a correlation between y_e and v_e. The intuitive belief being that a driver entering at a higher speed would tend to cut the curve, implying an exterior lane positioning. Figure 5 shows the scattered plot of v_e in function of y_e. Indeed, the widespread shape of the graph does not indicate any correlation between speed and position.

Hence it has been chosen to separate the drivers classes only according to their initial lateral position y_e. Four classes of 50 cm width are created, as shown by the different colours in Figure 5. In each of these classes, the reference

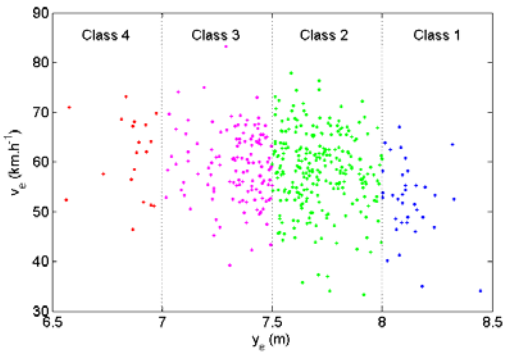

Figure 5. Scattered plot of initial speed as a function of initial lateral position.

trajectory is defined by the mean of the experimental trajectories. Results are presented on Figure 6. Classes are numbered from the interior (class 1) to the exterior (class 4).

Command computation

Once the reference trajectory is defined, the corresponding driver commands (steer angle and associated speed) must be computed to start the risk estimation process. This is done by inverting the vehicle dynamics model at each of the *N* steps of the simulation, thus resolving for all $n \in [1, N]$:

$$d_{lat}(\beta_n) = 0 \qquad (9)$$

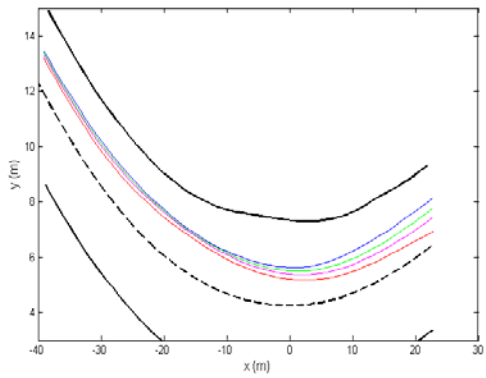

Figure 6. Reference trajectory for each driver class (not to scale).

where d_{lat} expresses the lateral distance between the reference trajectory and the simulated one, and $(\beta_n = \beta(t_n), n \in [1, N])$ the searched steer angle. There exists a different β for each speed profile due to the variation of the slip angle. The equation (9) is solved using a Newton-Raphson method.

RISK ASSESSMENT

Once the initial conditions known and the adequate reference trajectory defined, the last part of this work consists in the evaluation of a risk index, through the stochastic modeling proposed previously. The chosen risk indicator is the failure probability noted P_f, evaluated by a Monte-Carlo method [8]. While requiring a great number of simulations for accurate results, the advantage of this indicator is that it constitutes a reference solution for stochastic problems.

Probabilistic method

<u>**General principle**</u> – Let (Ω, F, P) be a probability space, where Ω is a sample space, F a σ-algebra on Ω and P a probability measure on F. The uncertain parameters of the mechanical model are gathered on a n-dimensional vector modeled as a continuous $\Re^n$-valued random variable $\boldsymbol{X} = (X_1, \ldots, X_n)^T$ defined on (Ω, F, P) whose probability density function (pdf) p_X is assumed to be known. We denote by G the limit-state function associated with the safety criterion chosen for the study. It's a measurable mapping from $\Re^n$ into $\Re$ which defines two complementary subsets of $\Re^n$: D_s and D_f, such that:

$$D_S = \{\boldsymbol{x} \in \Re^n : G(\boldsymbol{x}) > 0\} \quad (10)$$
$$D_f = \{\boldsymbol{x} \in \Re^n : G(\boldsymbol{x}) \le 0\} \quad (11)$$

called respectively the safety domain and the failure domain.
Two events are associated with these domains : the safety event $E_s \in F$ and the failure event $E_f \in F$, such that

$$E_S = \{\omega \in \Omega : G(\boldsymbol{X}(\omega)) > 0\} \quad (12)$$
$$E_f = \{\omega \in \Omega : G(\boldsymbol{X}(\omega)) \le 0\} \quad (13)$$

and which verify :

$$E_S \cup E_f = \Omega \text{ , } E_S \cap E_f = \Phi \quad (14)$$

The objective of the reliability analysis is then to evaluate the probability $P(E_s)$ or $P(E_f)$, called safety and failure probability respectively, given by :

$$P(E_s) = \int_{\Re^n} 1_{D_s}(\boldsymbol{x}) p_X(\boldsymbol{x}) d\boldsymbol{x} \quad (15)$$
$$P(E_f) = \int_{\Re^n} 1_{D_f}(\boldsymbol{x}) p_X(\boldsymbol{x}) d\boldsymbol{x} \quad (16)$$

and such that, according to Equation (14) :

$$P(E_s) = 1 - P(E_f) \quad (17)$$

where $\boldsymbol{x} = (x_1, \ldots, x_n)^T$, $d\boldsymbol{x} = dx_1 \ldots dx_n$ and 1_A (with $A = D_s$ or $A = D_f$) is the indicator function of $A \subset \Re^n$, such that : $1_A(\boldsymbol{x}) = 1$ if $\boldsymbol{x} \in A$ and $1_A(\boldsymbol{x}) = 0$ if $\boldsymbol{x} \notin A$.
Owing to Equation (17), generally only $P_f = P(E_f)$ is considered. In practice an exact calculation of P_f is not possible and a Monte-Carlo procedure must be used.

Application to the studied case – Let us recall that the vector $\boldsymbol{x}$ gathers the four parameters M, a_r, D_0, V_0 and that $\boldsymbol{X}$ is its probabilistic model. Each of its components $\boldsymbol{X_i}$ follows a truncated Gaussian distribution whose characteristics are given in Table 1. The solution $\boldsymbol{x_s}$ depends on $\boldsymbol{x}$ through the mechanical model and consequently, from Equations (7) and (8), so do the control variables $a_y(t)$ and $d(t)$. Therefore we can formally write $d(t) = d(t, \boldsymbol{x})$, $a_y(t) = a_y(t, \boldsymbol{x})$ and the safety criteria can be rewritten :

$$\overline{d} - \sup_{t \in [0,T]} |d(t, \boldsymbol{x})| > 0 \quad (18)$$
$$\overline{a_y} - \sup_{t \in [0,T]} |a_y(t, \boldsymbol{x})| > 0 \quad (19)$$

From these criteria we can define the associated limit-state functions :

$$G^D(\boldsymbol{x}) = \overline{d} - \sup_{t \in [0,T]} |d(t, \boldsymbol{x})| \quad (20)$$
$$G^A(\boldsymbol{x}) = \overline{a_y} - \sup_{t \in [0,T]} |a_y(t, \boldsymbol{x})| \quad (21)$$

and the corresponding failure events :

$$E_f^D = \{\omega \in \Omega : G^D(\boldsymbol{X}(\omega)) \le 0\} \quad (22)$$
$$E_f^A = \{\omega \in \Omega : G^A(\boldsymbol{X}(\omega)) \le 0\} \quad (23)$$

The aim of this study is then the computation of the occurrence probabilities of these failure events, given by :

$$P_f^A = P(E_f^A) \text{ , } P_f^D = P(E_f^D) \quad (24)$$

Numerical application

A set of $N = 10^7$ simulations is needed to obtain accurate probability estimations for $P_f \approx 10^{-4}$. With the specific vehicle dynamics model, the operation requires less than 2 hours on a standard PC (2GHz). The probabilities to violate the lateral acceleration criterion P_f^A and the lateral position criterion P_f^D are computed for each driver class and for speed varying from 45 to 80 km.h^{-1} (Figures 7-9).

Figure 7 shows that P_f^A vary suddenly from 0 to 1 around 60 km.h^{-1}. The driver class seems to have little influence on the probability, except for the first one that corresponds to the most interior position. Due to the fact that the curvature radius is slightly smaller, the criteria is violated at a lower speed. This first result indicates that the lateral acceleration criterion is weakly sensitive to hazard. Indeed, the speed for which P_f^A changes from 0

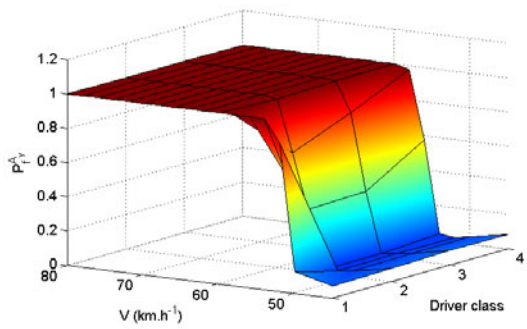

Figure 7. P_f^A as a function of speed and driver class (linear scale).

to 1 corresponds to the one that leads to reach the threshold of 3 m.s^{-2} on the different reference trajectories. This means that no information are added on this criterion compared to a deterministic study. On the contrary, Figures 8 and 9 reveal the usefulness of this probabilistic approach.

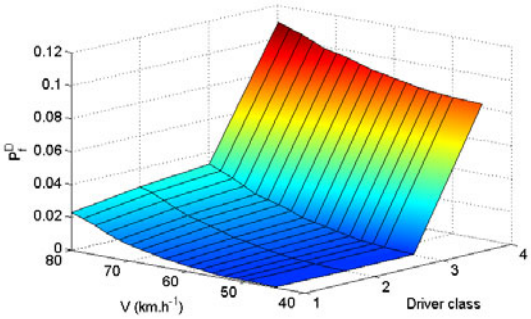

Figure 8. P_f^D as a function of speed and driver class (linear scale).

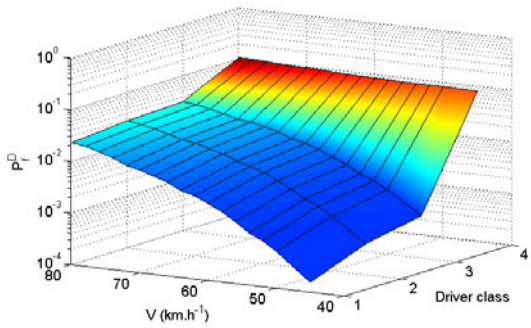

Figure 9. P_f^D as a function of speed and driver class (logarithmic scale).

Evolutions of P_f^D as a function of the speed and driver class are visible on Figure 8 (in linear scale) and on Figure 9 (in logarithmic scale). It reveals that both speed and driver class have influence on the lateral position criterion. P_f^D ranges from 10^{-4} to 0,11. The probability is always rising with increasing speed, and with the class number. This probabilistic study allows to obtain a gradation of the roadway departure risk versus speed for each driver class. This result, which could not be brought by a deterministic study, is of first interest here given the aim to trigger warning signals.

The smooth variation of P_f^D for the first three classes reveals the importance of hazard in the system. Concerning the fourth class, the probability is almost constant for all speed. This is due to the fact that it corresponds to the most exterior lane positioning (starting at only 60cm of the lane boundary) while the first class remains roughly in the middle of the lane.

In order to control a warning device, an acceptable roadway departure risk must be chosen by road safety experts considering for example real traffic analysis. Then, once a threshold on P_f^D is defined, the results of this study can be exploited to identify the critical initial conditions leading to risky situations.

CONCLUSION

This study proposes an application of probabilistic methods to the road safety domain with a view to develop a SVRD warning system. The interest of this approach is clearly highlighted for the case of an alarm triggering decision, as it leads to the direct computation of a risk indicator. This constitutes the first important difference compared to other SVRD studies. The other originality relies on the in-pavement integrated measurement devices that will be used for the initial conditions determination. This ensures a minimization of the necessary on-board equipment, which is an advantage for a mass implementation.

The results presented here show that both lateral position and speed have a great influence on the roadway departure risk. Even though these contributory factors were already well-known, the risk indicator computation allows to quantify the combined effects of these two factors. This can hardly be done with statistical post-accident analysis. Hence it has been noticed that the lateral acceleration criterion is weakly sensitive to hazard, due to the paramount influence of speed. Inversely, the lateral position criterion presents a smooth variation of probability between 10^{-4} and 0,11. Once a threshold on P_f^D is defined, the acceptable initial conditions can be selected through the results of this study. In the case where the arriving vehicle

does not respect these initial conditions, an alarm must be triggered to notify the driver to change his trajectory.

Concerning the system implementation, combined speed and lateral position measurement devices integrated in the pavement are under experimental validation. The equipped curve is the one presented in this study. The envisaged alarm system consists in warning lights positioned on the curve announcement traffic sign.

Two steps are considered for the prospects of this work. First, in the line with the driver/vehicle/road infrastructure stochastic modeling, time dependant perturbations will be added to the reference steer angle to represents the difference between the trajectory that the driver is willing to realize, and the one actually done. This involves the notion of stochastic processes, and thus requires more complex simulation and resolution methods. The statistical characteristics of this random process can be identified from experimental data and driver's actions studies. Second, a calculation time reduction will be obtained using different risk indicators and efficient structural reliability methods.

ACKNOWLEDGMENTS

This work is supported by the "Agence Nationale de la Recherche" through the project CISSSI reference ANR-06-CIS6-003.

REFERENCES

[1] G. Rey and al., "Towards a probabilistic alert procedure of roadway departure", Proceedings of the IEEE SSCI 2009 (Nashville, TN, March 30-April 2)
[2] D. Leblanc and al., "Road departure crash warning system field operational test: methodology and results", UMTRI, Tech. Rep., 2006
[3] P.H. Batavia, "Driver-adaptative lane departure warning systems", CMU, 1999
[4] D. Pomerleau and al., "Runn-off-road collision avoidance using IVHS countermeasures', NHTSA, 1999
[5] Y. Zhou and al., "A lane departure warning system based on virtual lane boundary", Journal of Information Science and Engineering 24, pp.293-305, 2008
[6] T. Piluti and A. Ulsoy, "Fuzzy-logic-based virtual rumble strip for road departure warning systems", IEEE Transactions on Intelligent Transportation Systems 4, pp.1-12, 2003
[7] A. Eidehall and L. Petersson, "Statistical threat assessment for general road scenes using monte carlo sampling", IEEE Transactions on Intelligent Transportation Systems 9, pp.137-147, 2006
[8] O. Ditlevsen and H. Madsen, "Structural Reliability Methods", Wiley, 1996
[9] A. Saltelli, K. Chan and E. Scott, "Sensitivity analysis", Wiley, 2004
[10] I. Sobol', "Global sensitivity indices for nonlinear mathematical models and their Monte-Carlo estimates", Mathematics and Computers in Simulation 55, pp.271-280, 2001
[11] J.P. Brossard, "Dynamique du véhicule : modélisation des systèmes complexes", Presses polytechniques et universitaires romandes, 2006
[12] T.D. Gillepsie, "Fundamentals of Vehicle Dynamics", Warrendale SAE, 2002
[13] H.B. Pacejka, "Tyre and Vehicle Dynamics", Warrendale SAE, 2002
[14] H. Radt and W. Milliken, "Non-dimensionalizing tyre data for vehicle simulation", Road Vehicle Handling, Institute of Mechanical Engineers, 1983
[15] D. Lechner and al., "Méthodologie de validation du logiciel de dynamique automobile CALLAS", Ingénieurs de l'automobile 713, pp.42-48, 1997
[16] J. Lauffenburger and al., "Driver-aid system using path-planning for lateral vehicle control", Control Engineering Practice 11, pp.217-231, 2003
[17] L.K. Chen and A.G. Ulsoy, "Identification of a driver steering model, and model unvertainty, from driving simulator data", Journal of Dynamic Systems, Measurement, and Control 123, pp.623-629, 2001
[18] M. Gabibulayev, "A stochastic form of a human driver steering dynamics model", Journal of Dynamic Systems, Measurement, and Control 129, pp.322-336, 2007
[19] J. Edelmann and al., "A passenger car driver model for higher lateral accelerations", Vehicle System Dynamics 45, pp.1117-1129, 2007
[20] Y. Goyat and al., "Vehicle trajectories evaluation by static video sensors", 9th International IEEE Conference on Intelligent Transportation Systems, Sept 2006

VALIDATION OF HARDWARE IN THE LOOP (HIL) SIMULATION FOR USE IN HEAVY TRUCK STABILITY CONTROL SYSTEM EFFECTIVENESS RESEARCH

Alrik L. Svenson
Paul A. Grygier
National Highway Traffic Safety Administration

M. Kamel Salaani
Transportation Research Center Inc.

Gary J. Heydinger
The Ohio State University
United States of America

Paper number 09-0189

ABSTRACT

A Hardware in the Loop (HiL) system was developed to investigate heavy truck instability due to loss of control and rollover situations with and without ESC/RSC systems for a wide range of maneuvers and speeds. The purpose of this HiL model is to examine the safety benefits of the emerging electronic stability systems (ESC/RSC) in heavy trucks that are designed to prevent yaw instabilities (e.g., jackknife) and rollovers. This paper outlines the process for validating the HiL model so that the simulation closely represents the expected outcome for a similar maneuver conducted on a test track. The HiL system was built in a laboratory using the brake system of a truck and the actual stability control system control units supplied from a manufacturer. The dynamics software uses TruckSim, and the simulation results were validated using NHTSA collected field data. The HiL model is being used to examine yaw instability and rollover scenarios that would not be possible to conduct in actual track testing. Driving scenarios were developed through an examination of Large Truck Crash Causation Study (LTCCS) cases. These scenarios were based on realistic events and were developed to replicate typical crash situations. The scenarios use a path-following driver model to drive through curves of various radii, a curve with a reduced radius, and variations of lane change maneuvers that are representative of obstacle avoidance. An overview of the scenario development, HiL system design, and the results of the validation of the HiL model are presented. The results of the validation show that the vehicle dynamics and hardware responses of the HiL are comparable to actual heavy truck test track results and can be helpful in determining the benefits of stability control technologies in varied driving situations.

INTRODUCTION

The National Highway Traffic Safety Administration (NHTSA) has funded the University of Michigan Transportation Research Institute (UMTRI) to study the potential safety benefits from two stability control systems developed for heavy truck tractor-trailers, Roll Stability Control (RSC) and Electronic Stability Control (ESC). The RSC systems sense lateral acceleration and apply the brakes when rollover is imminent. ESC systems sense vehicle speed, yaw rate, lateral acceleration, and apply brakes to assist a driver in avoiding directional instabilities as a result of an understeer or oversteer mitigation process. ESC can also address vehicle rollover as well. Stability control technology is needed because by the time a driver is aware that the truck is beginning to roll or lose control, it is usually too late for a corrective action by the driver. Since these systems have been only recently introduced in heavy vehicles, there is a limited amount of heavy truck crash data to base a determination of system effectiveness. Therefore, a hardware-in-the-loop (HiL) simulation model has been developed to assess system effectiveness. The observed system effectiveness in varied driving situations from the HiL can then be used to determine the potential benefits of stability control technologies by developing simulated driving scenarios that are linked to actual crash data populations. A validation of the HiL system by comparing simulation results to actual vehicle test experiments was required to ensure valid results. NHTSA validated the simulation results with experimental test track data from ramp steer maneuvers using tractor-trailers. An overview of the scenario development, HiL system design, the methods used for validation, and the validation results are presented in this paper.

SCENARIO DEVELOPMENT

In order to link the performance of stability control technologies to crash reduction benefits, data selection algorithms compatible with the national crash data files of the General Estimates System (GES), Trucks Involved in Fatal Accidents (TIFA), and Large Truck Crash Causation (LTCCS) databases were developed [1]. This information was used to create driving scenarios for the HiL simulation to study the effectiveness of ESC and RSC systems in addressing crashes involving directional loss of control and rollover.

The LTCCS database was analyzed to determine the factors that were used to define simulation scenarios. This analysis classified factors according to road radius of curvature (<100m, >100m, or straight), roadway friction (high or low), the position along the curve of rollover onset, driver control inputs (none, steer only, steer and brake, or brake only), trailer load (full, medium, or empty), center of gravity height (high, medium, or low), and whether the roll occurred at an intersection. UMTRI developed simulation scenarios representative of these factors that may lead to rollover and directional loss of control. [1] These scenarios were:

Transient to Constant Curve

This maneuver represents a typical entrance to a freeway exit ramp, and its geometry consists of two constant radius curves. The curve radii were 68 m and 227 m which represent the mean values for roads with a curvature less than 100 m or greater than 100 m respectively in the LTCCS database. The geometry is shown in Figure 1. The transition from a straight line to a constant radius curve provides a smooth vehicle dynamics transition as road curvature changes from infinity (straight roadway) to the desired radius. In this maneuver, increasing vehicle speed increases lateral acceleration and vehicle roll motion, and accordingly RSC, ESC, and ABS (baseline) have been evaluated iteratively to determine the speed for rollover onset, which is referred to as the critical speed.

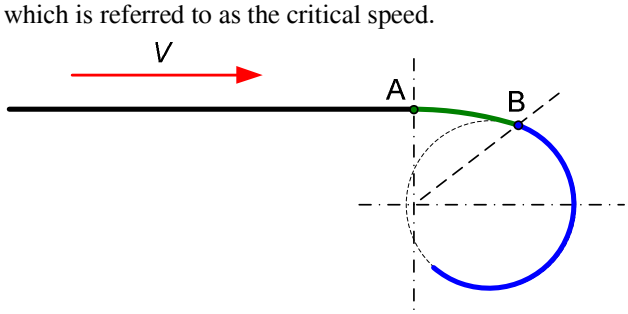

Figure 1. Transient to constant curve.

Constant Radius to Diminishing Curve

This maneuver represents a scenario where the vehicle enters the curve at a speed just below the critical speed, but the reduction in curvature increases the vehicle's lateral acceleration and roll angle to initiate rollover. The schematic of this maneuver is shown in Figure 2. The diminishing radius portion of the curve begins at 90 degrees beyond point A (see Figure 2). RSC, ESC, and ABS have been compared based on their critical speed.

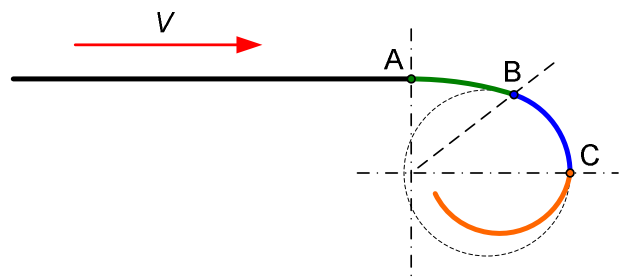

Figure 2. Constant radius to diminishing curve.

Single Lane Change in Curve

This maneuver represents the scenario of a truck changing lanes to the outside of the curve on a road resembling a freeway exit ramp with multiple lanes in the direction of travel. The schematic of this maneuver is shown in Figure 3. Critical speeds for the RSC, ESC, and ABS have been determined iteratively.

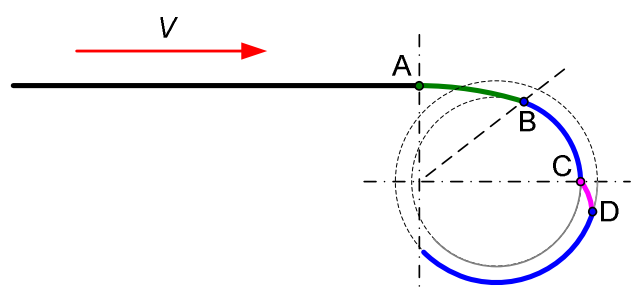

Figure 3. Single lane change in curve.

Single Lane Change on Straight Road

This maneuver is associated with most rollovers on straight roads. It tends to occur when truck drivers try to avoid an obstacle on the road, e.g., a slowing vehicle or an incursion from an intersecting road. ISO 14791 lane change geometry is used and critical speeds for RSC, ESC, and ABS have been determined iteratively.

Turn at an Intersection

Several rollover scenarios have been identified in the LTCCS that occur while the truck is turning at intersections. The radius of this maneuver is 20 m, and critical speeds for the RSC, ESC, and ABS system have been determined iteratively (see Figure 4).

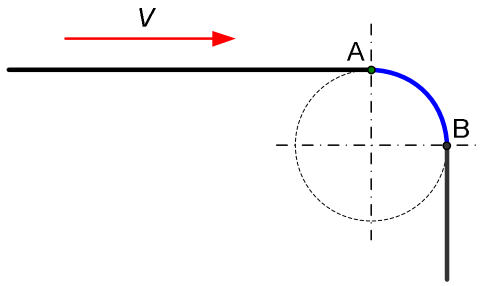

Figure 4. Turn at an intersection.

HIL SYSTEM DESIGN

To evaluate the effectiveness of stability control systems in the driving scenarios developed, a HiL system was built in the UMTRI laboratory. The HiL included the pneumatic brake system of a tractor-trailer and the actual stability control system control units supplied from a manufacturer. For this study, Meritor WABCO systems were used. The HiL system is a combination of hardware and software components, and includes simulated truck dynamics, a driver model, pneumatic brake system hardware, and the electronic control systems (RSC, ESC, and ABS). The dynamics were modeled using TruckSim software. Road geometry and surface conditions were modeled by variables in TruckSim. The driver model used a path-follower model at a constant speed. Also, the driver was modeled as a continuous controller. Using this method, lateral errors were reduced. The parameters of the controller were adjusted to provide a realistic closed loop vehicle driver simulation and were sufficient for this task.

The pneumatic brake system hardware is shown in Figure 5. Hardware was used to avoid modeling complex mechanical systems that included: compressible fluid mechanics, valve dynamics, and nonlinear frictional and system properties. This method eliminated the need for validating brake pressure models, as the actual hardware (typically installed on five axles and ten brake actuators) was used. The pressures that actuate the brakes were taken from TruckSim and the braking torque was determined from a table lookup of experimental data measured on a brake dynamometer. Brake line pressures and time delays were generated by a physical replica of an actual braking system.

Figure 5. Pneumatic brake system hardware.

Figure 6 shows the major components of the HiL system. TruckSim and Simulink were used and executed on real-time computers running on OPAL-RT software on a QNX operating system. System motion variables (speed, acceleration, yaw rate) were modeled in software (TruckSim and Simulink) and provided the inputs to the hardware control variables (steering and treadle displacement) and wheel speeds. The treadle displacement was converted to actual displacement via an electro-mechanical servo. Wheel speeds were transformed to appropriate hardware inputs that replicated wheel-speed magnetic pickups. The electronic stability system responded by providing control commands for engine brake applications, throttle inputs (disengage throttle), or actuation of the air brakes.

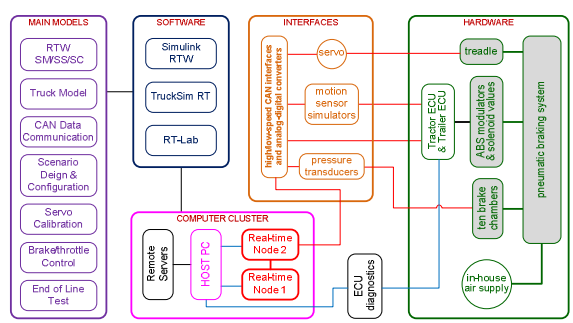

Figure 6. HiL system overview.

Heavy Truck Dynamics Model

The tractor-trailer modeled in TruckSim was based on collected test data from a 1992 White-GMC truck manufactured by Volvo GM Heavy Truck, model WIA64T, and a 1992 Fruehauf van trailer, model FB-19.5NF2-53. UMTRI measured geometric and inertial parameters for the chassis, steering, and suspension components. The performance properties of the three suspensions and torsional stiffness of the vehicle frames and fifth wheel coupling were also measured [2]. The geometric measures of the tractor and trailer are shown in Figure 7.

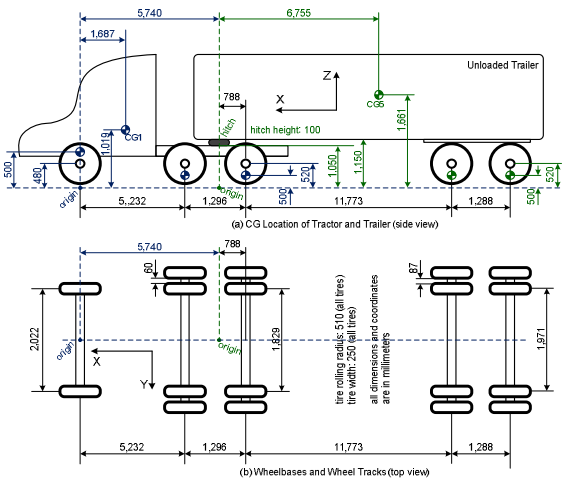

Figure 7. Heavy truck geometry.

Additional details for the TruckSim model used can be found in references [3-8].

Tire Data

Results from an SAE Cooperative Research Project [9] provided the tire data for the tractor-trailer. The SAE experimental tire data for lateral forces were limited to 16 degrees of slip angle, and data beyond that level were interpolated using the data point at pure sliding at 90 degrees of slip angle. These data represented typical tires produced in the 1990's as current data for state-of-the-art tire designs were not yet available. Despite this limitation, simulation results presented reasonable replications of typical heavy truck responses where comparative analysis can be done.

The dynamics delay or relaxation length for lateral force was set to 300 mm and for the longitudinal force it was 100 mm. The lateral relaxation length was not based on direct measurements of tire forces, but it was set to produce reasonable frequency response of lateral dynamics [10]. The longitudinal relaxation was set to produce reasonable stopping dynamics at zero speed after hard braking, and it had a secondary effect on the ESC/RSC systems.

HIL MODEL VALIDATION

NHTSA conducted the validation of the heavy truck HiL system developed by UMTRI. The simulation results were compared to experimental test track data for a typical tractor with a 53-foot semitrailer that was heavily loaded with a high C.G. location. Test track data were collected at the NHTSA Vehicle Research and Test Center (VRTC) in East Liberty, Ohio. These data were taken from the NHTSA stability control research program and were not conducted solely for the purpose of this validation. This resulted in some differences in the test track conditions and the HiL system. However, the data were useful for qualitatively checking the response of the HiL.

Ramp Steer Maneuver

The Ramp Steer Maneuver (RSM) formed the basis of the validation of the HiL simulation with test track data. The RSM is similar to a J-Turn maneuver. It was performed by inputting the steering profile shown in Figure 8. The severity of the maneuver was controlled by incrementally increasing speed until rollover occurred.

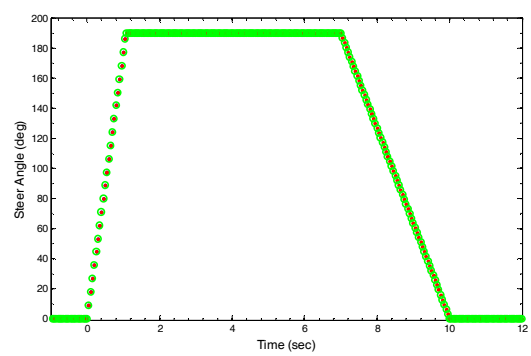

Figure 8. RSM steering profile.

Validation Results

For the HiL simulation, the RSM (using the steering profile shown in Figure 8) was applied to these three configurations: ABS-only (baseline), RSC, and ESC. The speed was increased gradually until rollover occurred. The ABS-only configuration did not involve ABS operations because driver braking was not included in the maneuver. For all runs, the driver input consisted of steering actions only. Differences between test track and HiL conditions were that the track maneuver was performed with a dropped throttle and

for the HiL it was performed at a constant speed provided by the simulated driver model. Also, there were some differences in the tires, suspensions, and compliances used on the actual truck, as opposed to the simulation.

When analyzing simulation results, it should be noted the extent of roll motion where model predictions are accurate. The parameters used in simulation models such as for TruckSim are typically based on measurements and estimations of vehicle motion that do not have excessive roll. Rollover events in simulations may result in numerical inaccuracies in the model as a result of complete vehicle roll. Although the predicted rollover mechanics beyond a certain roll angle (typically higher than six degrees) are not entirely valid, the simulation is useful for predicting the onset of vehicle rollover.

The tire data did not account for excessive vehicle roll and inclination effects. Data for the roll centers at each axle, suspension compliances, suspension kinematics, and many other aspects of the vehicle model were not formulated to accurately handle extreme roll mechanics. From a physical standpoint, it was sufficient to analyze wheel liftoff as a sign of rollover when using simulation results. The Load Transfer Ratio (LTR) metric was used to analyze rollover potential for both the tractor and trailer. This method was valid and yielded accurate and consistent results.

LTR is given by:

$$LTR = \left| \frac{\sum_{Left} F_{Ni} - \sum_{Right} F_{Ni}}{\sum_{Left} F_{Ni} + \sum_{Right} F_{Ni}} \right| \qquad (1)$$

LTR varies from 0 to 1. When LTR is equal to 1, it indicates a complete rollover. This is because, at the onset of rollover, all of the tires do not lift from the ground at the same time. An LTR value of approximately 0.9 indicates an onset of rollover.

Table 1 lists the HiL simulation and experimental results. The threshold speeds of the ABS-only and the RSC conditions were comparable with the speeds observed during test track testing (within 1 mph difference). However, the ESC speeds were quite different. The HiL driver model maintained throttle (in order to maintain constant speed) during the test maneuver. This likely produced a different response by the ESC controller for the HiL than observed in the test track runs.

When compared with test track data, the HiL simulation results showed the correct trends for ABS and RSC. For ESC the differences in the constant speed maintained by the driver model had a pronounced effect on system activation. The fact that the driver model in the HiL simulation maintained throttle resulted in the ESC controller intervening very quickly and earlier than on the test track. This permitted a higher speed at the start of the maneuver than what was achieved on the test track. As the test track runs were performed with dropped throttle, the ESC controller delayed intervention until it identified a loss-of-control situation. Therefore, the results were not expected to exactly match the speed obtained from test track measurements given this difference. However, the activations of the ESC were appropriate for the given simulated conditions.

Table 1.
RSM results – Speed (mph) at which first wheel lift occurs

Type	HiL Simulation		VRTC Data
	LEFT	RIGHT	LEFT
ABS only	27	27	27
RSC	34	35	35
ESC	42	41	32

Figure 9 shows a comparison of lateral accelerations, yaw rates, and roll angles for the three tractor-trailer electronic stability configurations for the RSM. Simulation results show that the truck dynamics model and the HiL systems were tuned appropriately. Both systems showed a substantial advantage in improving tractor-trailer stability as evidenced by the greater speed at which rollover was initiated for the RSC and ESC runs over the baseline condition of ABS. Figure 10 shows tractor decelerations for the three configurations. The ESC system had a higher deceleration level than the RSC system due to the additional steer axle braking of the ESC system. The ESC and RSC systems showed that wheel liftoff occurred at a higher speed than with the ABS-only system.

Figures 11 and 12 show experimental test track results from RSC and ESC systems compared to baseline runs (ABS only). Figures 13 and 14 show the generated brake line pressures as a result of RSC and ESC system activations respectively. Figures 15 and 16 show the simulation results that can be compared to the experimental results in Figures 11 and 12.

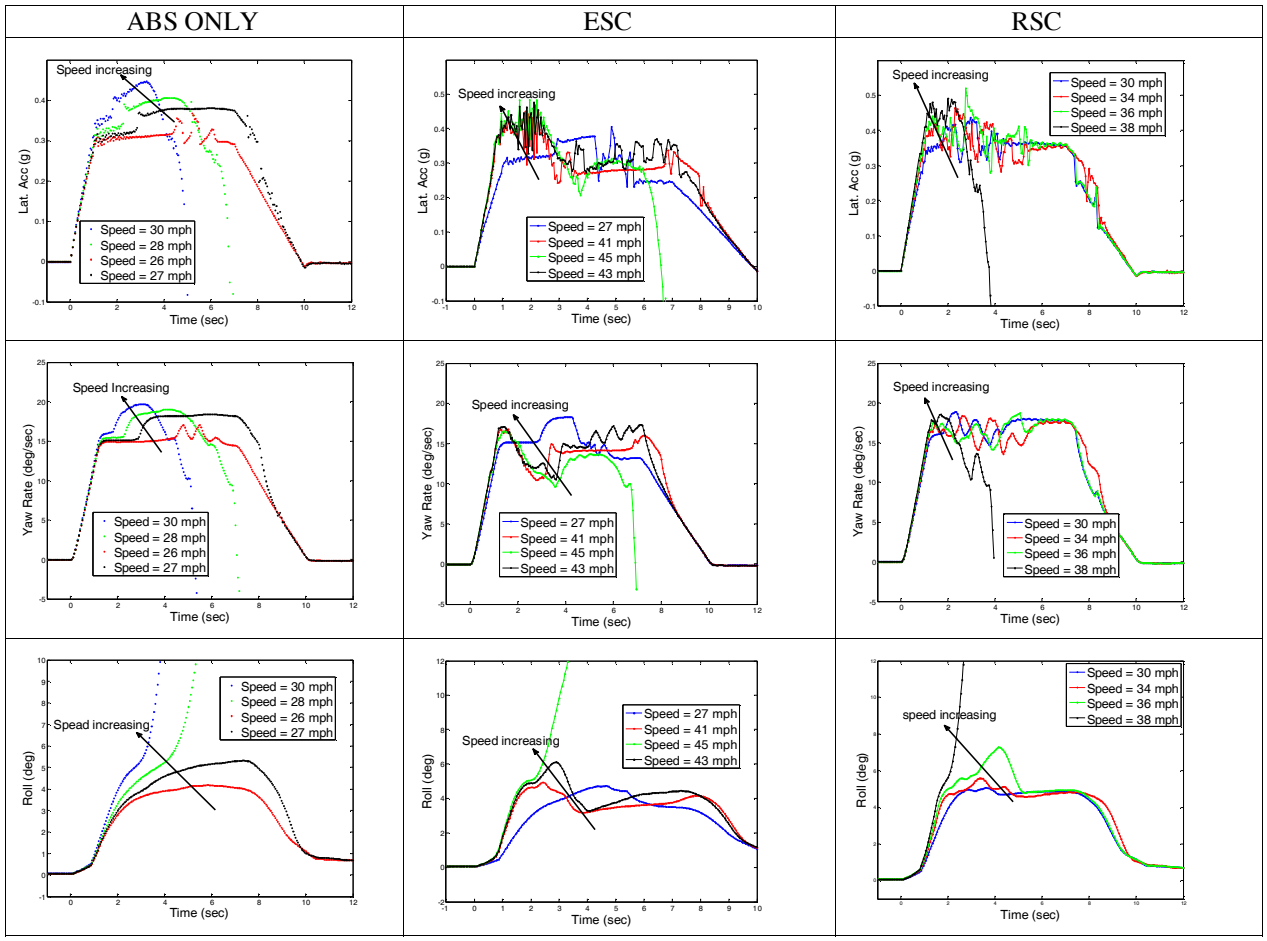

Figure 9. Lateral accelerations, yaw rates, and roll angles for the tractor.

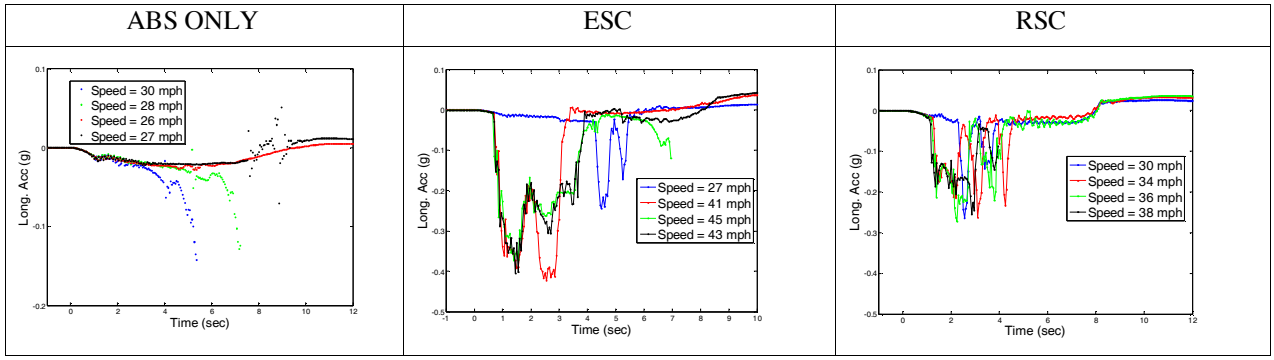

Figure 10. Longitudinal accelerations for the tractor.

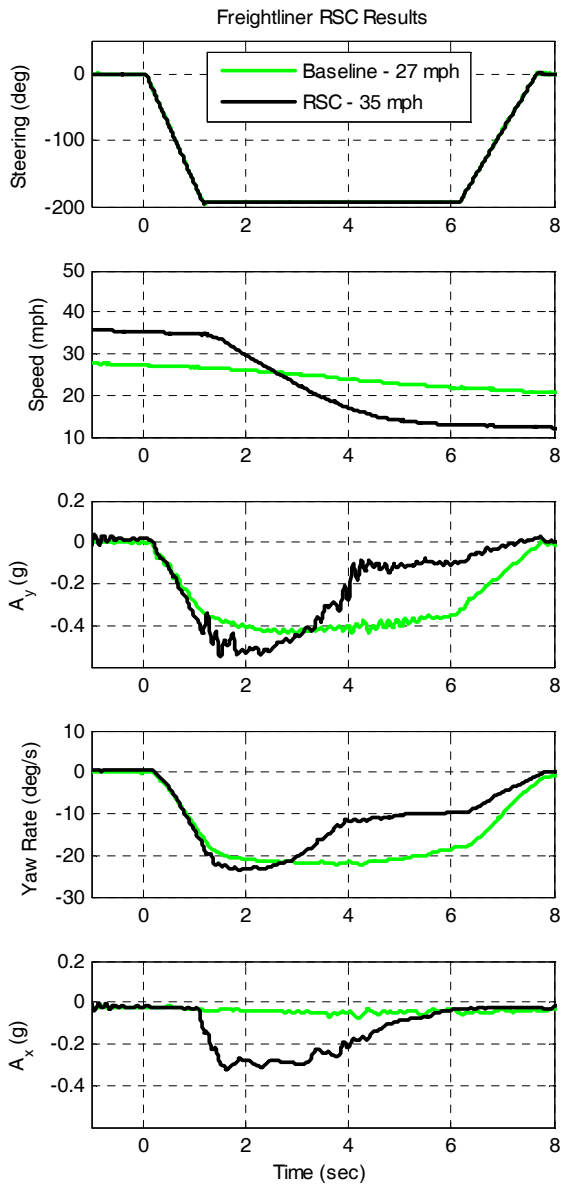

Figure 11. Experimental steering inputs and vehicle responses: baseline and RSC results: 2006 Freightliner.

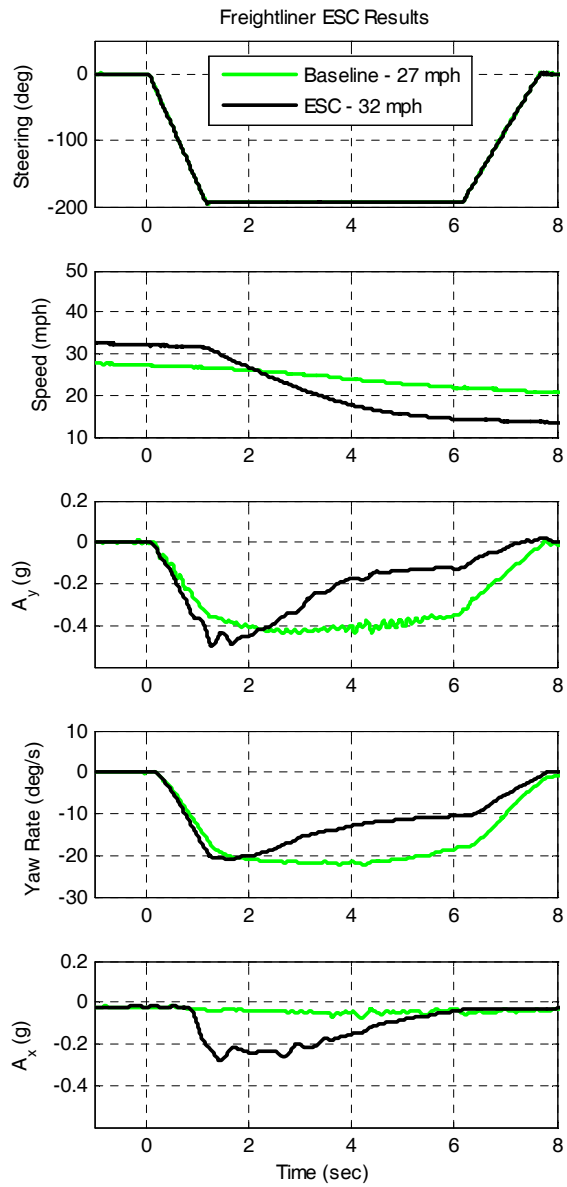

Figure 12. Experimental steering inputs and vehicle responses: baseline and ESC results: 2006 Freightliner.

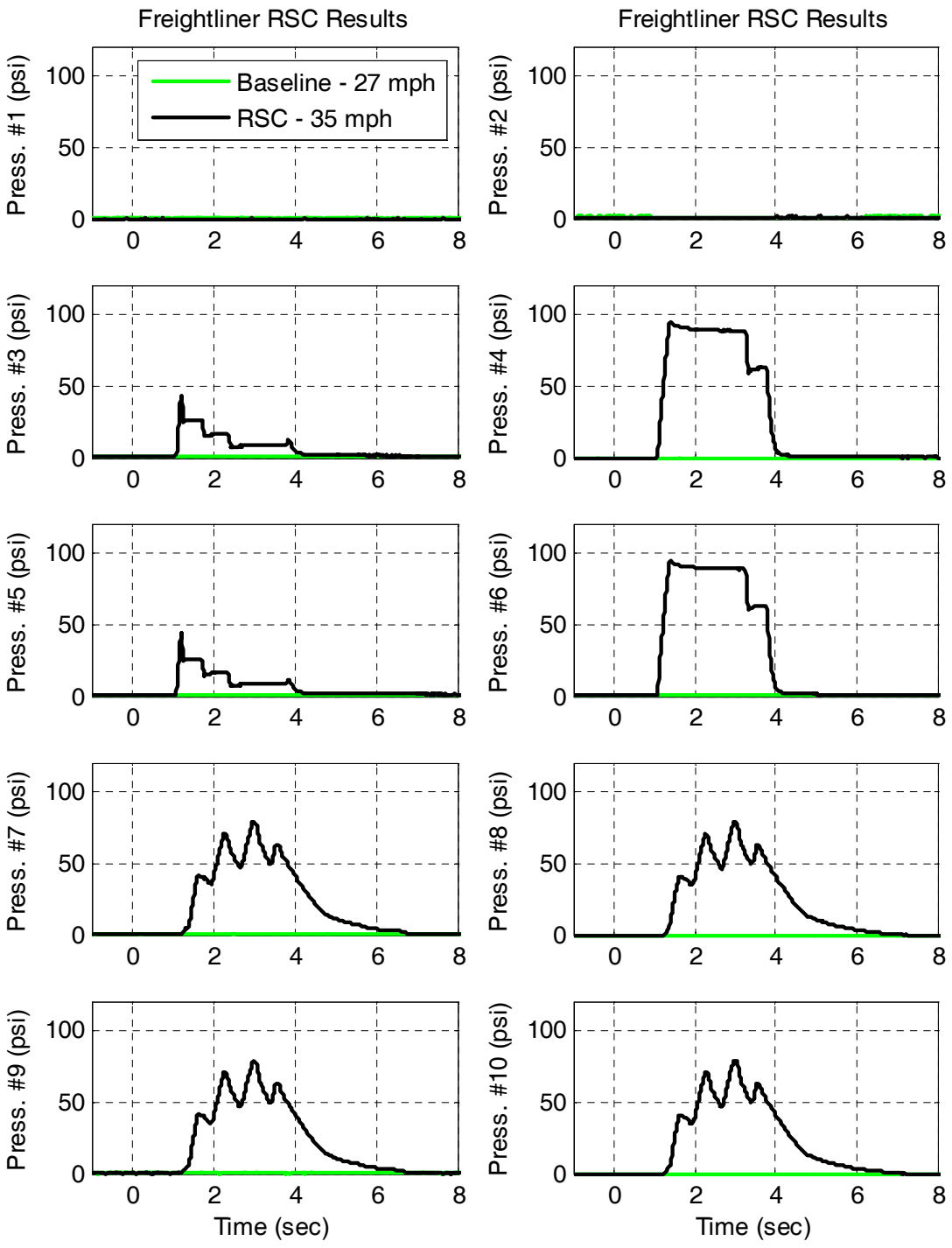

Figure 13. Experimental brake pressures: baseline and RSC results: 2006 Freightliner.

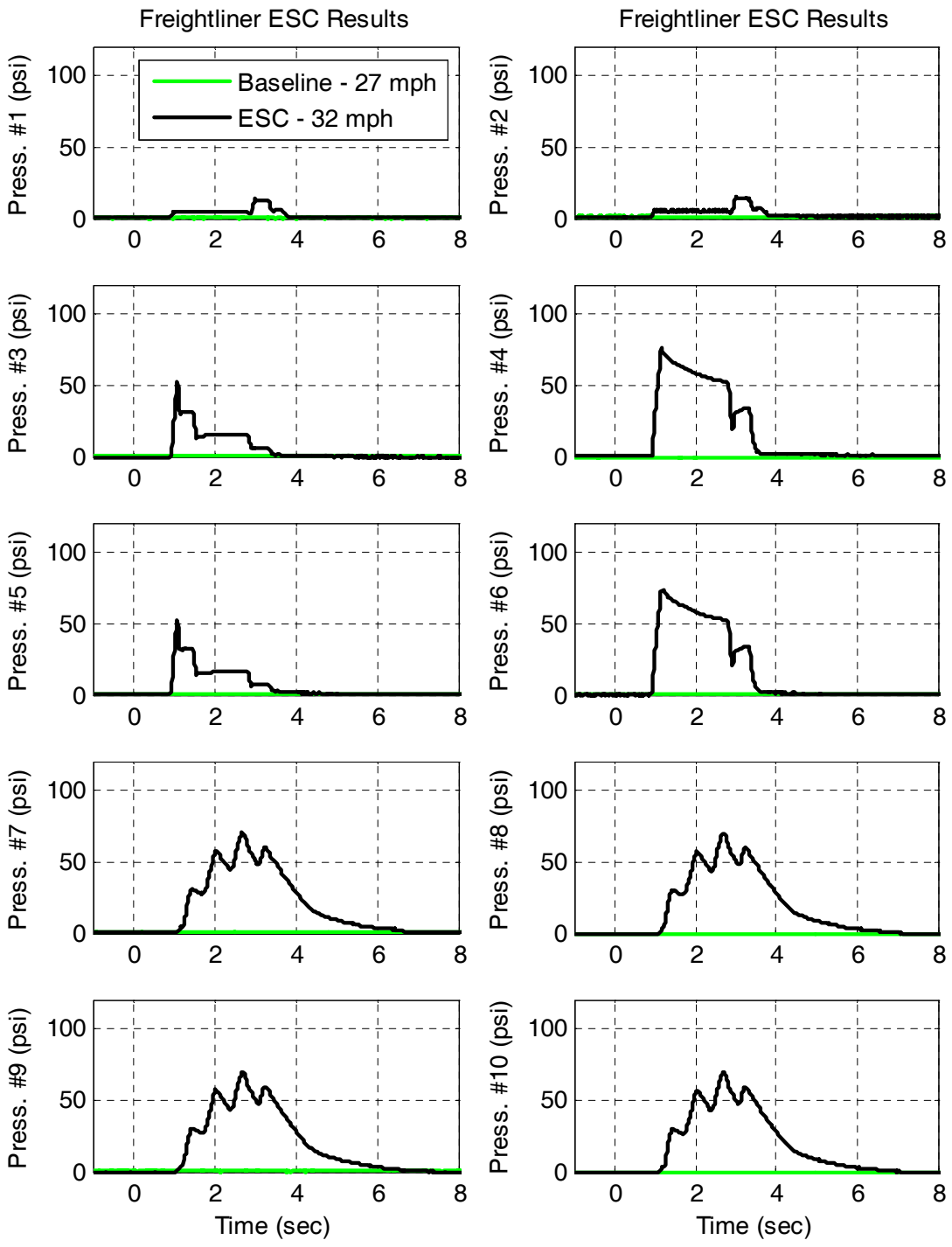

Figure 14. Experimental brake pressures: baseline and ESC results: 2006 Freightliner.

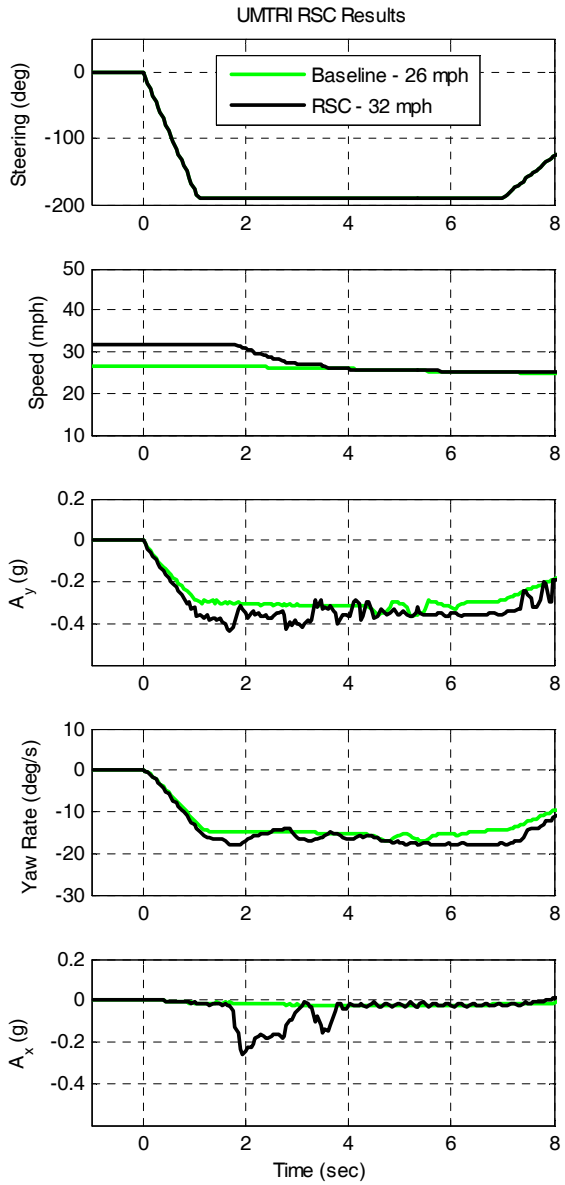

Figure 15. UMTRI HiL simulation steering inputs and vehicle responses-baseline and RSC results.

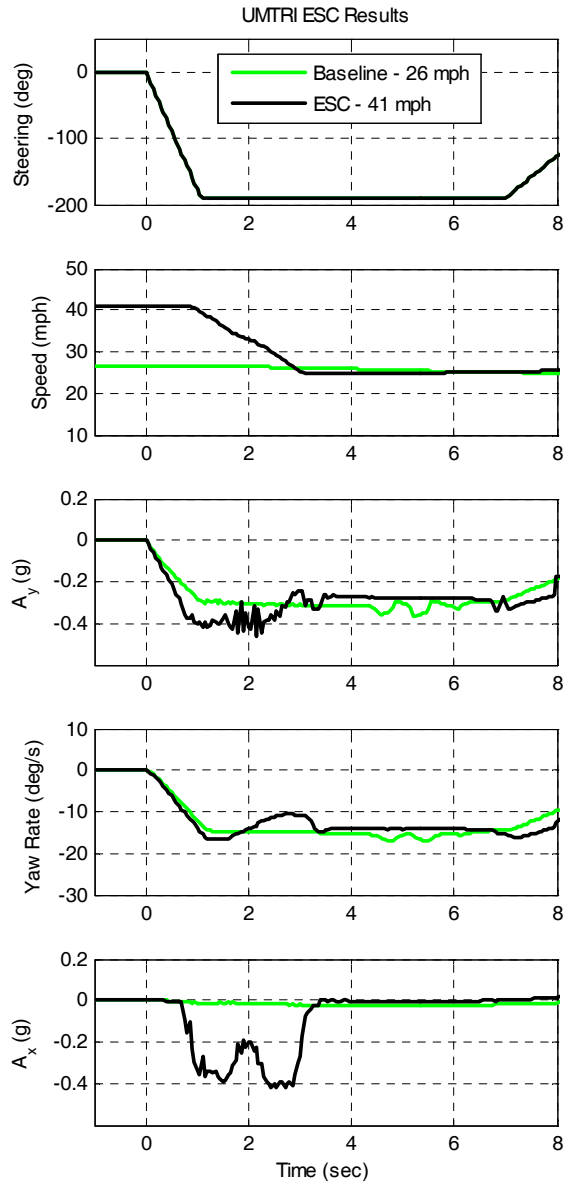

Figure 16. UMTRI HiL simulation steering inputs and vehicle responses-baseline and ESC results.

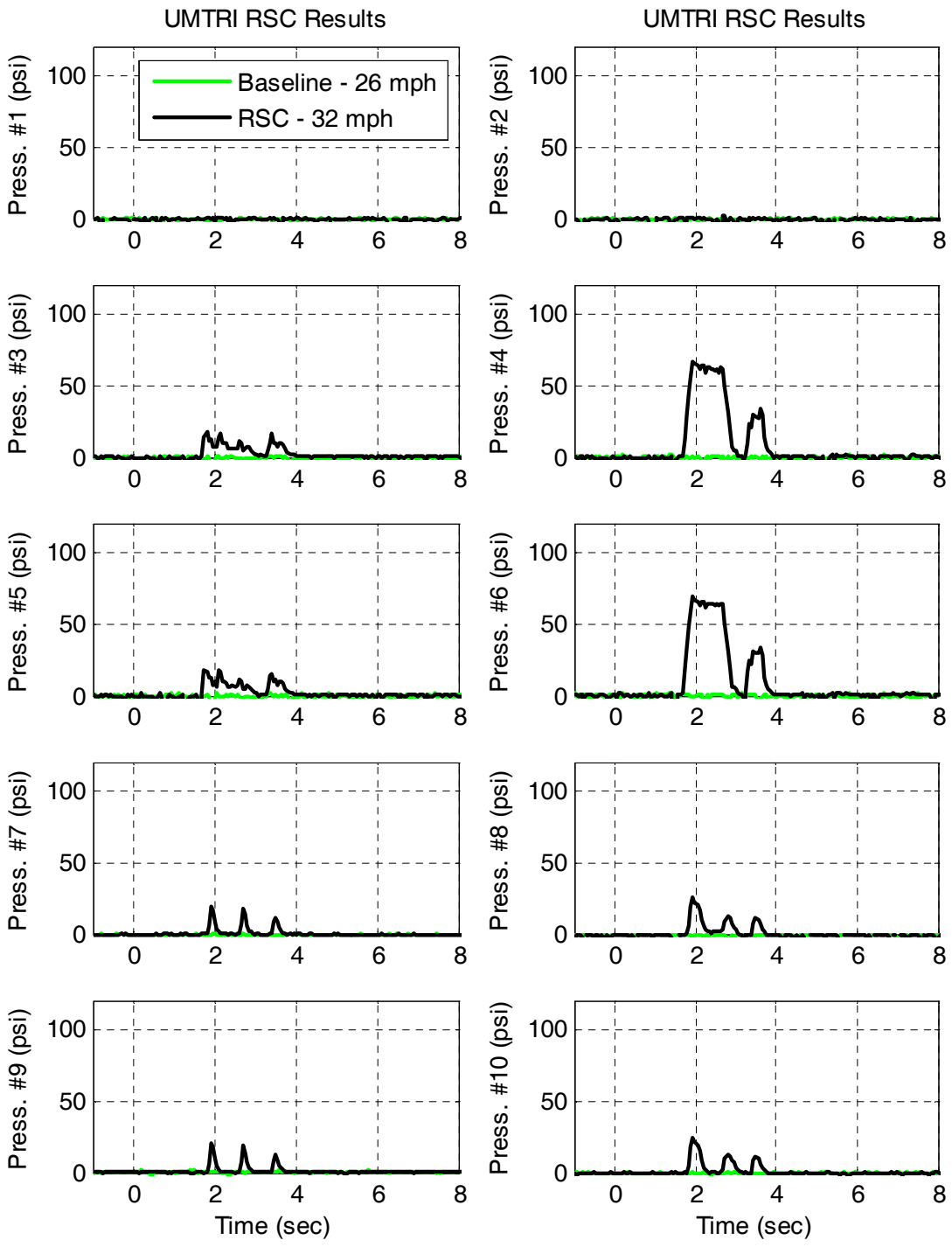

Figure 17. UMTRI simulation HiL brake pressures: baseline and RSC results.

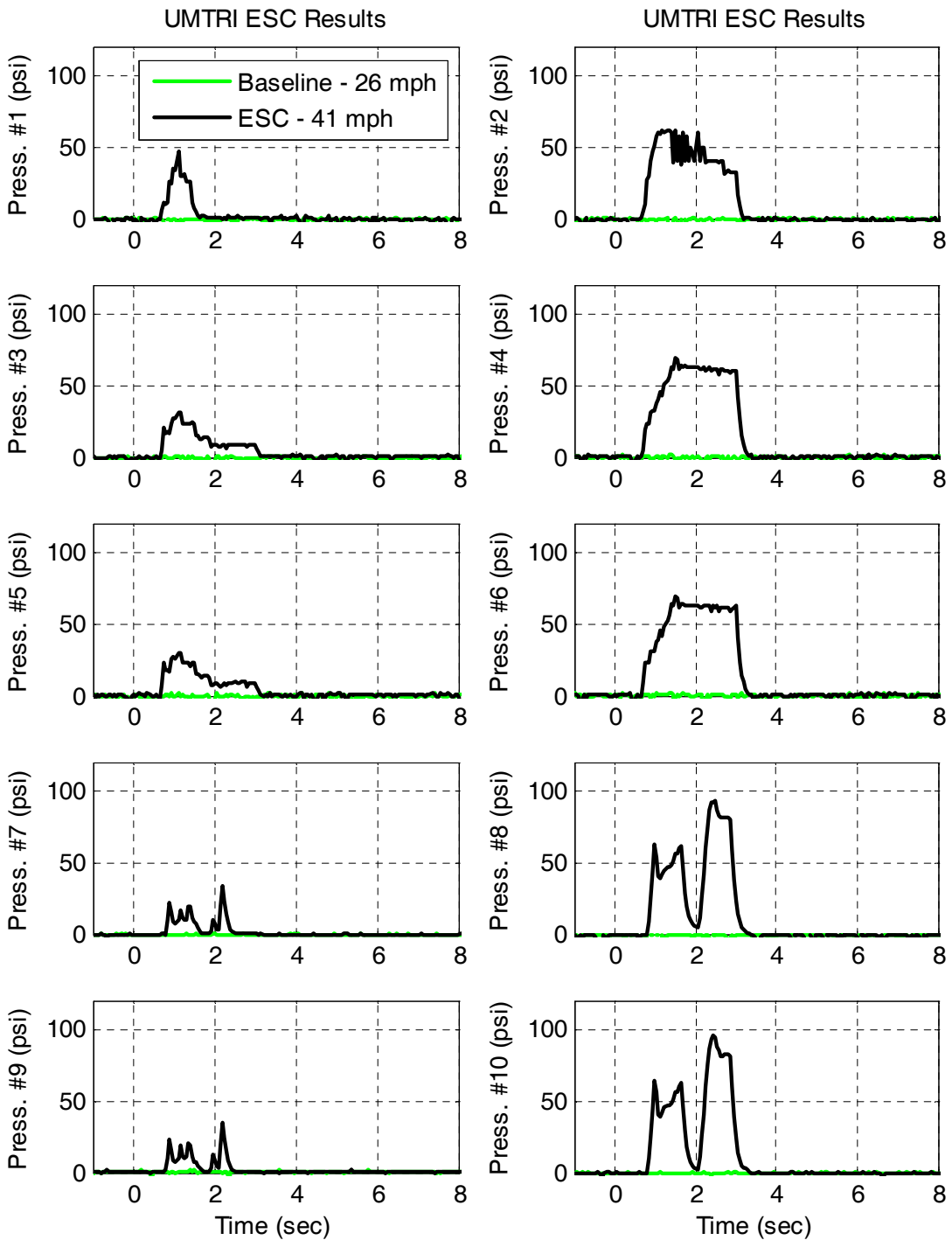

Figure 18. UMTRI simulation HiL brake pressures: baseline and ESC results.

The comparison shows that the lateral accelerations, yaw rates, and longitudinal decelerations reach about the same maximum levels. However, the driver model in the HiL attempted to keep the speed of the tractor-trailer constant, and the speed was not reduced further after rollover was avoided. This explains the constant speed profile and the change in deceleration after about 3 seconds of RSM initiation. The RSC system in both the HiL and the test track vehicle reduced the yaw rate and lateral acceleration levels to the baseline levels. The ESC system in the HiL activated slightly more than 0.2 seconds earlier than the system on the test track vehicle. Also, the longitudinal deceleration was almost twice as much.

Figures 17 and 18 show the brake line profiles at each wheel. Comparing Figures 14 and 18 reveal that the steering axle brakes of the simulated vehicle provided far more braking force than those of the test track vehicle, which explains the higher threshold speed achieved by the simulated vehicle.

Overall, the qualitative differences in results between the HiL simulations and test track experiments were minor. An exact match between test track and HiL data was not possible due to differences in the hardware between the tested vehicle and the simulation. Also, the constant speed maintained by the driver model in the HiL produced an effect that was more pronounced in the ESC than the RSC in the comparison with test track RSM data. However, the HiL system functionality and results were valid for a comparative analysis of system effectiveness for the constant speed driving scenarios developed in this study.

CONCLUSIONS

A HiL system has been developed by UMTRI to evaluate the effectiveness of stability control technologies in tractor-trailers. Driving scenarios have been developed to evaluate the effectiveness of ESC and RSC in addressing crashes involving directional loss of control and rollover. These scenarios have been created using LTCCS cases to replicate typical crash situations and have been linked to national crash data bases (GES, TIFA).

The HiL system was validated by NHTSA through a comparison of RSM test data. The results of the validation showed that the vehicle dynamics and hardware responses were comparable to actual tractor-trailer test track results. Differences in the test track conditions and the HiL system did not allow for a direct comparison of track data and simulated results. However, the data were useful for qualitatively checking the response of the HiL. The constant speed maintained by the driver model in the HiL produced an effect that was more pronounced in the ESC than the RSC in the comparison with test track RSM data. This resulted in the ESC system in the HiL activating approximately 0.2 seconds earlier than the system on the test track vehicle, but this was appropriate for the given simulated conditions. Despite the differences, the HiL system functionality and results were valid for a comparative analysis of system effectiveness for the constant speed driving scenarios developed in this study.

The fact that the HiL system provides valid predictions means that this HiL simulation environment can be used reliably to study heavy vehicle response with these technologies. This is true not only for evaluating RSC and ESC effectiveness in the driving scenarios developed in this study, but for other future scenarios that would be difficult or impractical test using an actual vehicle. The observed system effectiveness in varied driving situations from the HiL can be used for the determination of potential benefits of stability control by using driving scenarios that are linked to actual crash data populations.

REFERENCES

[1] Woodrooffe, J., Blower, D., Gordon, T., Green, P.E., Liu, B., and Sweatman, P. 2009. *Safety Benefits of Stability Control systems for Tractor-Semitrailers*, The University of Michigan Transportation Research Institute, Ann Arbor, Michigan, to be published.

[2] Winkler, C.B., Bogard, S. E., and Karamihas, S. M. 1995. *Parameter Measurements of a Highway Tractor and Semitrailer,* The University of Michigan Transportation Research Institute, UMTRI-95-47, NHTSA Contract Number DTNH22-95-C-08125.

[3] Milich, E. 1999. *An Evaluation of VDM-Road and VDANL Vehicle Dynamics Software for Modeling Tractor-Trailer Dynamics*, M.S. Thesis, The Ohio State University, USA.

[4] Zaugg, B. C. 2004. *Development of Heavy Truck ABS and Limit Maneuvers*, M.S. Thesis, The Ohio State University, USA.

[5] Zagorski, S.B. 2003. *Compatibility of ABS disk/Drum Brakes on Class VIII Vehicles with Multiple Trailers and their Effect on Jackknife Stability*, M.S. Thesis, The Ohio State University, USA.

[6] Dunn, A. 2003. *Jackknife stability of Articulated Tractor Semitrailer Vehicles with High-Output Brakes and Jackknife Detection on Low Coefficient Surfaces*, Ph.D. Dissertation, The Ohio State University, USA.

[7] Shurtz, M. L. 2006. *Effects of ABS Controller Parameters on Heavy Truck Model Braking Performance*, M.S. Thesis, The Ohio State University, USA.

[8] Chandrasekharan S., Guenther, D.A., Heydinger, G. J., Salaani, M. K., Zagorski, S. B. 2009. "Development of Roll Stability Control Model for a Tractor Trailer Vehicle," SAE 2009-01-0451.

[9] *Truck Tire Characterization*. 1995. SAE Cooperative Research Report, CRP-11.

[10] Salaani, M. K., Heydinger, G. J., and Grygier, P. A. 2003. "Evaluation of Heavy Tractor-Trailer used in the National Advanced Driving Simulator," SAE Paper 2003-01-1324.

ENHANCED BRAKING PERFORMANCE BY INTEGRATED ABS AND SEMI-ACTIVE DAMPING CONTROL

Marcus Reul
Hermann Winner
TU Darmstadt, Chair of Automotive Engineering
Germany
Paper Number 09-0204

ABSTRACT

This paper is on focused on the optimization of the braking process integrating Antilock Braking System (ABS) and Continuous Damping Control (CDC). Strategies for reducing the braking distance derive from theoretical approaches. These strategies deal with sharing information between ABS and CDC in order to improve the slip-control quality and adjusting braking torque (ABS) and / or wheel load (CDC) coordinately. Quantities which influence the amount of the mean braking force and therefore the braking distance are identified methodically, regarding a standard control loop. Furthermore the influence of the time course of wheel load on the braking process is discussed.
In the second section of this paper, experimental results of straight-line ABS-braking tests for two methodically identified strategies are discussed. The results of the first experiments show the influence of passive damper settings (hard, soft) and the MiniMax damping control on the braking distance for various braking conditions (dry an wet roads, flat and unevenness roads,…). The MiniMax damping control aims for reduced body induced slip oscillations that usually disturb standard ABS-control. This damping control reduces the braking distance significantly in a statistical manner. The second experiment has been performed with a modified ABS which takes into account the information of the dynamic wheel load (due to pitching and lifting) additionally for the calculation of the braking force operation point. It is shown that the braking force operation point changes more, if dynamic wheel load information is implemented in ABS-control. Indeed the amount of modulated braking force operation point due to pitching or lifting is too small with respect to the demand, so further modifications are necessary.
Finally an outlook on the next steps for improving the braking process by integrated ABS and Continuous Damping Control is given.

INTRODUCTION

When designing a chassis of a passenger car, ride and handling are important criteria. In order to improve driving safety and comfort, several chassis control systems that control the vehicle's longitudinal, lateral and vertical dynamics were developed and introduced in production cars in the last decades. Regarding vehicle safety, most important chassis control systems are ABS (Antilock Braking System) and ESP (Electronic Stability Program). These systems control longitudinal and lateral tire forces by adjusting tire slip, based on wheel speed sensor information. However, horizontal tire forces are limited by the amount of wheel load and friction. With information available in today's ABS the wheel load is estimated taking the vehicle mass and axle-load transfer into account only.
According to comfort, mainly the vehicle's vertical dynamic characteristics are important. With passive suspensions a known trade-off between comfort (usually measured as RMS on vertical body acceleration) and safety (usually measured as RMS on wheel load) exist. Thus, a compromise between different optimal suspension parameters for ride and handling has to be found. With adjustable damping and / or spring forces, vertical body accelerations and wheel loads can be influenced depending on the situation. Available for production cars are either semi-active, e.g. Continuous Damping Control (CDC), or active systems, e.g. Active Body Control (ABC) or Anti-Roll-System (ARS). In normal driving situations damping and / or spring forces are usually adapted according to a Skyhook algorithm in order to reduce vertical body movements (lifting, pitching and rolling). For this control strategy, vertical wheel accelerations and vertical body displacements or accelerations are detected by several sensors. Currently, semi-active suspension systems have greater market share compared to active suspension systems probably due to less energy consumption and component costs. This makes Continuous Damping Control interesting for the topic of this research: It is investigated if CDC in conjunction with ABS has potential to improve the braking process.

State of the Art

In critical driving situations, as ABS controlled braking or lane changing, the time course of wheel load should be optimized in order to realize maximum horizontal forces. In today's production cars, semi-active or active suspensions support slip-control systems (ABS or ESP) reducing body movements as pitching or lifting. These body movements cause wheel load oscillations which

disturb slip-control and lead to less mean horizontal tire forces. Therefore, for straight-line ABS-braking an aperiodic pitching behavior is intended in order to reduce disturbances. In production cars equipped with semi-active damping, this objective is aspired by switching the dampers to a rather hard setting, if ABS-braking is detected (refer to Becker et. al. [1]). However wheel load oscillations depend not only on body movements but on pavement excitations as well. This fact is not considered in this usually used control strategy. Apart from the Boolean signal "ABS-activity", it is not of the author's knowledge that additional information between ABS/ESP and semi-active or active suspension are shared in today's production cars. So, information of "dynamic wheel loads" caused by pitching, rolling, lifting and pavement excitations are not taken into account in today's ABS-control although the knowledge of the overall wheel load is necessary to adjust the braking force operation point correctly in today's ABS systems.

In a research project, Niemz [2] developed a control strategy for semi-active damping, which is able to modify wheel load induced slip. For modifying slip in this control strategy, the wheel load is changed by means of switching the damper from hard to soft and vice versa. This control strategy has been reduced the mean ABS-controlled braking distance by 1.3% compared to those with series damper setting (constant hard setting), tested with an initial velocity of 70 km/h on a dry road in real braking tests. However, this damping control and the production ABS of the vehicle worked independently from each other, data exchange between both systems has not been taken place. Moreover, the performance and robustness of this control strategy for varying braking conditions is not investigated yet.

Motivation and Objective

For several years, coordination and information exchange of different control systems has been focused more and more by industry and research. This is based on the fact that in addition to ABS and ESP, other control systems as semi-active and active suspensions or Active Front Steering (AFS) take place in production cars. Sharing information between systems and coordination of those systems may provide greater overall performance compared to different stand alone working control-systems – often without additional production costs. As an example, the combination of ESP with AFS to so the called ESP II reduces the braking distances in μ-split situations [4]. Moreover, the combination of active antiroll-bars (ARS) with ESP and AFS reduced the braking distance even further (refer to [5]). Referring to previous research at TU Darmstadt which deals with ABS-controlled braking and semi-active damping (refer to [2] and [3]), an increased overall performance is expected if ABS and CDC share information and work in conjunction. So, the results of this research project shall answer the question if and to what extend there is potential for reducing the braking distance by coordination of the chassis control systems ABS (as part of ESP) and CDC. This potential could be used both by sharing information and by modifying the horizontal and vertical tire forces in conjunction.

This paper is focused on the identification of possible strategies for improving the braking process with Continuous Damping Control in conjunction with ABS. Furthermore the results of braking tests with a modified damping control (MiniMax control) and a modified ABS are presented which show the potential of optimizing the braking process by means of integrated ABS and CDC. The modified ABS takes the dynamic wheel load in a very easy manner into account. Based on the theoretical approaches and experimental results, other strategies will be tested in the future which let expect potential for improving the braking process.

STRATEGIES FOR IMPROVING STRAIGHT-LINE BRAKING

Objective of this research project is the determination if and to what extend the braking process can be improved with combined operation of ABS and CDC systems. Improving the braking process to the authors view means:

- Reducing braking distance, which possibly avoids accidents or reduces their severity at last
- Faster decrease of the vehicle's kinetic energy with respect to travelled distance, which reduces the severity of accidents that cannot be avoided
- Braking stability (lateral offset, yaw rate variation) must not be degraded

The braking distance is directly connected to the braking force, as can be seen in equation. (1).

$$d_B = \frac{1}{m_v} \cdot \int_{t_{BB}}^{t_{BE}} \int F_{B,total}(t) \cdot dt' \cdot dt \qquad (1)$$

Due to the fact that total braking force is limited by friction coefficient μ_{max} and wheel load F_z it cannot be increased above a certain value. The average total braking force for braking to standstill is limited by friction coefficient and vehicle mass.

$$F_B = \mu \cdot F_z \qquad (2)$$

$$F_{B,total,mean} = \mu_{mean} \cdot m_V \cdot g \qquad (3)$$

The braking distance can be reduced either by increasing the mean friction coefficient μ_{mean} or by modifying the time course of wheel load. Neglecting aerodynamic effects the mean value of wheel load must be constant over the whole braking process – namely equal to the vehicle mass multiplied by gravity. This is due to the fact that the vehicle mass

cannot be changed within the braking procedure. The effect of wheel load distribution on the braking distance will be discussed latter.

Increasing the mean braking force

Regarding the first optimization aspect - increasing mean friction coefficient μ_{mean} to increase mean braking force - the friction-slip characteristics is important (refer to Figure 1). For stationary conditions, the maximum friction coefficient can be obtained with a characteristic slip value $\lambda_{B,opt}$, which depends on tire properties and road condition. If this slip value could be controlled exactly, the maximum total braking force for a given vehicle mass could be achieved. Braking slip λ_B is defined physically by the ratio of the wheel's rotational velocity v_W and the translational velocity of the wheel's center point $v_{W,x}$. For ABS control, $v_{W,x}$ is assumed to be equal to the vehicle velocity:

$$\lambda_B = 1 - \frac{v_W}{v_{W,x}} = 1 - \frac{r_{dyn} \cdot \dot{\varphi}_W}{v_{W,x}} \approx 1 - \frac{r_{dyn} \cdot \dot{\varphi}_W}{v_V} \qquad (4)$$

Of course, braking distance can be reduced by increased friction as equation (2) and (3) show. For a given tire - road combination this can be achieved by modifying the tire properties. Although this is possible in certain applications as e.g. racing cars demonstrate this come along with other negative tire properties which usually are not acceptable for production cars. Optimizing the tire properties is not discussed within this research; hence a standard tire is assumed and used for the experiments of this research project.

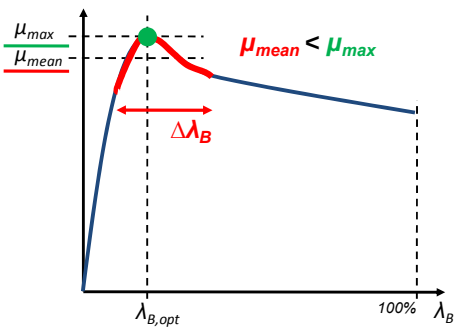

Figure 1. Example of friction-slip characteristics

For production ABS-controller, the so called target slip $\lambda_{B,Z}$ is less than $\lambda_{B,opt}$ and depends on the vehicle velocity among other things to keep slip-control smooth and effective. However in braking maneuvers slip oscillations exist. Assuming that $\lambda_{B,Z}=\lambda_{B,opt}$, slip oscillations in the nonlinear section of the μ-λ_B characteristics lead to a mean friction coefficient that must be less than the maximum friction coefficient. Therefore, as a first optimization parameter for this research, braking slip oscillations has to be as small as possible to obtain the mean friction coefficient of a braking process μ_{mean} as close as possible to the maximum friction coefficient μ_{max}. This holds true for quasi-stationary conditions which are represented by the friction-slip characteristics in Figure 1. For dynamic situations, fast alternations of the braking torque or wheel load lead to even greater braking slip and friction oscillations, referring to Zegelaar [7]. The hypothesis "shorter braking distances are obtained by less slip oscillations" is not disproven yet and therefore hold true. This is shown in previous research [2] analyzing the correlation between braking distance and velocity difference (v_V–v_W), which is in fact the braking slip weighted with the vehicle velocity. According to [2] the correlation coefficient is between 41-63% depending on the damper settings. The physical mechanisms of the dynamic transfer behavior of braking torque and wheel load modifications on the braking slip will be examined in further research. So far it is assumed that the objective

$$\mu_{mean} \rightarrow \mu_{\max} \qquad (5)$$

can be achieved by minimizing slip oscillations:

$$\left(\lambda_{B,Z} - \lambda_B\right) \rightarrow 0 \qquad (6)$$

<u>Quantities which cause braking slip oscillations</u> - In order to increase the mean braking force for a given friction-slip characteristics by means of increased mean friction due to decreased slip oscillations, the influences on braking slip have to be known. Taking a view on a rotating and braked wheel (Figure 2) with neglected vertical and longitudinal stiffness of the tire the principle of angular momentum delivers:

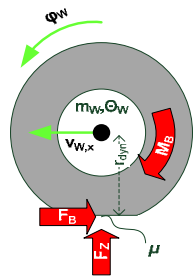

Figure 2. Quantities at a rotating wheel

$$\Theta_W \ddot{\varphi}_W(t) = F_B(t) \cdot r_{dyn} - M_B(t) \qquad (7)$$

Integrating eq. (7) leads to

$$\Theta_W \left(\dot{\varphi}_W(t) - \dot{\varphi}_{W,0}\right) = \int F_B(t) \cdot r_{dyn} dt - \int M_B(t) dt \qquad (8)$$

Substituting the angular velocity of the wheel with the definition of slip (eq.(4)), eq. (8) delivers:

$$\lambda_B(t) = 1 - \frac{r_{dyn}}{v_{x,W}(t)} \cdot \left(\Delta\dot{\varphi}_W + \dot{\varphi}_{W,0}\right) \qquad (9)$$

Defining differences of the angular velocity with respect to a free rolling wheel as:

$$\Delta\dot{\varphi}_W = \frac{\int \mu(\lambda_B(t)) \cdot F_Z(t) \cdot r_{dyn} dt - \int M_B(t) dt}{\Theta_W} \qquad (10)$$

Equation (10) shows that differences in the wheel's angular velocity result from the integral of wheel load and /or braking torque variations in time domain. This means, there is a time delay between torque or force variations and the reaction of braking slip. Comparing the integral with a low pass filter this shows that torque or force variations with lower frequencies take even more effect on braking slip oscillations compared to higher frequencies with equal amplitudes. This means, that both increased amplitudes of braking torque or wheel load variations and low variation frequencies lead to higher braking slip oscillations. If those braking torque and wheel load variations are based on disturbances, this could result in less mean total braking force and longer braking distances. For straight-line braking, especially pitching and lifting influence wheel loads with low frequencies and high amplitudes and hence the braking slip with respect to eq. (10). Braking torque disturbances result e.g. from friction oscillations of the brake disc / pad combination. Furthermore ABS-control is not perfect due to several assumptions and actuator properties which can cause braking slip oscillations as well.

Strategies for decreasing braking slip oscillations - The previous section deals with the identification of variables which possibly cause braking slip oscillations. Thus less mean total braking force would be obtained. Braking torque and wheel load oscillations have been identified as disturbance variables. What can be done to reduce braking slip oscillations? In today's standard ABS, slip is controlled adjusting the braking torque only. Amongst others, inaccurate slip control could cause differences between applied and optimal braking torque. The latter is defined as the braking torque which is required for a specific situation. So, an increased accuracy of slip control has the potential to reduce slip oscillations, which would increase the mean total braking force.

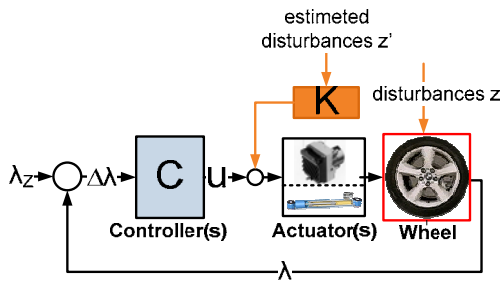

Figure 3. Simplified control loop with disturbance feed-forward (K)

Taking a view on a real ABS-control loop for straight-line braking we get to know that several quantities of the control loop (Figure 3) are estimated based on wheel angular velocities and the master brake cylinder pressure. These estimations are necessary for ABS-control because direct measurands are not available (referring to Figure 2 e.g., longitudinal wheel velocity, braking torque, braking force,…).

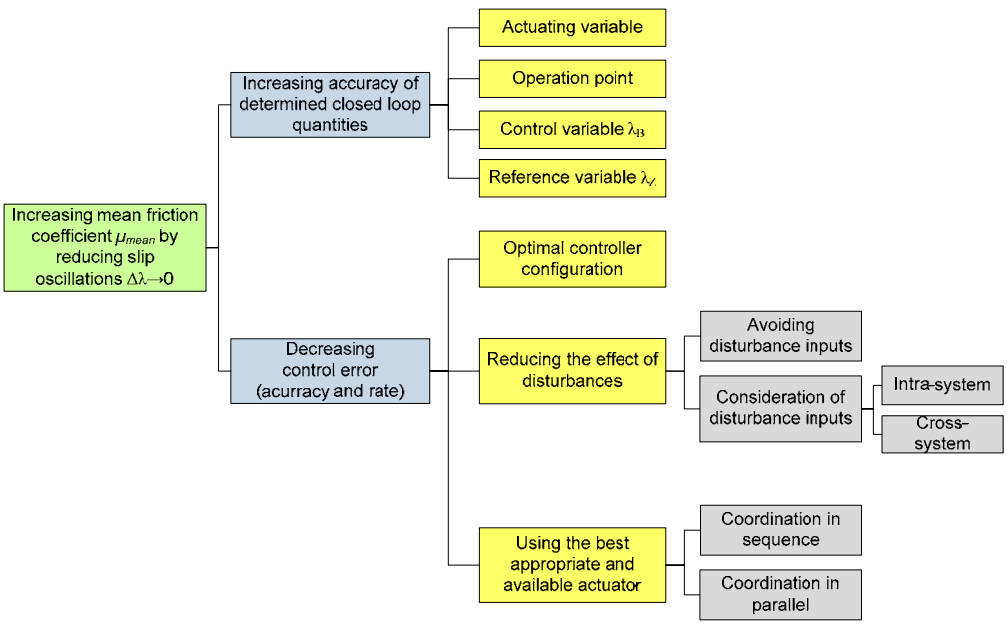

Figure 4. Strategies for increasing the mean total braking force $F_{B,total,mean}$

The control variable "braking slip" has to be determined by measuring the wheel's angular velocity and the vehicle's velocity. Assuming that vehicle velocity equals the wheel's longitudinal velocity, which means that the longitudinal suspension flexibility is neglected, braking slip is calculated. However for ABS-controlled braking, the vehicle velocity is estimated as well because all wheels possess slip. So, the control variable "braking slip" is based on several estimations and might be inaccurate.

For slip control a reference variable "target slip" is needed. Desiring a high friction coefficient and braking stability (which means sufficient potential for lateral forces) the target slip derives from the friction slip characteristics for stationary conditions. This tire-characteristic varies by several inputs as wheel load, velocity, road conditions, temperature etc. Lots of these inputs are not well known and therefore not all of these influences are considered in the target-slip which results in deviations to the desired optimal target slip.

The actuating variable determines the desired braking torque of a wheel. Both operating point and the required braking torque differences to reduce control errors (controller output) are translated into caliper pressure that is influenced by the brake valves. So, the quality of slip control is also influenced by operating point and actuating variable.

In summary all of the control loop variable possibly influence slip control quality and thus braking slip oscillations which should be minimized. This is shown in the upper part of Figure 4.

As mentioned before, major task of the control loop is to minimize control errors. Regarding the control loop shown in Figure 3 and assuming target-slip and braking slip as determined precisely two components influence the control quality mainly: The controller configuration and the properties of the actuator(s), especially its dynamics and operation range. For the optimization of the controller settings the trade-off between fast error compensation and overshooting has to be dealt with. Although the controller compensates control errors the control quality can be improved by reducing the effects of disturbances on the control variable. Avoiding of disturbance inputs in general would be the best option in order to reduce slip oscillations. Instead of a closed-loop control this would allow an easier open-loop control. Although this is not possible for ABS braking the reduction of disturbance inputs should be aspired because of less control errors anyway.

Among other quantities, e.g. braking torque variations, dynamic wheel load variations due to low frequency pitching act as disturbance variable on slip control, as equation (10) shows. For ABS-controlled straight-line braking pitching results from the height difference between center of gravity and pitching center. The effect of pitching on wheel load oscillations can be reduced by increasing damping or spring forces – no or aperiodically pitching is aspired ideally. If the vehicle's suspension is passive, a trade-off with respect to comfort exists. For today's production cars equipped with Continuous Damping Control (CDC) damping is switched to rather hard setting when ABS braking is detected so that wheel load oscillations and their effect on ABS control are reduced. As a consequence, hard damping results in shorter braking distances on flat roads compared to soft damping, referring to [2]. Taking into account that the integral of dynamic wheel load changes braking slip (eq. (10)) the ABS controller reacts on wheel load oscillations with a time delay in braking torque. This could be improved using the dynamic wheel load information additionally for slip control in order to decrease wheel load induced slip oscillations. In literature algorithm for active or semi-active suspension control principles are known which reduce wheel load oscillations (e.g. "Ground Hook control" [6], "Constant wheel load control" [3]) or that control wheel load induced slip oscillations directly [2]. All of these methods consider the disturbance variable "wheel load oscillations" intra-system with adjusting the vertical suspension parameters of the vehicle. However connecting semi-active or active suspension control with ABS wheel load could be taken into account for ABS control additionally which possibly reduces slip oscillation even further.

Apart from the controller, actuation of the control system "wheel" with its control variable "braking slip" is very important. In today's production cars hydraulic valves moderate the braking pressure applied by the driver. So the braking torque is controlled by ABS. Referring to equation (10), apart from braking torque the wheel load modulates braking slip as well. With an active or semi-active suspension system that acts in vertical direction, wheel load and thus braking slip can be influenced temporarily. In order to modify braking slip, there are two different actuators available with brake torque (ABS) and wheel load (e.g. CDC) modulators. Depending on their properties ABS and CDC could act in sequence or in parallel but coordinated. The method of coordination depends on the specific properties of the actuator principle which could be different with respect to operation range, "minimal step size" and dynamics.

Wheel load influence on the braking process

At the beginning of this section it is shown that both mean friction coefficient and wheel load take effect on the braking distance in principle. In the previous section strategies for increasing the mean friction coefficient and so mean total braking force are deduced within a theoretical approach. The next section will discuss the influence of wheel load on the braking process.

Neglecting aerodynamical effects which may change wheel load with higher vehicle velocities the

overall wheel load has to be constant in steady state. Assuming wheel load and friction to be constant for the whole braking procedure the total braking force is constant, too:

$$F_{B,total}(t) = \mu \cdot m_v \cdot g \tag{11}$$

As a result of constant braking force, the braking distance is calculated by eq. (1):

$$d_B = \frac{1}{2}\frac{v_{x,0}^2}{\mu \cdot g} \tag{12}$$

Taking into account that the mean total braking force has to be constant over the whole braking process due to the constant vehicle mass (refer to eq.(11)) and assuming a linear decrease of braking force over time with eq. (14) this leads to a shorter braking distance for κ>1, as eq. (15) shows. The factor κ describes the raise of the braking force at the beginning of the braking process (Figure 5):

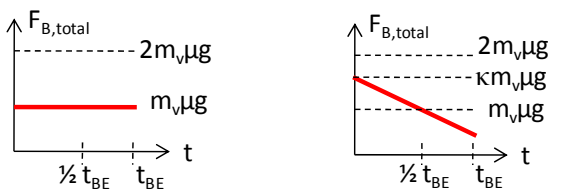

Figure 5. Constant (left) and time-variant (right) distributions of total braking force in time domain

$$\text{For } 0 \le \kappa \le 2\text{: } \kappa = \frac{F_{B,total}(t=0)}{F_{B,total,mean}} \tag{13}$$

The time course of total braking force is defined as

$$F_{B,total}(t) = \kappa \cdot \mu \cdot m_v g \cdot \left(1 + 2\left(\frac{1}{\kappa} - 1\right)\frac{t}{t_{BE}}\right) \tag{14}$$

$$d_B = \frac{v_{x,0}^2}{\mu \cdot g}\left(\frac{4-\kappa}{6}\right) \tag{15}$$

Defining $\kappa = 2$ and assuming a linear decrease of braking force over time the braking distance is minimized to:

$$d_B = \frac{1}{3}\frac{v_{x,0}^2}{\mu \cdot g} \tag{16}$$

Compared to eq. (12) the braking distance is reduced by $^1/_3$ in this theoretical approach. The result shows that the time course of braking force influences the braking distance at a given mean total braking force, which depends on the vehicle mass and mean friction coefficient μ_{mean} mainly. The higher the braking force at the beginning of the braking process the shorter the braking distance. So as a second optimization parameter, the braking force at the beginning of the braking process has to be maximized.

But how could the time course of the braking force be influenced? Of course the friction coefficient could be maximized especially at the beginning of the braking process. But this objective is aspired for the whole braking process and should not be considered at the beginning only.

Apart from the friction coefficient, the wheel load derives as a second quantity which influences the braking force (equation (2)). Controlling the time course of wheel load this could deliver higher but decreasing braking forces from the beginning of the braking process. It is possible to influence wheel load temporarily with active and semi-active suspensions. Wheel loads can be changed temporarily with these systems by adding additional spring and / or damping forces. In case of adjustable damping switching the damper in compression from soft to a hard setting increase damper force and thus wheel load (please see Niemz [2] for more details). The effect time is limited because additional suspension forces acts both on the wheel (increasing the wheel load) and the body. The latter accelerates the body upwards as long as the wheel load increases. Due to the raising displacement between body and wheel greater spring forces decelerate the body which decrease wheel load. The average wheel load equals zero but the time course of wheel load is changed temporarily.

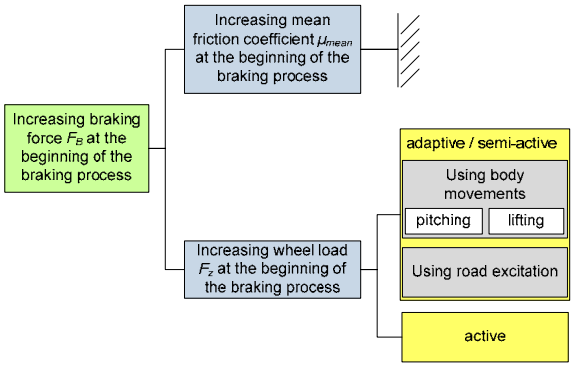

Figure 6. Strategies for increasing braking force F_B at the beginning of the braking process

Contrary to active systems with good controllability semi-active suspensions have to use system inherent energy for changing wheel loads which is less predictive. In case of semi-active damping, damper forces depend on damper velocity and damping characteristics which can be changed by a proportional valve. Without any damper velocity wheel load cannot be influenced. Energy that can be used for changing wheel load results from body movements due to pitching and lifting which appear in straight-line braking situations. Rolling can be used

in cornering situations to change wheel loads – but this is not taken into account for straight-line braking. In addition to body movements road excitations cause damper velocities as well and can therefore be used for changing wheel loads by semi-active systems too.

Summary of strategies for improving the braking process

Previous section deals with the identification of strategies in order to improve the braking process. Two quantities are identified which influence the braking process mainly:
The first is the mean friction coefficient. Limited by tire properties mainly that value should be as high as possible. This could be realized by minimized slip oscillations. A theoretical approach shows that slip oscillations result from both braking torque variations and wheel load oscillations. Strategies for reduced slip oscillations are deduced methodically considering a standard control loop. For minimized braking slip oscillations the quantities of the control loop have to be known as accurate as possible. In addition, disturbance inputs as wheel load oscillations can be reduced potentially by additional feedforward controls in ABS and / or by control of vertical suspension systems. At last it is discussed that different actuator principles as ABS and CDC, which could be used coordinately, have the potential to improve the overall control performance "adjusting the braking slip to the target slip". As a result it is expected that the braking distance is reduced due to higher mean braking forces.
As a second quantity, the wheel load should be maximized at the beginning of the braking process. Semi-active or active suspensions allow changing the total wheel load temporarily and can be used for this application in principle. Contrary to active suspension systems with a good controllability, semi-active suspensions systems as Continuous Damping Control have to use system inherent energy for changing wheel loads temporarily. This energy results either from body movements or road excitations.

EXPERIMENTS

In the previous section strategies for improving the braking procedure are deduced with theoretical approaches. The following section investigates the influence of selected strategies on the braking procedure in driving tests. Referring to (Figure 4) the following theoretical strategies are considered in the following sections:

1. The disturbance variable "wheel load induced slip oscillations" is minimized intra-system by using the semi-active damping control "MiniMax-control". No ABS- modification or interaction takes place.
2. The "dynamic wheel load" is taken into account for a modified ABS-control in order to estimate the overall wheel load for each wheel. The braking force operation point is adjusted to dynamic wheel load oscillations due to pitching or lifting in order to decrease slip oscillations.

Test design - For statistical reasons straight-line braking tests with varying damping-control or ABS settings are usually repeated N=35 cyclically in order to compensate slow changing parameters as tire wearing or test track temperature. The start of the braking procedure, initiated automatically by a braking machine, is changed with respect to the position on the test track in order to compensate potentially particularities of the test track. The braking distance is determined using an optical Correvit-sensor, which measures the longitudinal velocity, and several light barriers reflectors with defined gaps. The braking distance is defined as the travelled distance during the time interval of $[t_{BB}, t_{BE}]$ – which represents the beginning and the end of the braking procedure in time domain. The beginning of the braking procedure is defined by a threshold of the left front calliper pressure which corresponds to the beginning of the maximal longitudinal deceleration of the vehicle. The end of the braking procedure is defined by the vehicle velocity $v_x \leq 3$ km/h. With this method, the braking distance is determined with an average accuracy of below 0.2 %. The determined braking distance cannot be compared to those which can be found in literature because the built-up time for braking pressure is not taken into account. However it is a proper method for the comparison of different damper or ABS settings with respect to braking distance because the built-up time is reproducible due to the braking machine.

1. Reducing wheel load induced slip-oscillations by semi-active damping control (MiniMax-control)

The MiniMax control strategy has been developed in previous research by Niemz [2]. Referring to equation (10) the integral of wheel load oscillations leads to slip oscillations. In order to decrease slip oscillations the MiniMax-controller switches the dampers to a hard or soft setting depending on the damper stage and the amount of the integral of dynamic wheel load which represents wheel load induced slip oscillations. For a detailed description of the controller refer to Niemz [2]. It has been proved that reducing the braking distance with this strategy is possible for an initial velocity of 70 km/h on a dry road with unevenness representative for a German Autobahn. The following results deal with the transferability to other conditions of the braking procedure. The braking tests were performed with the same test vehicle (referring to [2]), a GM Opel Astra

H equipped with CDC dampers (Continuous Damping Control). The dynamic wheel load information is estimated wheel individually by means of vertical accelerometers. The following parameters were varied in additional braking tests in order to prove the robustness of the MiniMax-controller:

- initial velocity: 70km/h and 100 km/h
- road condition: dry and wet road to vary the overall friction coefficient
- road roughness: flat, Germ. Autobahn like, very rough (nondeterministic)
- tire type: 205/55R16 summer (standard) and winter tyre of the same manufacturer

In addition to the MiniMax damping control, the braking tests have been performed with passive hard (standard setting for the production car) and soft damper setting. Any test design consists usually of N=35 braking tests per damper setting, 105 ABS-controlled braking tests overall. If less braking tests were performed for a scenario, it is noted in the figures. In order to compare the performance of the control strategy for different tests-conditions, the braking distance is normalized by the mean braking distance of all three damper settings hard (h), soft (s) and controlled (c):

$$d^{h,s,c}_{B,i,norm} = \frac{d^{h,s,c}_{B,i}}{\frac{1}{3N}\sum_{i=1}^{N}\left(d^{h}_{B,i} + d^{s}_{B,i} + d^{c}_{B,i}\right)} \qquad (17)$$

It is defined that a parameter influences the performance of the control strategy (braking distance reduction) significantly if the range between minimum and maximum braking distance reduction of two test-scenarios does not overlap on a significance level of α=5%. A t-test is used to calculate the minimum difference of braking distances on a level of significance of α=5%, for the maximum difference of braking distance the 2σ limit of a Gaussian distribution is used.

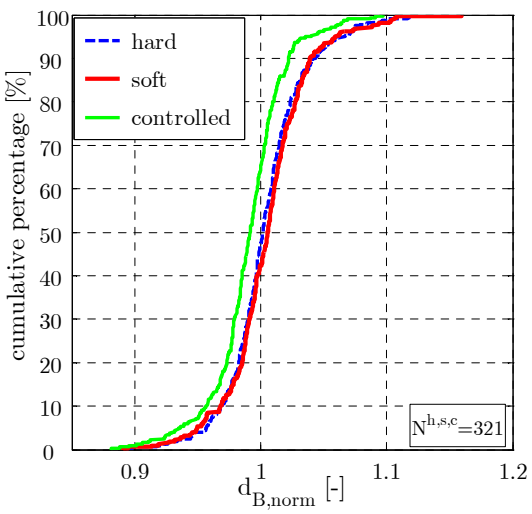

Figure 7. Overall results of N=963 braking tests

In summary, N=963 ABS-controlled braking tests with different damper settings were carried out. Figure 7 shows the normalized results of the braking distance. Assuming a Gaussian distribution, the control strategy reduces the mean braking distance compared to hard damping by approx. 1% and for soft damping by approx. 1.3% (level of significance α=5%).

The distributions of normalized braking distances for summer and winter tires and for the defined initial velocities do not show any significant differences with respect to the mean braking distance and deviation (refer to Figure 8 for some results of the influence of initial velocities). So, these results are not represented by a figure in this paper. For these test scenarios, the MiniMax control reduces the braking distance on dry roads significantly compared to the best passive damping (usually hard, except for very rough roads, where soft damping leads to better results).

The next sections describe the influence of different damper settings for different road roughnesses and friction conditions on the braking distance in more detail:

Influence of friction - With reduced friction μ on wet roads, less effect of the damper setting on the braking distance is expected due to less pitching and less body-induced wheel load oscillations. The mean acceleration (which is proportional to the mean total braking force and thus the braking distance, referring eq. (1)) on varying road conditions and initial velocities is presented in Figure 8. Contrary to dry roads different damper settings do not change the mean deceleration on wet "German Autobahn" like roads significantly (α=5%). Due to smaller damper velocities, the damping forces on wet roads distinguish less. Thus the influence of different damper settings on the wheel load oscillations is reduced. On a wet rough road, the control strategy increases the mean deceleration and reduces the braking distance significantly. A reason for this effect could be greater road induced wheel load oscillations compared to the body induced wheel load oscillations. With higher damper velocities on rough roads, the effect of switching the damper from one setting to another generates more effect on wheel load and braking slip. For proving this hypothesis, more tests are necessary.

Influence of road roughness - Driving tests on roads with varying roughness reveal the relevant excitation frequencies and the influence of damping on the braking distance. On flat roads (very flat test track), it is expected that the wheel load is influenced by pitching primary and only secondary by the road excitation. The expectation is based on the small power of road excitation compared to body induced wheel load. The influence of road excitation is expected to rise with increased road roughness.

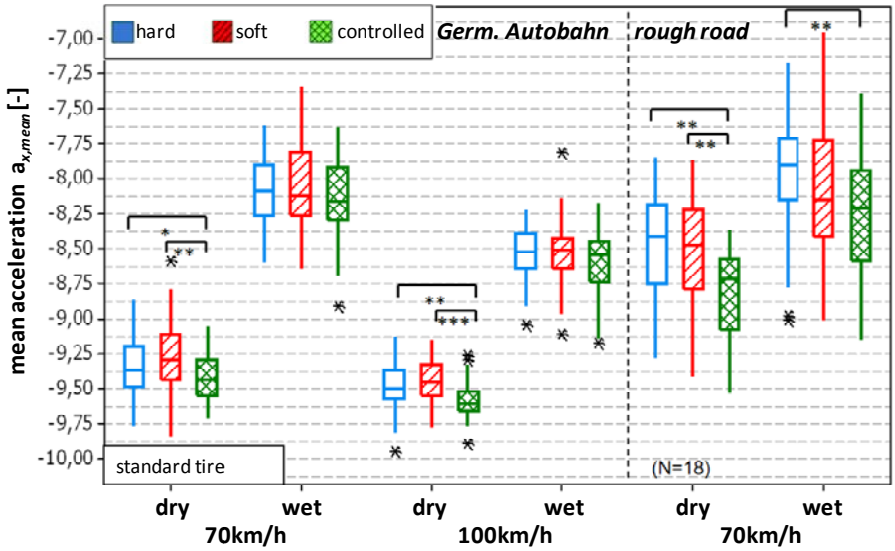

Figure 8. Variation of road conditions and initial velocities (significance levels: *(5%), **(1%), ***(0.1%))

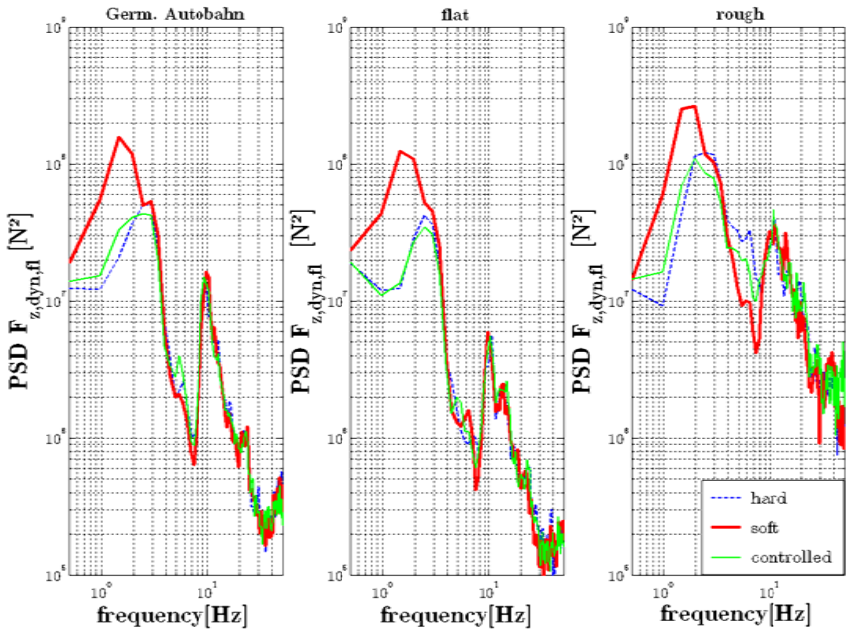

Figure 9. Mean Power Spectrum Density for the dynamic wheel load front left on varying road roughness and an initial velocity of $v_{x,0}$=70km/h

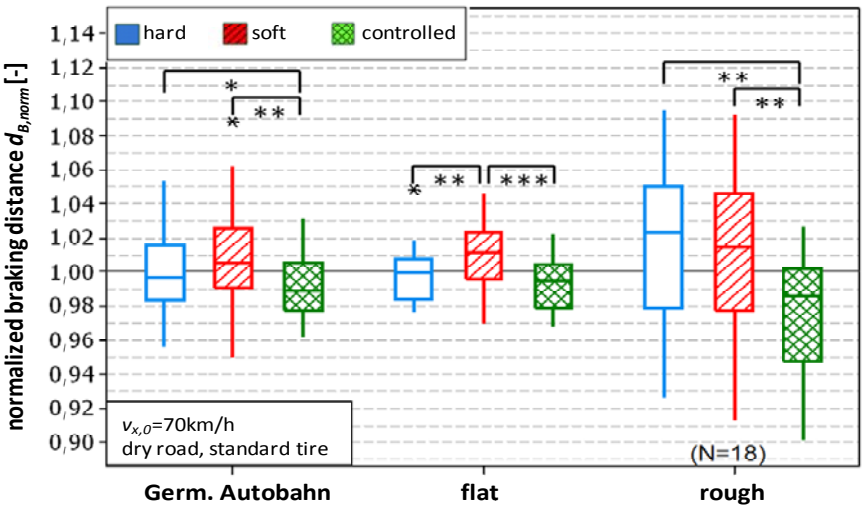

Figure 10. Variation of road unevenness (significance levels: *(5%), **(1%), ***(0.1%))

This effect is observed in the power spectral density of dynamic wheel load gained from the braking tests measured at the front left wheel, see Figure 9. As expected for the vibration characteristics the spectrum of 3-10 Hz between pitch eigenfrequency and vertical wheel eigenfrequency reveals greater wheel load oscillations with hard damping on rough roads than with soft damping. Next to the eigenfrequencies (especially pitch eigenfrequency at ~2-3 Hz), this behavior is quite contrary. The control strategy combines advantages of both damping characteristics: The wheel load oscillation in the spectrum of 3 – 10 Hz is reduced almost to the level of soft damping (see Figure 9 for rough roads). For flat roads the pitch eigenfrequency dominates the wheel load oscillation. For these roads the MiniMax control strategy produces the smallest wheel load oscillations. As a consequence, hard damping causes shorter braking distances on flat roads ("flat" and "German Autobahn") compared to soft damping (Figure 10). According to the power spectral density (Figure 9), the body-induced wheel load oscillation dominates on these roads. On rough roads, soft damping leads to shorter braking distances compared to hard damping.

In none of the test scenarios the mean braking distance with activated MiniMax damping is longer than with passive damping (on a level of significance of α=5%). On German Autobahn like roads and rough roads, controlled damping reduces the braking distance on a level of significance of α=5% (*) and α=1% (**) respectively, compared to the best passive damper setting. The results on German Autobahn affirm Niemz's results. MiniMax damping control reduces the mean braking distance by approx. 1%. On rough roads, the mean braking distance is reduced even by 3.5%. The control strategy solves the trade-off between hard and soft passive damper settings for different road roughnesses: hard damping for flat road surfaces, soft damping for rough roads. MiniMax control allows shortest braking distances and lowest standard deviations.

Interim Conclusion - Almost thousand braking tests analyzed with statistical methods show, that the semi-active damping control "MiniMax" can reduce the braking distance significantly, in a statistical manner. The performance depends on the conditions of the braking maneuver. With low friction and small body movements (due to pitching and lifting) the influence of damping on the longitudinal dynamics is small. On rough roads the trade-off between hard and soft damping with respect to the shortest braking distance is solved by MiniMax. Furthermore, the MiniMax controller reduces the mean braking distance by 3.5% compared to the best passive damping, which has been "soft" for these conditions. On a dry road with unevenness comparable to a German Autobahn, the MiniMax controller reduces the braking distance compared to best passive damping (hard), too. This holds true for an initial velocity of 70 and 100 km/h. Changing the standard tire (summer) to a winter tire (same dimension) has not changed the positive effect of the MiniMax controller on the braking distance.

In summary it is proven for several braking conditions that it is possible to improve the braking process if disturbances are minimized intra-system (refer to Figure 4).

2. Extended ABS-control using dynamic wheel load information

In a previous section it has been mentioned that taking into account additional information, e.g. the dynamic wheel load, lets expect an improved slip control (refer to Figure 4). For preliminary studies with adjusted ABS-control the answer of a simple question is aimed: How does the implementation of dynamic wheel load into ABS affects the quality of slip-control and the braking distance if the ABS control parameters are not adapted to this modification? In order to answer this question ABS is modified by adding the dynamic wheel load information to the wheel load information, which is estimated by the ABS already. A standard ABS estimates the wheel load (e.g. for the wheel front left "FL") by means of the longitudinal acceleration $\ddot{x}_V$ shown in eq. (18) (h_{CG}: center of gravity height, l: wheelbase; m_V: vehicle mass):

$$F_{z,\mathrm{ABS,standard,FL}} = F_{z,stat.,FL} - \frac{1}{2}\ddot{x}_V \cdot m_V \cdot \frac{h_{CG}}{l} \qquad (18)$$

The modified ABS uses the overall wheel load, which takes wheel load oscillation due to road excitation and due to the body movements as pitching and lifting into account as well:

$$F_{z,\mathrm{ABS,modified,FL}} = F_{z,\mathrm{ABS,standard,FL}} + F_{z,dyn.,FL} \qquad (19)$$

For ABS control wheel load and estimated friction define the optimal braking force operation point. The braking force operating point is an important quantity for ABS-control because it influences the amount of the caliper pressure and thus the amount of the braking torque strongly. If the operating point is chosen correctly in every braking situation, e.g. by a feed-forward-control, a slip controller would not be necessary. In previous industrial research with a BMW X5 (E70), the braking force operation point of the ABS has been adjusted continuously to the amount of weight transfer. As a result, the braking performance of this prototype ABS has been improved compared to the standard ABS.

Test vehicle and design - A BMW X5 (E70) with a programmable prototype ABS and CDC (Continuous Damping Control) is also used as test vehicle for this research. The ABS system, which only uses the weight transfer (eq.(18)) for adjusting

the braking force operation point, is used as reference for this research ("Reference-ABS").

The vehicle is equipped with a braking machine due to reproducibility reasons. The dynamic wheel load is measured front left by a measurement rim. The dynamic wheel load information for the left front wheel is copied to the signal for the front right wheel assuming that the dynamic wheel load is dominated by pitching and lifting instead of road excitations. For the rear axle, no dynamic wheel load information is used in ABS-control. However the pitching centre is close to the rear axle, it is expected that pitching influences the wheel load oscillations of the rear axle less compared to the front axle. The determination of the dynamic wheel load by the use of a measurement rim reduces the transferability to further prospective applications, because the dynamic wheel load would be estimated by vertical sensors in productions cars. For further research the dynamic wheel load will be estimated by information which are available due to the Continuous Damping Control. The dynamic wheel load information are transferred using the vehicle's chassis high-speed CAN. The braking tests were performed according to the described test design (refer to the beginning of this section), which means N=34 cyclical repetitions of each ABS-setting with an initial velocity of 70km/h. The production car's standard damping control has been used for these tests.

Results - The following section discusses the influence of adding dynamic wheel load information on the braking force operating point in addition to weight transfer (eq.(19)), which has been already implemented in the test vehicle's prototype ABS ("Reference ABS"). Apart from changing the wheel load calculation - in order to take oscillations due to pitching and lifting into account - the algorithms of the Reference-ABS have not been changed. However, for preliminary tests a very simple method has been chosen for orientation. Though, if this very simple method "adding the dynamic wheel load" already improves the braking process in terms of shorter braking distances it would be very easy to extend prospective standard ABS systems for productions cars if they were equipped with semi-active or active suspensions. The Reference-ABS includes a feed-forward control in order to increase the slip control dynamics if wheel loads change (wheel load is estimated by horizontal accelerations only). If wheel load changes the braking force operating point for this wheel is adjusted directly to those changes. However, dynamic wheel load oscillations due to pitching or lifting are not taken into account for standard ABS- and Reference-ABS-control currently. As a result, the braking force operating point is not adjusted directly by the feed-forward control and so the braking slip changes slowly and with a delay due to the low-pass filter characteristics of the integral (refer to equation (10)). The braking torque is not modified till then a difference between target slip and braking slip is detected. It is assumed that taking the dynamic wheel load into account for feed-forward control of the braking force operating point this will improve ABS-control due to more dynamics.

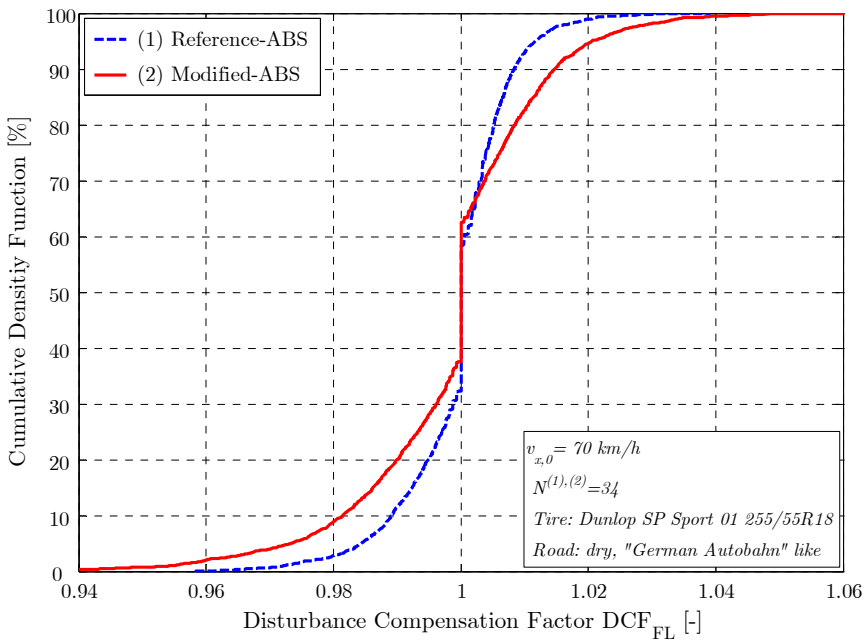

Figure 11. Deviations of the braking force operating point for Reference-ABS and Modified-ABS. The latter takes the dynamic wheel load into account

Taking a view on the results of the performed braking tests, the so called "Disturbance Compensation Factor" (*DCF*) is analyzed. This factor influence the braking force operating point: If the wheel load increase, the braking force operating point will be increased as well, i.e. *DCF*>1. Figure 11 shows the effect of the dynamic wheel load on *DCF*. Providing the dynamic wheel load in ABS-control this modifies the braking force operating point more compared to the Reference-ABS algorithm. This is shown by the cumulative density function which is obtained from all of the carried out measurements. It can be interpreted as follow: In 50 % of the time, the *DCF* equals one, which means that the mean braking force operating point is not adapted in total. Regarding the range of the distributed values, with Reference-ABS (no dynamic wheel load is taken into account) the braking force operating point is adjusted by max. ±4 %. Taking the dynamic wheel load for the feed-forward control of the braking force operating point into account, the range of the *DCF* is increased by ±2 % to ±6 % in total. This is because of the fact that wheel load oscillations due to pitching and lifting are now considered by ABS-control additionally. In summary, Figure 11 shows that the dynamic wheel load information takes effect on adjusting the braking force operating point - the range is increased by max. ±2%. Although the braking force operating point is more adjusted by the dynamic wheel load the demand is still unknown. The measurements in Figure 12 show that the amplitude of the dynamic wheel load oscillation is approx. 2000 N in its maximum. Taking into account that the weight transfer is approx. 3000 N this is a rather high amount of wheel load which is not considered in standard ABS- and Reference-ABS-control. Assuming that it is optimal to adjust the braking force operating point to the time course of wheel load, the demand on a Disturbance Compensation Factor can be calculated by

$$DCF_{opt} = \mu(\lambda_Z) \cdot \frac{F_{z,total,FL}}{F_{z,loadtransfer,FL} + F_{z,static,FL}} \qquad (20)$$

Figure 12 shows the plot for a braking test with modified ABS. The disturbance compensation factor takes the dynamic wheel load into account. However it adjusts the braking force operating point in a range of ±6 %, as described before. Regarding the assumed DCF_{opt} for $\mu = 1$ on dry roads (for this pavement and tire $\mu_{max} = 1.15$), Figure 12 shows a demand of up to -20 % to +10 %. So, the effect of the dynamic wheel load on adjusting the braking force operating point seems to be too small. The disturbance of wheel load oscillations due to pitching is much higher than expected from the ABS's feed-forward control. As a consequence, the feed-forward control of the Reference-ABS should be adapted for further research.

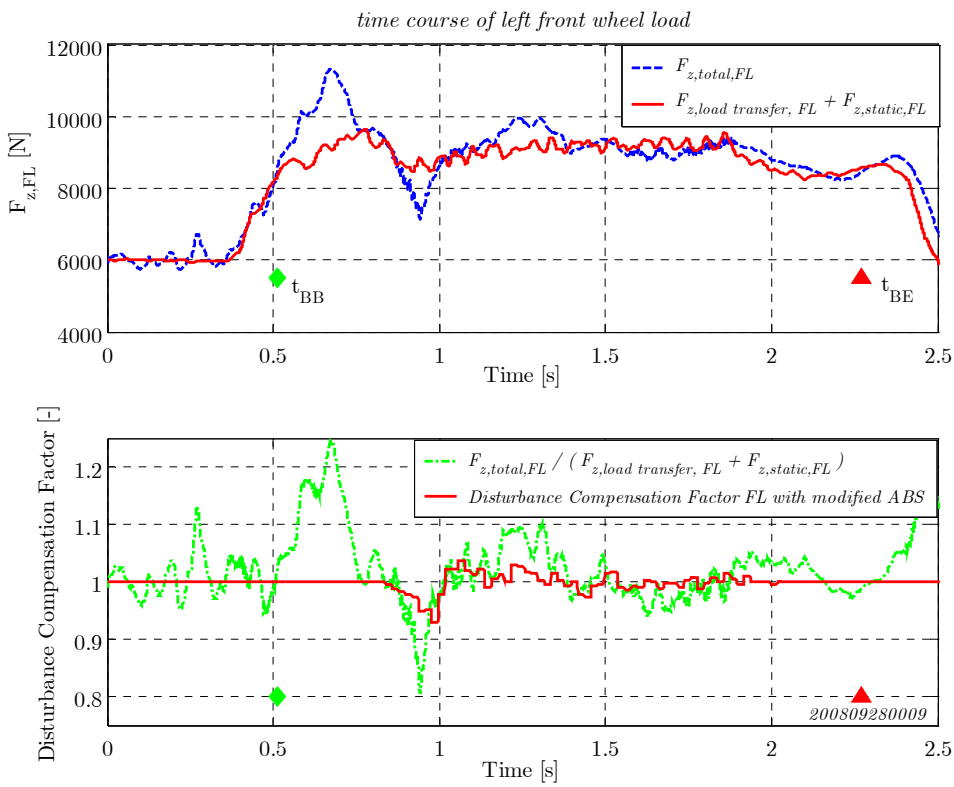

Figure 12. <u>top</u>: wheel load provided for standard and Reference-ABS (based on weight transfer only) and for Modified-ABS (total wheel load); <u>bottom</u>: available DCF vs. estimated demand

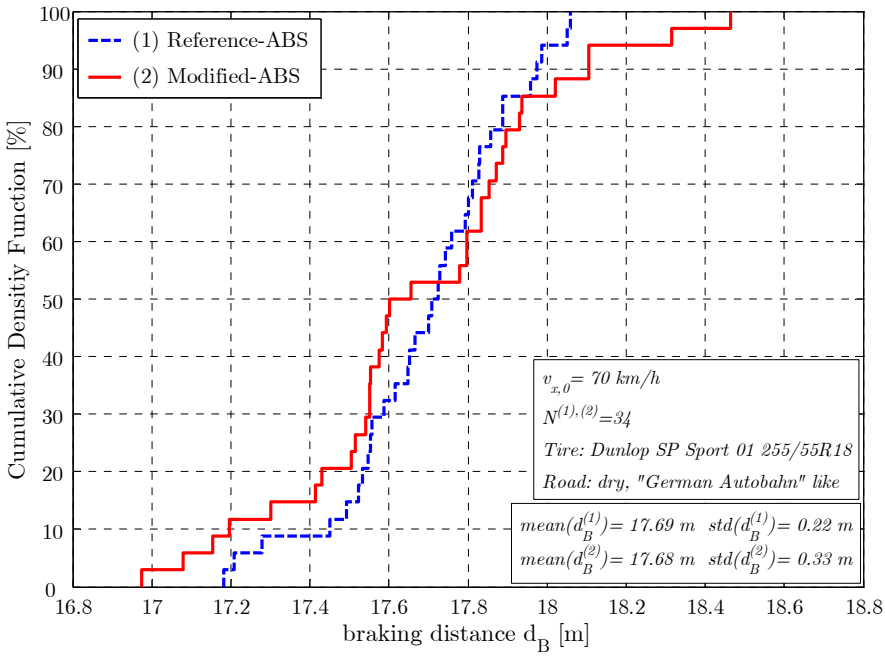

Figure 13. Braking distances, comparing Reference-ABS and Modified-ABS with dynamic wheel load

Looking at the measured braking distances no differences of the mean braking distance can be verified on a significance level of α=5%. It is checked with a t-test due to the normal distribution which is proven by a Lilliefors test. Figure 13 shows that the mean braking distances are similar. In addition the deviation of the braking distances with modified ABS increase which reduce the reproducibility of the braking procedure. Neither a positive nor a negative effect of the adjusted braking force operating point is proven statistically using both the feed-forward control of the Reference-ABS and the dynamic wheel load information. However it has to be considered that the dynamic wheel load has not influenced the braking force operating point only but other quantities as well during the tests. For one of these quantities, a strong negative influence of the dynamic wheel load is identified. With the available measurements, it cannot be excluded that an adjustment of the braking force operating point by adding the dynamic wheel load takes effect on the braking distance. Further braking tests are necessary to analyze the influence of dynamic wheel load on the braking force operating point and other quantities separately. It is estimated that adjusting the braking force operation point on the time course of dynamic wheel load allows shorter braking distances due to higher mean friction coefficients.

CONCLUSION AND OUTLOOK

Goal of this research project is the improvement of straight-line ABS-braking. The braking process is influenced by the vehicle's longitudinal and vertical behavior, or in more detail the braking torque and wheel load, mainly. Adjusting the braking torque and the wheel load by ABS and Continuous Damping Control (CDC), two actuating quantities which influence the braking process mainly can be modified.

Based on theoretical approaches, the paper presents several strategies which seem to have potential to improve the braking process. They can be separated in those which increase the mean braking force by a greater mean friction coefficient and those which modify the time course of the braking force. For both optimization objects, possible strategies derive from a methodical analysis. With semi-active or active suspensions the time course of wheel load and thus the braking force can be influenced temporarily. This topic will be investigated in further studies by use of Continuous Damping Control.

Regarding the objective of less slip oscillations, the paper presents results of the MiniMax damping control for various braking conditions and the results of a preliminary study which deals with the modulation of the ABS internal braking force operation point depending on dynamic wheel load information. The braking distances with different damper settings show that in combination with a standard ABS the MiniMax controller reduces the braking distance significantly adjusting the wheel in a special matter. Furthermore the results let expect less potential for improving the braking process by means of integrated ABS and CDC control on wet roads than on dry roads due to less wheel load oscillations on wet roads.

In a preliminary study the dynamic wheel load is taken into account for ABS-control of the front wheels. A measurement rim has been used for these tests. Further tests will be performed with estimated dynamic wheel load information, based on sensors

similar to those used with CDC. In summary, taking the dynamic wheel load into account for ABS-control does not yet reduce the braking distance significantly in these preliminary tests. However it has to be considered that the dynamic wheel load has adjusted not only the braking force operating point but influences also other ABS-modules. In one of these modules, the additional dynamic wheel load information has lead to a negative effect, which possibly affects the braking distance as well. In further braking tests, the dynamic wheel load will be taken into account in ABS-modules separately in order to identify the influence of each modified module on the braking distance.
Furthermore the transfer mechanisms of both the braking torque to braking force and the wheel load to braking force will be investigated with theoretical approaches and experiments. The knowledge of both transfer mechanisms is aspired in depth in order to allow an optimization of the braking process which is transferable to other applications and vehicles. Research is ongoing and results will be published in the future.

ACKNOWLEDGEMENTS

The authors would like to thank ZF Sachs AG and Robert Bosch GmbH for funding and supporting this research-project.

REFERENCES

[1] BECKER, A.; FOLCHERT, U.; KLUGE, S.; ET. AL.,: Integration von Fahrzeugkomponenten am Beispiel des verkürzten Anhaltewegs. Reifen Fahrwerk Fahrbahn. VDI-Verl., Düsseldorf, 2001, S. 466

[2] NIEMZ, T.: Reducing Braking Distance by Control of Active Dampers. VDI-Verlag, Düsseldorf, 2007

[3] REICHEL, J.: Untersuchungen zum Einfluss stufenlos verstellbarer Schwingungsdämpfer auf das instationäre Bremsen von Personenwagen. VDI-Verlag, Düsseldorf, 2003

[4] SEMMLER, S.; SCHWARZ, R.: ESP II – Der erste Schritt zum vollständig vernetzten Fahrwerk. 2004

[5] TRÄCHTLER, A.: Integrierte Fahrdynamikregelung mit ESP, aktiver Lenkung und aktivem Fahrwerk. *In: Automatisierungstechnik (at)* (2005)

[6] VENHOVENS, P. J. T.: Optimal Control of Vehicle Suspensions. Faculty of Mechanical Engineering and Marine Technology, Delft Univ. of Technology, 1993

[7] ZEGELAAR, P. W. A.: The dynamic response of tyres to brake torque variations and road unevennesses. Delft, Delft Univ. of Technology, 1997

AN ANALYSIS OF THE MECHANISM CAUSING LOSS OF CONTROL DURING A TIRE DELAMINATION

David Renfroe
Alex Roberts
The Engineering Institute
USA
Paper Number 09-0209

ABSTRACT

Electronic controls cannot always compensate for the destabilization of a poorly designed vehicle caused by tire delamination. Axle tramp caused from rubber strips on the track showed axle skate [1]. Further research, reported at ESV 2007 [2] demonstrated that lumps on a single rear tire caused 15+ degrees/g of oversteer.

The Engineering Institute has shown that the process of tire delamination causes some vehicles to become unstable at highway speeds. This was accomplished by actually preparing tires to partially delaminate while at 95 to 115 KPH on a remotely controlled vehicle. This testing demonstrated a severe loss of control as the tire was delaminating. The testing also showed that the predominate mechanism of control loss arises from the imbalance created during the delamination process.

A discussion of the testing illustrating accelerations on the rear axle as well as displacements of the shock absorbers will be used to illustrate the imbalance excitation and the tramping motion of the axle. Previous research indicated that the oversteer gradient during such an event to be between 15 and 20 degrees per g. This would then yield a critical speed of about 45 KPH. The testing illustrates how a vehicle loses control when the vehicle transitions from understeer to oversteer at highway speeds significantly above the critical speed from tire failure induced forces. Alternative suspensions were tested using the same simulated tire failure and illustrated how the vehicle stability is increased.

Using these results, a design criteria based upon a percentage of the critical rotational damping is proposed to control axle tramp from excitations at the harmonic frequency.

INTRODUCTION

Goodyear president John Polhemus has said, "[Tire] tread separation is the most common form of failure for all light commercial tires regardless of who manufactures them." [3] Complete loss of control of vehicles during testing has been demonstrated by Tandy [4] and Arndt [5] during tire delamination tests at highway speeds. In Florida (1993 – 2000) and in Texas (1994 – 1999) 220 and 550, respectively, fatal tire failure related rollovers in SUV's have been identified from databases maintained in the respective states. A report to NHTSA in June of 2001 identified significant differences between some SUV's with respect to others in their propensity to lose control and rollover from a tire failure based on those statistics [6]. This then brings up the question as to whether there is a design parameter that can be identified to increase the ability of drivers to maintain control of a vehicle in a tire failure situation, particularly a tire delamination.

Two mechanisms for loss of control during the tests in References 4 and 5 have been suggested. One suggested cause was that there was hard braking on the rear wheel that pulled the vehicle to the side due to tread interaction with the vehicle [4]. This is very unlikely since testing by Tandy, et al. (see figure 1) shows that the longitudinal forces caused by a braking effect of the delaminating tire is insufficient to cause such a course altering pull to the right [7]. The longitudinal force is varying from positive 1000 lbs to negative 1000 lbs. This would certainly shake the vehicle but not cause sufficient force on the right rear corner to pull the vehicle to the right.

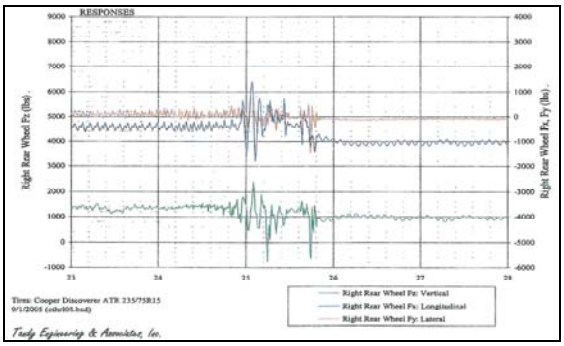

Figure 1. Wheel forces of delaminating tire. Test 41A [7]

A closer examination of the data presented in Figure 1 revealed that the forces being shown were not solely the result of a braking effect of the tire tread separation process. By zooming in on the data, it is seen that during the delamination, the peak of the longitudinal force corresponds to the neutral value of the vertical force, and vice versa. This is demonstrated in Figure 2 and indicates that the force values are more likely due to a rotating imbalance than a braking effect. The slopes of the neutral value lines are due to instrument drift. This is more evident in the vertical force plot. The vertical force begins at a neutral value of 6561 N (1475 lbs), which is consistent with the pre-test weights recorded. However, after the delamination, the neutral value is around 4448 N (1000 lbs).

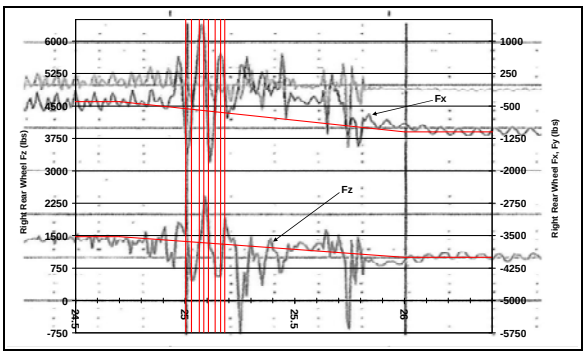

Figure 2: Zoomed view of Figure 1.

Gardner stated, "The results of the testing show that the forces developed during a tread belt detachment are well within the range of a driver's ability to control a vehicle [8]. Fay reported that while driving a Ford Taurus, "Little or no corrective steering action was needed to maintain control of the vehicle during the tread separation events [9]." Klein [10] stated that maintaining control of the vehicle after treadbelt separation required a steering torque similar to that required for a lane change maneuver. Were braking the causative factor of the loss of control, there would be no differentiation between vehicle brands and the propensity to lose control and rollover as was found in the Reference 5. Kramer [1] has determined that insufficient rotational damping can cause loss of control from rear axle tramp initiated by bumps to the wheel.

Based on Kramer's work, Renfroe [11] has proposed that the cause for the loss of control is rear axle tramp caused by the imbalance of the delaminating tire. Kramer, et al [1] found that the rear axles of Ford light trucks were susceptible to rear axle tramp and what he called "skate" between wheel bump impact frequencies of 10 to 15 hertz. "Skate" is a term used by Ford that describes an oversteer condition caused by rear axle tramp and the resulting reduction of lateral force capability of the rear tires. That skate tendency of certain Ford vehicles could account for the statistical difference between vehicle brands as seen in field data from Reference 5. From Figure 1 it can be seen that vertical forces on the order of 3558 to 4448 N (800 to 1000 lb) are occurring at a frequency of about 10 hertz, the rotational frequency of the wheel while traveling about 97 kph (60 mph) during the tire delamination process. Control was not lost in that test since delamination was over in 5 revolutions of the wheel or ½ of a second. In the test 2030 G [5] half of the tread remained attached through out the test and control was never regained even with a trained driver applying significant counter steer to the left. In Run 10 by Tandy [4], the delamination process lasted about 1.5 seconds and the vehicle traversed more than one lane to the right while significant counter-steer to the left was employed by a professional driver. When the tread finally released the vehicle responded to the steering input of the driver. In observing the video of Run 10, the wheels on both sides of the vehicle can be seen to alternately bounce. Alternating skipping tire marks from Arndt Run 2030 G can be seen on the pavement after the event indicating rear axle tramping while yawing. In testing of a Ford Excursion with ½ of the tire tread attached to the rear wheel conducted by the authors, control was lost and the vehicle veered across the track to the right. Alternating skipping marks were also seen on the pavement as a result of the tramping of the rear axle. This is shown in the figure below. Note in the figure, the left rear is the modified tire, yet distinct gaps are seen in the yaw marks of the right rear.

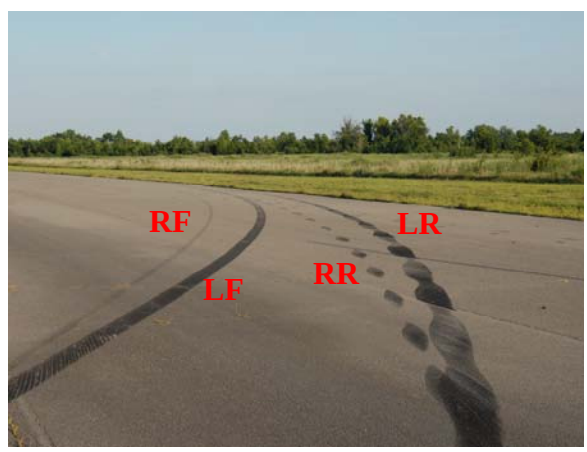

Figure 3. Photographs of tire marks from Excursion testing

Kramer found that control of the tramping motion can be accomplished by increasing the rotational damping of the rear axle. This could be

accomplished by stiffening the shock absorbers and/or moving them further outboard on the axle. Renfroe, et al [2, 11, 12] have validated Kramer's findings and quantified the magnitude of oversteer caused by the rear tramp and the effects of his alternative designs. This paper will suggest a rotational damping design criteria, a percentage of critical damping, for the solid rear axle whereby the designer may be assured that sufficient rotational damping is designed into the vehicle to maximize vehicle handling stability during a tire disablement or while traveling over rough roads.

First, a more complete discussion of the forces from the delaminating tire will be given and why they are being generated. This will be followed by a description of testing from many researchers using devices to generate rear axle tramp under various damping conditions. From that testing we will be able to determine the axle/spring system critical damping, and then calculate the actual rotational damping on the particular vehicle system. Knowing the control characteristics of the particular axle/shock system, correlation can be made between the percentage of critical rotational damping and the level of control.

FORCES GENERATED DURING A TIRE DELAMINATION

Forces on the wheel during a tire delamination are vertical and longitudinal in nature as shown in Figure 1. The longitudinal forces will be generated from the retardation of the rotation caused by impacts of the tire flap with the fender and other body parts while rotating resulting in wheel braking. The effects on the retardation of the vehicle cannot exceed the coefficient of friction of the tire interface with the pavement. That interface will most often be the steel belt on the carcass from the tire and the pavement. Previous studies have shown that the friction at that interface is around 50% of the normal friction between the tire and pavement [13]. This is consistent with what others have found in other studies, except for Reference 4. The premise for conducting that research was based in part on results reported in Reference 13 wherein they stated that longitudinal forces ranged between 361 and 1151 lb. Unfortunately, the authors of that paper later recanted their statement and said that the forces were ½ as large as previously stated [14]. Although the researchers in Reference 4 were able to achieve yaw effects similar to a rear tire delamination as shown in 2030 G, they could only do so by installing a racing tire on the single rear braked wheel. That tire, the G-Force Radial from Goodrich, was advertised as the stickiest road tire in the world developing a friction coefficient of 1.06. Also during their test where the similar yaw velocity occurred there was little or no counter steering. In Arndt's and Tandy's experiences, they steered up to 300 degrees opposite the direction of the yaw with no effect. Thus, consistent with the measured forces from a wheel force transducer and the experience of other researchers, the effect of the drag associated with the process of tire delamination is similar to a gust of wind and not from very large drag effects of the delaminating tire.

The cyclic vertical component of forces is generated due to the imbalance of the tire caused as sections of the tire tread are releasing. The tread flap and remaining tread cause significant imbalance in the tire and are experiencing 250 G's while turning at highway speeds. The magnitude of the vertical force will be affected by the weight of the attached tread and its radius from the axle, the weight of the detaching flap and the radius of the center of gravity of the flap from the center of rotation, and the rotational speed of the wheel. Testing reported by Arndt in Reference 15 illustrates how the response of the axle from a single tread section encompassing ½ of the tire causes a sudden growth in response as the harmonic frequency of the axle/tire-spring system are approached. However, instead of the response decreasing after the area of harmonic frequency is passed as the speed increases to 112 KPH (70 MPH), the response shows a slight decrease then continues to grow. This would be due to the increase in force from the dynamic imbalance increasing as a square of the velocity of the tire. As the high side of the harmonic frequency band is reached, the tire force has grown sufficiently to continue to drive the tramp motion of the axle. Thus for an under damped axle system cyclic tramping motion will continue beyond the band associated with the harmonic frequency, 10 to 15 hertz.

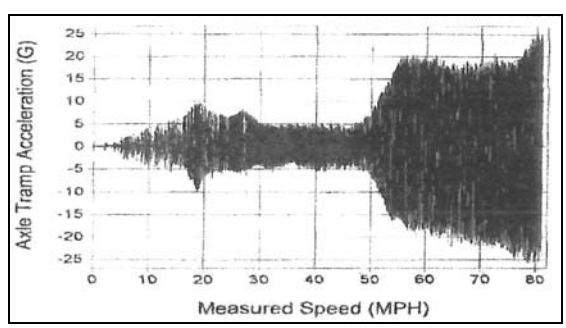

Figure 4. Axle motion from ½ of tread remaining on tire with a small step from tire carcass to the tread strip [15].

For example, a mere 15 cm (6 inch) section of tire tread weighs 1 kg (2.2 lb). At 80 kph (50 mph) this section of tire tread will generate 1.23 kN (277 lb) of cyclic force. At 112 kph (70 mph) that same piece of tread will generate 2.42 kN (544 lb). While the tire is delaminating the section of tread will begin as a 244 cm (8 foot) long section of rubber and steel and begin to decrease in size in an unpredictable manner throughout the process of delamination. Thus, there is significant potential for large cyclic forces on the order of 4478 N (1000 lb) to be generated during delamination. One mechanism suggested in the past for the generation of the large cyclic forces on the wheel was bumps created by the delaminating tire. Creation of bumps on the road and on the tire have been effective in the study of the axle motion and the effects on vehicle handling from a tramping axle [2, 11, 12]. That method has also allowed the quantitative study of the effects of various damping methods to control axle motion and thus vehicle handling through the application of quasi-static tests such as SAE J266. However, this study and others have clearly shown the actual mechanism of force generation during tire delamination is from the imbalance. The first clue was in observing both the 2030 G and Run 10. Both began with a severe loss of control when the tire began to separate at speeds above what would be considered the harmonic frequency of the system, indicating large driving forces to cause the tramping. When the vehicle begins to decelerate from 112+ KPH (70+ MPH) it immediately enters the harmonic range of axle oscillation that only makes control more difficult. Oscillation from imbalance was further illustrated in the study from Arndt [15]. The vehicle was placed on a chassis dynamometer with ½ of the tread attached to the tire, and a very small step at the front edge of the tread piece of only 5/8 of an inch. The data showed the effects of imbalance with increasing force from increasing speed, but there was no real second force occurring from the leading edge of the tire striking the roll. Then in a recent study by Pascarella [16] a single 15 cm (6”) long strip of rubber with a 3 cm (1.25”) step was vulcanized to a detreaded tire carcass similar to what was done by Renfroe, et al [2, 11, 12] and similar to the cross section of the rubber strip on the track utilized by Kramer [1]. He then drove the vehicle to 100 KPH (60+ MPH) and measured the response. What the data shows is that as the harmonic frequency of the axle is approached, the bump produces a significant vertical force pulse, but the imbalance also produces a vertical pulse that is increasing by the square of the speed. By the time the rotating tire system reaches the speed where the bump would cause a harmonic response, the imbalance is causing a vertical response as shown in Figure 5.

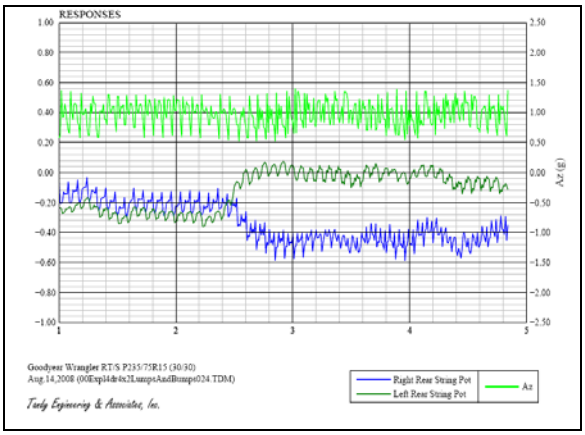

Figure 5. Motion from a single stepped lump vulcanized to the tire.

Thus, as the wheel approaches the harmonic rotational frequency, forces from the step of the rubber block occur, and simultaneously, imbalance forces begin to grow with increasing speed. As the rotational frequency approaches the harmonic frequency of the axle/spring system, the imbalance forces grow as a square of the rotational velocity approaching the same magnitude as that produced by the step. As is seen in Figure 5 at the harmonic rotational frequency of approximately 12 hertz the recorded motions show 24 hertz. The resulting motion of the axle is very small, 0.45 cm (0.18”) as measured at the shock absorber, and this vehicle remains stable as was demonstrated in the testing.

This conclusion was confirmed by testing performed for this study. Ninety degrees of the tread was removed, and ninety degrees was cut in from each side leaving a small amount bonded along the circumferential center. Figure 6 shows an actual delaminated tire at the scene of an accident and Figure 7 shows a tire prepared for the referenced testing. The step of the rubber on the leading edge of the attached tread was only 1.5 cm (5/8 “).

Figure 6: Photograph of an actual delaminated tire taken at the scene of an accident.

Figure 7. Picture of prepared tire.

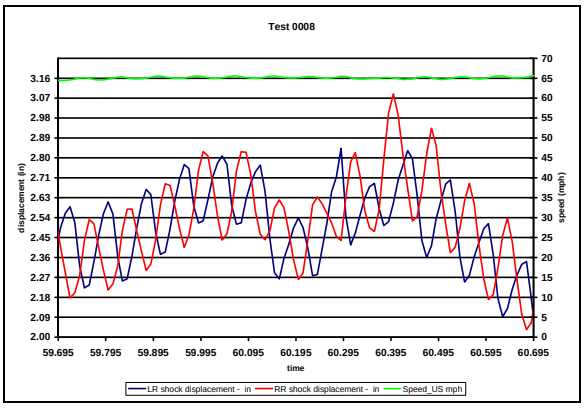

Figure 8. Axle motion for Test 0008 with ½ tread attached and 90 degree flap prepared to separate at speed. (RR Shock: blue; LR Shock: red; speed: green)

Figure 9: Screen capture shots from Test 0008 illustrating shock absorber motion.

When the vehicle was tested by driving it with a remote control up to 100+ KPH (60+ MPH) the axle began to tramp and control was lost as the tread separated. This motion is shown in Figures 8 and 9 and can be compared to the motion seen in testing with the single stepped block as illustrated in Figure 5.

First note how the axle motion is at the expected frequency of the rotation of the tire. Then note how the two sides of the axle are out of phase 180 degrees with similar vertical motions of the shock absorber of 1.0 cm (0.39”). In the video of the testing the tires can be seen having significantly more motion than 1 cm.

That is explained from the geometry of the suspension. With the shocks placed 77.5 cm (30.5”) apart and the track width being 148.5 cm (58.5”), the

motion at the tire is approximately double that of the shock. Also, the compliance in the bushing is about 3 mm (0.125") which will add more to the actual wheel motion. As the motion of the wheels is alternately bouncing on each side, control of the vehicles in these tests was lost in several cases. From Tandy's testing [7], vertical wheel motion of 3.6 cm (1.4 in) was recorded while the tire was delaminating. The motion in the tests where control was lost appears to be more.

Therefore, with a single force input at the frequency of the turning wheel at or above the natural frequency the axle tramps on each side and control can be lost. Whereas when there is a single stepped rubber block attached to the tire carcass the forces from the impact of the step in conjunction with the increasing forces from imbalance occur at twice the rotating frequency as highway speed approaches. Then there is insufficient time for the axle mass to react with an actual vertical motion. Therefore, there will be no tramp; and, therefore, no transition to oversteer and loss of control. So we conclude that the mechanism of force input to cause tramping and loss of control, as seen from 2030G and Run 10, is from tire imbalance occurring during the delamination process.

MANAGEMENT OF AXLE TRAMP THROUGH DESIGN

Kramer [1] noted in his study that "skate" can be controlled by increasing the axle tramp damping. This can be accomplished by increasing the stiffness of the shock absorber and/or by moving the shocks further apart. Renfroe, et al [2, 11, 12] measured the handling characteristics of a vehicle experiencing tramp excited by bumps on one rear tire causing force inputs at the axle harmonic frequency, and noted the effects of various shock absorber damping rates and placement on the understeer of the vehicle. As noted by Kramer [1] increased control occurred when the shocks were either stiffened and/or moved outboard. This is effectively increasing the rotational damping of the rear axle along the longitudinal axis or tramp mode.

Critical Damping of axle/spring system-In this section we derive the equations that define the rotational damping of the rear suspension of a vehicle and the critical damping. Then we will examine damping characteristics of various shock absorbers and look at the effects on handling that has been recorded. From these observations we will be able to look at the percentage of critical damping where control was maintained or lost or an understeer gradient was shown to be negative. From this limited set of data we can indicate the approximate value of the percentage of critical damping where control will be maintained under the conditions that would most likely cause axle tramp.

Critical damping is the damping at which a spring/mass system will return to equilibrium position in the least time. This particular system is for the rotational damping of the rear axle. The moment of inertia for the axle along a longitudinal axis with respect to the vehicle will be defined as I (length-force-time^2), rotational displacement will be θ, rotational damping coefficient will be C (length-force-time), and rotational stiffness K_{rot} (length-force/radians). The general equation of motion for the axle system is

$$I\ddot{\theta} + C\dot{\theta} + K_{rot}\ \theta = 0 \qquad (1)$$

Substituting $\theta = e^{\lambda t}$ and then divide by $e^{\lambda t}$ and I yields

$$\lambda^2 + \frac{C}{I}\lambda + \frac{K_{rot}}{I} = 0 \qquad (2)$$

Solving for the roots gives

$$\lambda = -\frac{C}{2I} \frac{+}{-} \sqrt{\left(\left(\frac{C}{2I}\right)^2 - \frac{K_{rot}}{I}\right)} \qquad (3)$$

Critical damping C_c occurs when the value under the radical is zero. Then

$$\left(\frac{C_c}{2I}\right)^2 - \left(\frac{K_{rot}}{I}\right) = 0 \qquad (4)$$

From equation 4 the critical damping is

$$C_c = 2I\sqrt{\frac{K_{rot}}{I}} \qquad (5)$$

Note that since the tires are the springs of this system, they can never go into tension. Thus there are two conditions of vibration, (1) where the tires never leave the ground and (2) where one tire is in the air and one is on the ground. For the purposes of this discussion, the idea of the critical damping is merely to characterize the system and to use a percentage of the system characterization to quantify the damping needed to manage the tramping rear axle and maintain control of the vehicle. Therefore, when speaking of critical damping we will be considering the first condition where both tires are on the ground.

Shock absorber damping-The damping considered in the equations is a linear function of a force generated by the shock being moved at a certain velocity. Actual shock absorbers usually have a preloaded force from a gas charge in the shock and the design of the valves in the shocks can allow it to have a non-linear response to the velocity of the shock. During the tramping of an axle, testing has measured displacements of 12.5 mm (0.5 in) and velocities in the 25 cm/s (10 in/s) range. Therefore, to characterize the shock absorbers used in these tests and to compare their relative effects the force versus velocity used will be that recorded at 34 cm/s (13.35 in/s). This was a standard recorded velocity and force measurement for the equipment being used and is the approximate velocity of the shock absorber while the axle is tramping in the harmonic range.

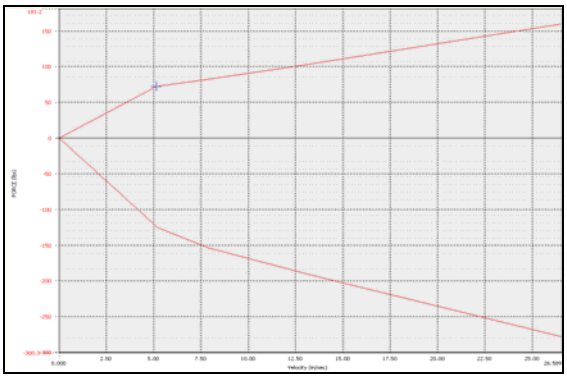

Figure 10. Typical Shock Curve Showing Force vs. Absolute Velocity

Vehicle testing and analysis-Over 50 different vehicle – shock absorber tests were conducted to determine the vehicle longitudinal stability. There were both circle tests with a lumped tire to input vertical forces at the harmonic frequency at low speeds, and straight line high speed tests with simulated delaminating tires to investigate controllability at highway speeds with vertical forces generated at and above the harmonic frequency. There were two general results, instability or stability. In the circle test instability was measured by recording a negative understeer. In the straight line high speeds instability was illustrated by the loss of control.

Appendix A is a tabular summary of those tests showing stable and unstable vehicle configurations and the associated percent of critical damping. In the cases where instability in both test conditions, low speed circle and high speed straight line driving, occurred the rotational damping of the axle was only 6% of critical. Maintenance of control was obtained in all instances for the high speed tests with the simulated delaminating tire when the rotational damping was 20% of critical. In the circle tests with the vertical forces cycling at the harmonic frequency with lateral accelerations at 0.2 – 0.3 g's stability was maintained with rotational damping of 31% of critical. This high percentage of critical damping was generated with a softer shock than the stable high speed example but with a wider spacing. As was discussed by Kramer, the spacing of the shock is the most effective method of increasing the rotational damping, since the rotational damping increases as a square of the spacing between the shocks. Also, by spacing the shock absorbers further outboard, there is increased motion in the shock which will minimize the effects of the undamped rubber bushings of the shock mounting.

CONCLUSIONS

In conclusion, it has been found that the destabilizing forces generated during the delamination of a tire will be from the imbalance of the tire due to the section of tread remaining on the tire. Until the tire is clear of tread there will remain the propensity to tramp if it is rotating at or above the harmonic frequency of between 10 and 15 hertz.

Secondly, increasing the percentage of critical damping of the axle/tire system to at least 20% appears to assure stability during tire delaminations at highway speeds. Added stability and a less harsh ride can be accomplished by moving the shock absorber outboard. Increasing the shock spacing will allow the shock to be softer while actually increasing the rotational damping of the system and thus allowing even greater control of the vehicle.

ACKNOWLEDGEMENTS

We would like to thank Tandy Engineering and Carr Engineering for their testing which provided some of the data for this study.

REFERENCES

1. Kramer, Kenneth D., Janitor, William A., and Bradley, Lawrence R., "Optimized Dampening to Control Rear End Breakaway in Light Trucks," SAE 962225, October 1996.
2. Renfroe, D.A., and H. A. Roberts and D. Beltran. "Effects of the Process of Rear Tire Delamination on Vehicle Stability." Paper Number 07-0142. ESV Conference. Lyon, France. June 2007.

3. Letter to Goodyear customers from John C. Polhemus, President, Goodyear North American Tire, 10/27/2000.
4. Tandy D. F., et al., “An analysis of Yaw Inducing Drag Forces Imparted During Tire Tread Belt Detachments,” SAE, 2007-01-0836, 2007.
5. Arndt, S. M., Arndt, M. W., “The influence of a Rear Tire Tread Separation on a Vehicle’s Stability and Control,” Proceedings of the 17th International Technical Conference on the Enhanced Safety of Vehicles, Amsterdam, The Netherlands, June 4-7, 2001.
6. Lampe, John, “Testimony of John Lampe, Chief Executive Officer, Bridgestone/Firestone, Inc., Before the Subcommittee on Commerce, Trade and Consumer Protection and the Subcommittee on Oversight and Investigations House Committee on Energy and Commerce,” June 19, 2001.
7. Tandy, Don, “Steering and Handling Evaluation With Tire Disablement and Wheel Force Transducers,” Unpublished Testing #41A, August 30-31, 2005 and September 1, 2005.
8. Gardner, “The Role of Tread Belt Detachment In Accident Causation,” ITEC 1998, Paper 27A, (1998).
9. Fay, Richard, et al., "Drag and Steering Effect from Tire Tread Belt Separation and Loss," SAE 1999-01-0447, 1999.
10. Klein, E. Z., "Anatomy of Accidents Following Tire Disablements," SAE 1999-01-0446, 1999.
11. Ipser, J., Renfroe, D. A., and Roberts, H. A., “Solid Axle Tramp Response Near the Natural Frequency and its Effect on Vehicle Longitudinal Stability.” Paper Number 2008-01-0583. SAE Conference. Detroit, MI. April 2008.
12. Renfroe, D.A., Roberts, H. A., “Designing for Vehicle Stability During Rear Tire Tread Separation Events”, ASME International Mechanical Engineering Congress and Exposition, Chicago, IL, November 5-10, 2006.
13. Arndt, M. W., Rosenfield, M. J., Arndt, S. M., and Stevens, D. C., “Force Response During Tire Tread Detachment Event,” SAE Paper 2004-01-1075, SAE International Congress. March 2004.
14. Arndt, Mark, Letter to SAE, referencing SAE Paper 04AC-57 Force Response During Tire Tread Detachment Event, July 27, 2007.
15. Arndt, Mark W., Rosenfield, Michael, Arndt, Stephen M., “Measurement of Changes to Vehicle Handling Due to Tread-Separation-Induced Axle Tramp,” SAE International Congress and Exposition, SAE 2006-01-1680, 2006.
16. Pascarella, R. et al., “Evaluation of Vehicle Performance with 1-Hump ‘Lumpy’ Tire and on Test Surface with Rubber Strips,” Tandy Engineering, August 13 & 14, 2008.
17. Dixon, John C., “Tires, Suspension, and Handling,” 2nd ed., SAE, Warrendale, PA., 1996.

Appendix A: Testing Details and Percent of Critical Damping for Each

Table 1.
Summary of Tests Relied Upon

Test Vehicle	Test Type	Shock Absorbers	Shock Placement	Compression Damping Force @ 13.2-13.3 in/s	Effective Comp Damping Due to Shock Angle	Rebound Damping Force @ 13.2-13.3 in/s	Effective Reb Damping Due to Shock Angle	Test Termination Condition	% Of Critical Damping
1994 Ford Explorer, 2dr, 2WD	Circle w/ lumps (CCW)	88134	Standard	103.6	91.2	191.8	168.8	OS	6
1995 Ford Explorer, 4dr, 4WD	Circle w/ lumps (CW)	Rancho RS9000X, Setting 5"	Outboard	189.0	189.0	468.0	468.0	US	31
1995 Ford Explorer, 4dr, 4WD	Straight line simulated delamination	New Monroe replacement shocks	Standard	81.5	71.7	229.1	201.6	Tramp/loss of control. Flap began to come unbonded around the mid-50s. Tramp then loss of control around 67 mph.	6
1995 Ford Explorer, 4dr, 4WD	Straight line simulated delamination	737971	Standard	199.7	175.7	805.8	709.1	Vehicle controllable throughout. 63 mph top speed. Some vertical motion seen on RR.	20

ESC STANDARD FITMENT AND FAILURE TO PROTECT YOUNG DRIVERS

Alix Weekes, Matthew Avery
Thatcham
United Kingdom

Richard Frampton, Pete Thomas
Loughborough University
United Kingdom

Paper Number 09-0278

ABSTRACT

The objective of the paper is to estimate UK fleet penetration of stability controlled vehicles, and casualty reduction, particularly for younger drivers. Two models (timeline 2003-2030) were developed for predicting UK fleet ESC penetration, one for Availability of ESC, and one for new car Registrations with ESC. Availability of standard ESC fitment increased from 40-53% from 2006-2008, whilst new car registrations increased from 20-56% from 2003-2008. EC regulation requires ESC new car penetration by 2014, and the models were modified to reflect this requirement. The models therefore project complete standard fitment in new cars by 2014, and full car stock penetration by 2021. The projections also reveal that another 3 million more new cars purchased without ESC in the interim from 2009 before ESC becomes mandatory in 2014, and these cannot be retro-fitted with ESC so represent a missed opportunity for casualty reduction. ESC casualty reduction was calculated using recent effectiveness values from UK studies based on a case control method and induced exposure. With full fleet penetration in 2021 ESC is projected to prevent 9,587 casualties annually including 382 fatalities, with £764 million savings (compared to no ESC). ESC effectiveness estimates reveal that ESC could be effective in reducing 14% of injury crashes for young drivers. These young drivers commonly drive small used cars with ESC rarely fitted. Since full fleet penetration could take 12 years, faster ESC introduction into smaller cars is needed for casualty reduction amongst younger drivers who represent 30% serious injuries & fatalities. Providing ESC on smaller cars so that younger drivers are protected equates to savings of £227 million and 2,844 casualties annually.

INTRODUCTION

Electronic Stability Control (ESC) is an important safety technology that is capable of preventing vehicles skidding or spinning out of control. ESC was first developed by Bosch in 1995, and the first manufacturer to fit ESC was Mercedes-Benz. The system compares a driver's steering wheel commands to the actual behaviour of the vehicle (direction of travel).When the sensors (lateral acceleration and yaw) indicate the vehicle is leaving the intended line of travel, ESC applies the brake pressure needed at each individual wheel to bring the vehicle back to the intended course. Some ESC systems also reduce the engine torque. ESC systems may differ in their response, with some programmed to intervene sooner and take away more driver control of speed than others. The driver is not normally aware of the operation of ESC. ESC is intended to be applied mostly in bends where the driver may lose control of the vehicle. Loss of control is likely when the driver is attempting to steer whilst the vehicle is skidding, or the driver enters a bend too quickly without applying the brakes (understeer). The vehicle may leave the road, sometimes rolling over, or it may collide with other vehicles. ESC can also help in oversteer situations, for example if you swerve to avoid an obstacle, oversteer can occur making the vehicle turn more than intended, ultimately spinning. The rear of the car might skid out and turn the car in the same direction as the intended steered direction, but at a faster rate and not under the control of the driver. ESC can prevent this by braking individual wheels to maintain control.

There is much research establishing the benefit of ESC for preventing crashes. Several authors have analysed the crash rates of cars equipped with ESC to compare with non-ESC vehicles [1,2,3,4,5,6,7,8,9,10]. These studies have covered a wide range of countries, road types and surfaces, weather conditions, crash types and severities. All of these studies conclude that ESC has a positive effect on reducing crashes, although there is a large variation in the level of the effectiveness. In a UK based study in 2007 Frampton and Thomas [10] established that ESC effectiveness is 7% in crashes of all severity. Serious crashes are 11% lower compared to non ESC cars and fatalities 25% lower. The potential savings in accident costs for a 100% take up of ESC amounts to some £959

million pounds annually by preventing some 7,800 crashes [10].

Since 2006 Thatcham has been publishing fitment information about the availability of ESC in new cars sold in the UK. This paper uses this fitment data to estimate the penetration of stability controlled vehicles into the UK car fleet over the next two decades. Combining this model of standard ESC penetration with the previous estimates from Frampton and Thomas [10] the paper also provides a new estimate of the effect of actual fleet penetration on casualty number and the severities over the time period. Additionally the paper will estimate the effect of ESC introduction on casualty rate for younger drivers given that they predominantly use older smaller vehicles.

ESC FITMENT RATINGS

Evidence from real world studies shows the effectiveness of ESC, so there is a need to promote fitment of ESC systems. In 2006 Thatcham began to publish ESC fitment ratings [11]. The ESC ratings are a form of public information to help guide new car buyers in their next car choice.

The ESC fitment ratings use a simple system associating colours with availability of ESC. Green indicates standard fitment, Yellow indicates optional fitment where the buyer will have to specify ESC on the order and pay extra when purchasing a new car, and Red indicates that ESC is not available at all. The rating is given as a coloured bar, with proportional areas of red, yellow and green, according to the availability of ESC for a particular car model. Only new passenger cars are rated, and the ratings are updated on an annual basis each summer. Car manufacturers sell their cars with ESC, but under different names such as ESP, DSC, VSA etc. Therefore alongside the ESC ratings bars the name of the ESC system for that particular manufacturer is also given to inform the new car buyer of the name of the system on the particular car they are buying.

The fitment information is gathered from publically available information from car manufacturers, so it directly represents the information on ESC fitment that an average new car buyer might receive in the real world. Data sources include price lists and brochures published by the vehicle manufacturers that include the derivative line up and the detailed specifications of ESC fitment for each vehicle model. The data is downloaded from websites as webpages, or PDF files, or sometimes requested as hardcopy in the post if electronic versions are not available.

The goals of the rating system are to raise awareness of ESC and increase sales of cars fitted with ESC. Also, the ESC ratings will encourage vehicle manufacturers to increase the availability of ESC as standard fit. Optional fitment is a useful step toward increasing ESC fitment in cars on the road, although it is not as effective as standard fitment. Take up of ESC as an option is low since buyers are not aware of the system, nor of its importance. According to manufacturer reports, take up of an ESC option is around 1% or less from new cars sold. Therefore, for increasing fitment of ESC in cars on the road, standard fitment is the most effective option since optional take up is so low. The ideal situation would be for every car sold to have 100% standard fitment – so the ratings would all be solid green bars. Standard fitment of ESC means that all car occupants will be protected by the system without having to select it or pay for it as an option.

Following Thatcham's work on the fitment ratings, Euro NCAP decided to introduce a similar scheme in order to promote ESC fitment throughout the EU. The data covers the 27 EU member states. Euro NCAP first published fitment ratings in 2007 [12], and has also updated the ratings in 2008.

Example ESC Rating: Volkswagen Polo

The Polo is a supermini car sold by Volkswagen. In August 2008 [13] there were 8 trim levels available. In total there were 32 variants (engine/gearbox/trim combinations) of Polo available. There were three trims (Dune, Bluemotion, and Bluemotion 2) where ESC was not available, which is 6 variants in total (19%). ESC was fitted as standard on the GTi trim level, which has 2 variants (6%). On the remaining 4 trim levels ESC was fitted only as an option on new car orders, and this represents 24 variants in total (75%). The cost of ESC as an option was £445 during 2008, and it is sold as Electronic Stability Program (ESP) by Volkswagen. So overall the ESC fitment on the VW Polo has the following proportions, in Table 1:

Table 1.
ESC availability on VW Polo for Summer 2008 - proportions for generation of ESC rating bar

ESC fitment	Variants	Percentage	Rating colour
Not available	6	19%	RED
Optional fit	24	75%	YELLOW
Standard fit	2	6%	GREEN

These percentages of availability for ESC are then used to generate the proportions of the colours in the rating bar for the VW Polo [13], as shown in Figure 1:

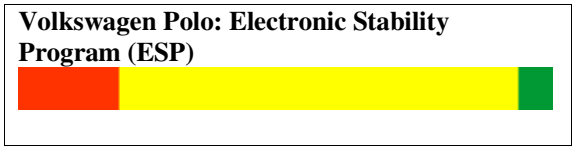

Figure 1. ESC rating for Volkswagen Polo (2008)

ESC Fitment Ratings for 2006 to 2008

ESC ratings have been generated for all new cars on sale in the UK during 2006 [11], 2007 [14], and 2008 [13]. One measure of ESC fitment rates that can be quantified is the number of models on sale with 100% standard fitment (solid green bars) as a proportion of the total models on sale; termed the "percentage of standard fit models". In 2006 the percentage of standard fit models was 40% i.e. 40% of models had 100% standard ESC fitment. In 2007 this rose to 47%, and by summer 2008 percentage of standard fit models had reached 53%. The progression over the years 2006 to 2008 for percentage of standard fit models is summarised below in Figure 2:

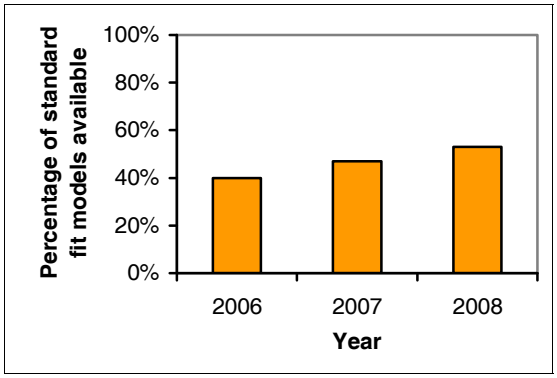

Figure 2. Percentage of standard fit models available for sale in the UK for 2006 to 2008.

MODEL OF ESC STANDARD FITMENT PENETRATION ON NEW CARS

Using the fitment information available it is possible to develop models of how ESC is penetrating the market within the UK. Two different models are developed based on two data sources. The first model uses the fitment ratings from Thatcham describing the availability of ESC on new cars. The second model uses new vehicle registration data from Bosch.

ESC Availability Model

The Thatcham ratings describe the availability of ESC in new cars as standard fitment. Using the data from Figure 2 the average increase in the percentage of standard fit models is 6.5%. This rate of increase is projected forward based on the assumption that the increase will remain at 6.5%, and this is modelled in Figure 3 up to the year 2030.

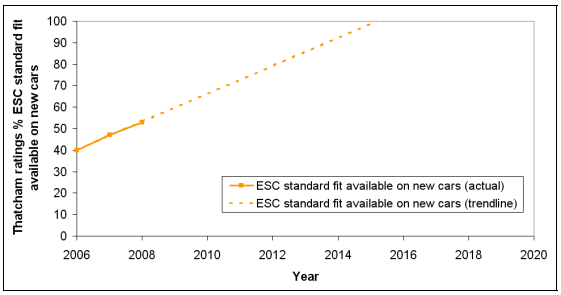

Figure 3. Model of ESC standard fitment availability 2006-2030 (data source: Thatcham ESC fitment ratings)

This model of ESC standard fitment availability reveals that it will take until 2016 before all new cars sold in the UK have ESC fitted as standard.

ESC Registrations Model

An alternative model uses data from Robert Bosch for the percentage fitment of ESC in new car registrations [15], which is data gathered by the agency R.L.Polk & Co for nine European countries including the UK. This data has been published from 2003 to date, and is shown in Figure 4.

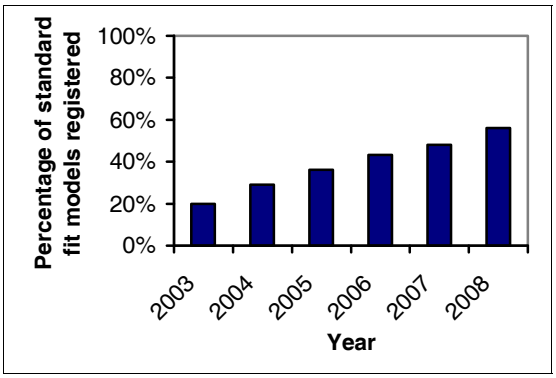

Figure 4. Percentage of standard fit models registered in the UK for 2003 to 2008.

Using the data from Bosch in Figure 4 the average increase in percentage of standard fit models is 6.97%. Based on the assumption that the increase will remain at 6.97% this rate of increase is projected forward to 2030, and this is modelled in Figure 5.

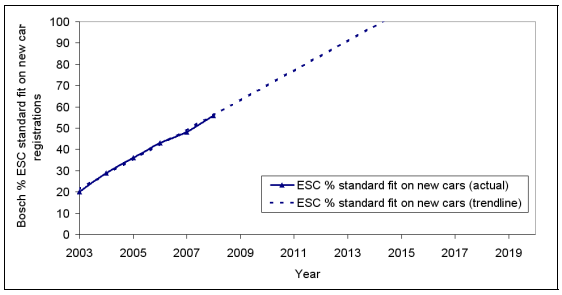

Figure 5. Model of ESC standard fitment registrations 2003-2030 (data source: Bosch new car registrations).

This model of ESC fitment registrations reveals that it will take until 2015 before all new cars sold in the UK have ESC fitted as standard.

Comparison of Availability and Registrations Models

The Availability and Registrations models are based on two different data sources, and are consequently slightly different. The Availability model uses Thatcham fitment ratings data [11,13,14], and the Registrations model uses new car registrations data from Bosch [15]. However both models make similar predictions for when 100% penetration of ESC standard fitment on new cars will be reached. The Availability model predicts 100% penetration by 2016, and the Registrations model by 2015. Since there is only one year difference as shown in Figure 6 it can be concluded that these models are in close agreement.

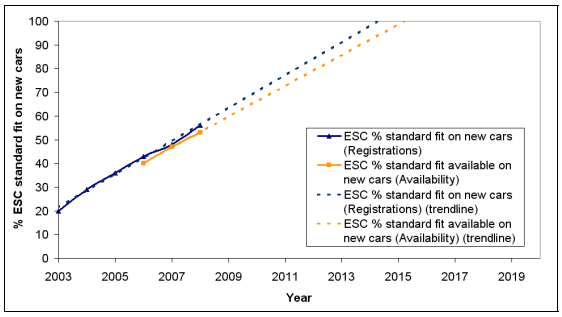

Figure 6. Comparison between Availability and Registrations models for new car penetration of ESC standard fitment.

Model of ESC standard fitment penetration on vehicle stock

Annually there are around 2,500,000 new cars sold in the UK [16]. Using this data on new car sales the proportion of new cars sold fitted with ESC can be calculated using the percentages from both the Availability and Registrations models. This is then used to find the proportion of cars fitted with ESC within the entire vehicle stock. Based on vehicle licensing data from the UK Department for Transport [17] the vehicle stock data is shown in Figure 7. The vehicle stock is currently approximately 28,000,000 cars, and this is also projected forward until the year 2030.

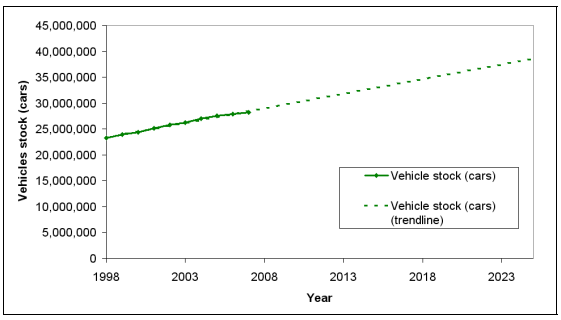

Figure 7. Vehicle stock on UK roads (1998-2030).

The proportion of ESC equipped cars in the vehicle stock is then calculated as the proportion of new ESC equipped cars entering the fleet each year cumulatively. This is modelled from 2005 to 2030. This model reveals that 100% penetration of ESC into the vehicle stock will be achieved in 2021 according to both the Availability and Registrations models. There is a close agreement between these two models, as shown in Figure 8.

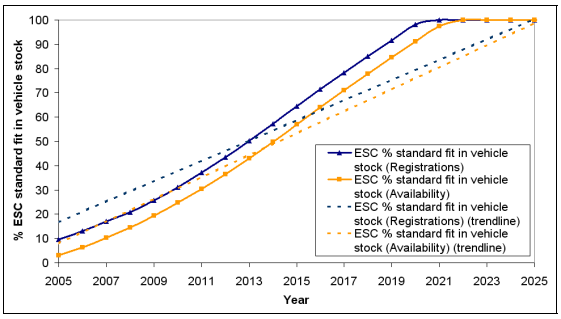

Figure 8. ESC penetration into UK vehicle stock: Availability model compared to Registrations model.

The Availability and Registrations models of ESC standard fitment into new cars and into the vehicle stock are based on two different data sources. However there is a close agreement between the two models with only one year difference between them for full fleet penetration. Since there is a close agreement it can be concluded that the estimate for 2016 for new car fleet penetration and 2021 for vehicle stock penetration is a reasonable estimate. Vehicle licensing statistics show that in the period 1998-2007 the average age of cars on the road was 6.6 years, which corresponds to the last cars registered in 2014 without ESC being taken off the road by 2021.

ESC Regulation and Vehicle Stock Penetration

On 10 March 2009, Members of the European Parliament voted for a compulsory introduction of ESC in all new types of vehicles from 1 November 2011, and for all new vehicles from 1 November 2014. This will have some impact upon the fitment of ESC in the vehicle stock. The Availability and Registrations models have been re-generated, but with fitment projections following the pattern required in order to meet the regulatory requirement of full penetration of new car sales by 2014. These models are shown in Figure 9.

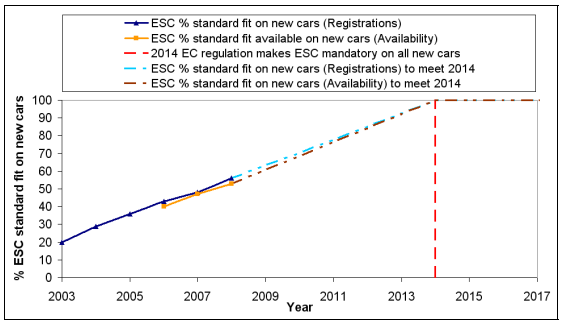

Figure 9. Availability and Registrations models for new car penetration of ESC standard fitment in order to meet EC regulatory requirement of standard fit by 2014.

This model indicates that there is a gap between the current market rate of ESC penetration (Figure 6) into the new car market, and the fitment rate required in order to meet the regulatory requirement in 2014 (Figure 9). Current market penetration rates will achieve new car fleet penetration by 2016, but it is required by the EC regulation by 2014. For some vehicle manufacturers this will simply mean providing ESC as standard, instead of as an option or being unavailable on some trim levels. For example the VW Polo in Figure 1 indicates that ESC is available on most trims, so the system need only be produced and sold as standard in order to meet the regulation. However for other manufacturers such as Proton this regulation for ESC will mean a substantial task since no Proton models in the UK are currently sold with ESC systems available at all [13].

The revised vehicle stock penetration, based on the models in Figure 9 to meet the requirement for standard fitment by 2014, therefore reveals that full stock penetration of ESC equipped cars will be achieved by 2021, as shown in Figure 10.

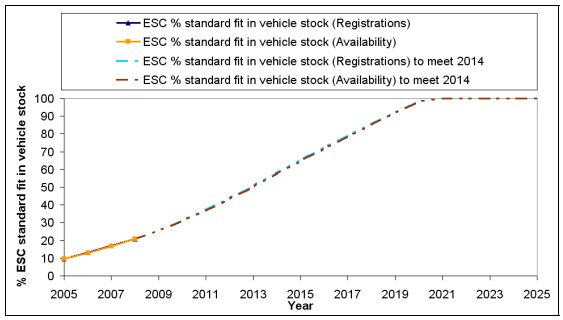

Figure 10. Availability and Registrations models of ESC penetration into the UK vehicle stock, with regulatory requirement for standard fitment of ESC by 2014 met.

In the period from 2009 before full stock penetration of ESC is reached another 3 million cars will be purchased as new without ESC fitted. ESC cannot be retro-fitted so all of these cars remain on the roads without this important safety technology.

This model (Figure 10) is used to generate estimates of casualty and cost savings offered by the standard fitment of ESC in accordance with the EC regulation by 2014.

CASUALTY AND COST SAVINGS FOR ESC

Using the ESC fitment and penetration models, it is possible to estimate the casualty and financial savings that can be projected when these models are combined with the true casualty numbers of occupants in cars. Like many other countries the UK has declining numbers of traffic casualties. Table 2 shows the average annual reduction since the current baseline values of the 1994-8 average. The reduction for all casualty severities is 1.2% annually, and the fatal casualty numbers have reduced by a mean of 0.5% each year.

Table 2.
Mean annual casualty reduction over 1994-8 baseline.

Total car occupants	1994-8 average	2005	Mean annual decline from 1996
Killed	1,762	1,675	0.5%
Serious	21,492	12,942	4.0%
Slight	180,034	163,685	0.9%

The most conservative estimate for fleet penetration is given by the Availability Model with a slightly slower fitment of ESC than in the Registrations model, so this Availability model is used to generate the casualty and cost reduction afforded by ESC. When the existing casualty

reduction rates are combined with the increasing fleet penetration of ESC equipped cars from the Availability model, estimates can be made for the reduction in total casualties due to the increasing ESC numbers in the fleet. These casualty and cost savings are shown in Figure 11, and this also shows the financial savings based on the standard UK model using willingness to pay methods [18].

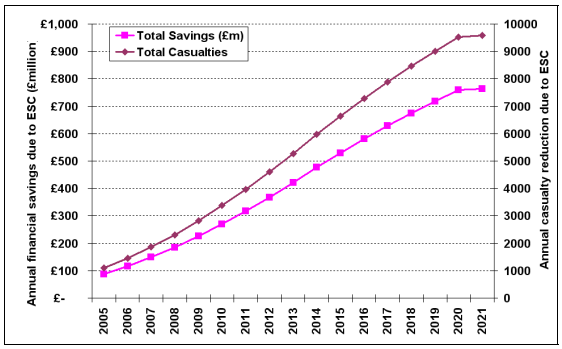

Figure 11. Annual casualty and financial savings with ESC.

By 2021 when full fleet penetration is achieved ESC systems are projected to be reducing total casualties by 9,587 each year, compared to the baseline of no ESC in the fleet. This includes 382 fatalities. Taking account of the different costs for each severity level, the value of these savings, equal £764 million (€1.1 billion) each year (at 2005 prices).

Table 3 shows the projected numbers of each injury category in 2010 and 2021 when all cars in the fleet are expected to be equipped with ESC for the two groups.

Table 3.
Casualty Reduction Projections.

	Total without further ESC		
Year	Slight	Serious	Fatal
2010	156451	10553	1634
2021	141640	6735	1546

	Reduction with ESC		
Year	Slight	Serious	Fatal
2010	2906	343	125
2021	8498	707	382

Comparing the estimates for ESC fleet penetration using these new models and the original model from Frampton and Thomas [10] also reveals similarities. The casualty and cost savings achieve similar levels, although over a slightly longer timescale taking approximately three years longer to reach the same level of savings. Furthermore the costs are based on data from 2005 so are probably underestimated, which might bring the estimates back to a similar time scale to the original.

EFFECTIVENESS OF ESC FOR YOUNGER DRIVERS

Over 3,000 car drivers aged under 25 are killed or seriously injured on Britain's roads each year [19]. A young driver is more than 2.5 times as likely to be involved in a crash as a mature driver [20]. Young drivers are more likely to be involved in single vehicle accidents involving loss of control, excess speed for conditions, and accidents on all-purpose single carriageway rural roads [20]. These are all the types of crashes where ESC is likely to be effective.

The effectiveness of ESC for young drivers (aged 25 and under) compared to mature drivers (aged over 25) has been calculated using the same method as in the previous study by Frampton and Thomas [10]. The analysis used a case-control method based on the induced exposure method [21]. Case vehicles were defined as those known to be equipped with ESC. A comparable group of control vehicles not fitted with ESC were also defined, and these were generally the previous version of a case vehicle. There were 10,475 case vehicles and 41,656 control vehicles in the dataset. The case control method also required vehicle manoeuvres to be separated into those where ESC may have an effect and those where no ESC effect is assumed. Table 4 shows the numbers of matched cases used to calculate effectiveness estimates.

Table 4.
Numbers of Cases used to Calculate Overall Effectiveness

Crash Severity	ESC Cars N	Non ESC Cars N
All Injuries	10,475	41,656
Fatal	110	491
Serious	846	3,564
Slight	9,519	37,601

ESC Effectiveness Estimates: Comparison of Young and Mature Drivers

Effectiveness estimates are calculated for drivers aged 25 years and younger, compared to drivers aged over 25 years. Driver age was known in 93% of cases. Figure 12 shows the distribution of young driver crashes compared to mature driver crashes. Crashes involving young drivers are in the minority at 13%.

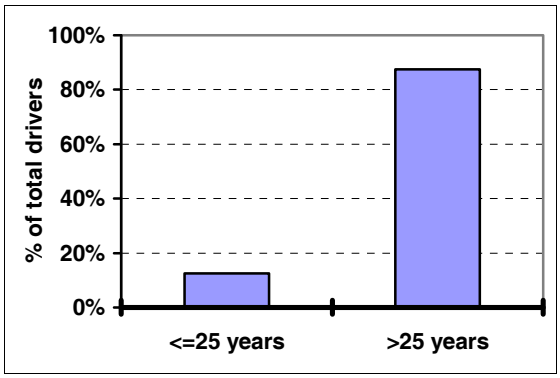

Figure 12. Numbers of Vehicles Involved in Crash.

Figure 13 shows effectiveness rates for cars equipped with ESC in young driver crashes. The best estimates are shown for different injury severity levels together with 95% confidence limits. Overall effectiveness for younger drivers is 14% dropping to 12% for slight crashes. For all fatalities and serious injuries (KSI) the effectiveness for younger drivers is estimated as 16%, which is greater than the effectiveness for all ages (12%) previously published [10]. ESC is shown to be more effective in reducing KSI for younger drivers than all drivers on the road.

Considering all injury levels (KSI and slight injuries), the overall effectiveness for all ages was 7% as previously published by Frampton and Thomas [10]. The overall effectiveness of ESC in reducing all injuries for young drivers is shown to be double (14%).

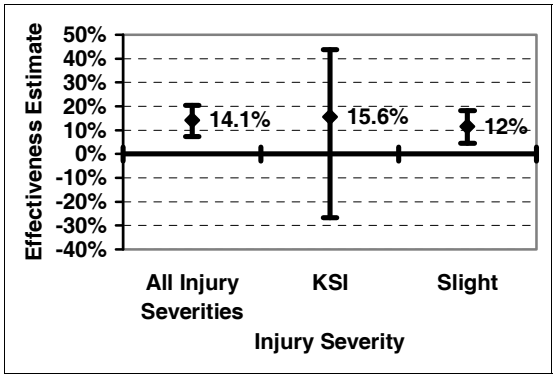

Figure 13. ESC reduction for young drivers.

Cost and Casualty Savings for Young Drivers

Young drivers account for 30% of car drivers killed or seriously injured on roads in the UK [22]. Applying this proportion to the casualty and cost savings reveals that when full fleet penetration is achieved by 2021 ESC systems are projected to be reducing total casualties by 2,844 each year for younger drivers, compared to the baseline of no ESC in the fleet. This includes 114 fatalities. The value of these savings, equal £227 million (€320 million) each year. These savings in casualties and costs are compared to the total annual savings in below in Table 5:

Table 5.
Summary of casualty and cost savings: total compared to young drivers.

	Young drivers	Total
Casualty reduction	2,844	9,587
Fatalities	114	382
Value of savings	£227 million (€320 million)	£764 million (€1.1 billion)

UK ESC Fitments in Young Drivers' Supermini Cars

Examining the ESC fitment ratings for 2008 reveals that only 5 models out of 47 supermini cars (11%) have ESC fitted as standard. Since younger drivers most commonly drive small cars this is a very small choice for the drivers who could benefit most from ESC technology. These models are relatively expensive within the supermini segment, most being priced from £12,000. The Suzuki Splash is cheapest from £9,000, but this is still expensive for a young driver.

Young drivers most commonly drive a second hand, older car. It will take a long time before ESC is available in the small used car market, which makes it extremely difficult for young people to drive cars fitted with this important safety system. The small car market is increasing, with new car sales data from SMMT indicating that the mini and supermini segments combined have increased their market share from 26% to 33% in the last decade [16]. Younger drivers are most likely to buy a second hand small car, but other drivers also buy these small cars – for example as a second car within the household. Given current economic and environmental concerns, households are potentially more likely to purchase a smaller car, and so small car sales are likely to continue to increase. With so few of the small cars fitted with ESC as standard, most of these cars will be entering the market without ESC, which is an opportunity missed in terms of safety provision. Small cars are still being brought to market without ESC fitted as standard. For example the latest Ford Ka launched in January 2009 in the UK only has ESC fitted as an option across the range, not fitted as standard. The small car segment has the largest gap in fitment to fill. In order to ensure that all drivers are protected by ESC it should be fitted as standard on all vehicles regardless of size. Results suggest that it would be most effective to introduce ESC into smaller cars

first in order to address the casualty rates amongst younger drivers.

LIMITATIONS

Both the Availability and Registrations models for standard ESC penetration are based upon the assumption that ESC standard fitment will increase in a linear manner, which may not be accurate. However the data does indicate a linear progression up to 2008.

Neither the ESC availability ratings from Thatcham, nor the ESC new car registrations from Bosch can indicate how many ESC equipped cars have actually been sold in the UK historically in the period before these fitment and registrations data were collected. The model of ESC cars in the vehicle stock therefore has to be assumed to follow the backward projection of the Availability and Registrations models.

A limitation of these models is the assumption that 100% standard fitment ESC throughout the entire vehicle stock can be achieved. In reality, there are likely to always be a small number of cars on the road that do not have ESC, for example classic cars and imported cars. However the models do provide an estimate of ESC penetration for the majority of passengers in the UK.

The model of new cars sales and vehicle stock is based on data up to 2008. Given the economic recession, it is evident that car sales are reducing during 2009. The effect might be to overestimate car sales, and therefore overestimate the benefit to be derived from ESC. However as ESC systems are sold in increasingly greater numbers of car models as the deadline for mandatory fitment in 2014 approaches, the unit costs for ESC systems will reduce. This will likely reduce the price of ESC as an option, and hence improve the take up of ESC as an option, which could mean the calculations of casualty and cost reductions are underestimated.

There are a number of factors to consider when interpreting the results of the effectiveness estimates for young drivers. The Great Britain national casualty data used in this analysis provides one of the largest samples of ESC equipped cars studied to date but further methodological procedures may be required to fully isolate the crash reduction benefits of the system.

The case-control method compares ESC and non-ESC cars in total and hence compares all the differences between these groups. It has been hypothesized that since all ESC cars have ABS systems, the differences in crash involvement could be due to ABS not ESC. However previous studies of ABS systems have shown the effects of ABS to be small [23,24], and most of the non-ESC cars in this study would also have been fitted with ABS.

The part played in injury reduction due to improvements in passive safety of the cars is also important to consider. There may have been further vehicle improvements introduced at the same time as ESC systems. Whilst vehicle safety improvements are unlikely to change driver behaviour, they would change injury outcomes. It was not possible to quantify the effects of passive safety improvements in this study, but the results are considered to be a measure of improvements in handling performance – mostly ESC.

In making the comparisons every effort was made to compare cars that were as similar as possible so that the major difference was ESC fitment. However it is possible that a few were mis-classified, although Kreiss et al [25] stated the effect will be to consistently underestimate the effects of ESC, so these study results can be viewed as conservative. Crashes involving vulnerable road users were excluded from this analysis because the effect on ESC effectiveness rates would have however been marginal [10].

The cost savings are based on the cost per casualty in 2005, where costs would be expected to raise meaning cost calculations are probably an underestimate.

CONCLUSION

Standard ESC fitment will reach 100% by 2014, as per the EC regulatory requirement. However current market rates indicate that fleet penetration of ESC in new cars will not be reached until 2016, revealing a gap in provision that vehicle manufacturers will have to fill. Full vehicle stock penetration will be achieved by 2021 according to the models. Projections also reveal that another 3 million cars will be purchased without ESC in the interim between 2009 and 2014 when it becomes mandatory. This means that the opportunity to reduce casualties is being missed. Earlier standard fitment of ESC could annually save £764 million and 9,587 casualties.

A previous study has shown that ESC effectiveness is 7% in crashes of all severity [10]. ESC appears to offer additional benefit for young drivers. Overall effectiveness was estimated as 14% for young drivers. For KSI the effectiveness for young drivers is 16%, and for slight injuries the effectiveness is 12%. For all these estimates, ESC effectiveness is around double the previously published overall effectiveness of 7% for all ages and all injury severities.

Young drivers commonly drive small used cars with ESC rarely fitted. Since full fleet penetration could take 12 years, faster ESC introduction into smaller cars is needed for casualty reduction amongst younger drivers where it will be most effective. These young drivers represent 30% of serious injuries and fatalities, equating to savings of £227 million and 2,844 casualties annually. With current economic and environmental concerns the small car market is likely to increase, so fitment of ESC as standard in small cars is key to increasing stock penetration of ESC.

There are many factors that can influence the rate of ESC fitment, including the national economy. In these current times of recession new car sales and second-hand cars are dropping. With decreased turnover in the vehicle stock, and people potentially keeping their vehicles for longer, full fleet penetration of ESC equipped cars may be limited. In these circumstances public awareness of ESC must be the focus, so that car buyers make an informed safety choice. Fitment ratings information published by Thatcham is useful tool for raising public awareness of the importance of ESC.

REFERENCES

[1] Aga, M. and Okada, A. (2003). Analysis of vehicle stability control (VSC)s effectiveness from accident data. 18th International Technical Conference on the Enhanced Safety of Vehicles (ESV), Nagoya, Japan, 541.

[2] Becker, H., Zobel, R., Donner, E. and Graab, B. (2003). Großzahlenmaterial, "In-Depth" Erhebungen und Einzelfallanalyse, Werkzeuge zur Verbesserung der Fahrzeugsicherheit im Volkswagenkonzern (Large number material, indepth studies and single case analysis – tools for improvement of vehicle safety at Volkswagen Group). Tagung: Verkehrssicherheit interdisziplinär. Dresdner. 27th - 28th June.

[3] Dang, J.N. (2004). Preliminary results analyzing the effectiveness of Electronic Stability Control (ESC) systems. Washington DC, National Highway Traffic Safety Administration. DOT HS 809 790. September 2004.

[4] Farmer, C.M. (2004). "Effect of Electronic Stability Control on automobile crash risk." Traffic Injury Prevention **5**:317-325.

[5] Langweider, K., Gwehenberger, J., Hummel, T. and Bende, J. (2003). Benefit potential of ESP in real accident situations involving cars and trucks. 18th International Technical Conference on the Enhanced Safety of Vehicles (ESV), Nagoya, Japan, 150.

[6] Sferco, R., Page, Y., Le Coz, J.-Y. and Fay, P.A. (2001). Potential effectiveness of Electronic Stability Programs (ESP) - What European field studies tell us. 17th International Technical Conference on the Enhanced Safety of Vehicles (ESV), Washington DC, 2001-S2-O-327.

[7] Thomas, P. (2006). "Crash involvement risks of cars with electronic stability control systems in Great Britain." International Journal of Vehicle Safety **1** (4):267-281.

[8] Thomas, P. and Frampton, R. (2007). Real-World Assessment of Relative Crash Involvement Rates of Cars Equipped with Electronic Stability Control. 20th International Technical Conference on the Enhanced Safety of Vehicles Conference (ESV), Lyon, France, 07-0184.

[9] Tingvall, C., Krafft, M., Kullgren, A. and Lie, A. (2004). "The effectiveness of ESP (Electronic Stability Programme) in reducing real life accidents." Traffic Injury Prevention **5**:37-41.

[10] Frampton, R. and Thomas, P. (2007). Effectiveness of Electronic Stability Control Systems in Great Britain. On behalf of the Department for Transport. Loughborough, Vehicle Safety Research Centre, Loughborough University. 15th March. http://www.dft.gov.uk/pgr/roads/vehicles/vssafety/safetyresearch/esc.

[11] Thatcham; the Motor Insurance Repair Research Centre (2006). Three letters to save your life - ESC, Thatcham MIRRC. August 2006.

[12] Euro Ncap (2007). Euro NCAP Recommends ESC. Brussels, Euro NCAP. 8th May.

[13] Thatcham; the Motor Insurance Repair Research Centre (2008). "Young drivers at risk in cars without ESC." Thatcham Research News **3** (8), August 2008.

[14] Thatcham; the Motor Insurance Repair Research Centre (2007). "New data shows that ESC technology could help reduce UK road deaths by 25%." Thatcham Research News **2** (7), July 2008.

[15] Robert Bosch Ltd (2009). ESP Installation Rate Europe by new car registration. Stuttgart, Robert Bosch Ltd. 4th March.

[16] Society of Motor Manufacturers and Traders (2008). Motor Industry Facts 2008. London, Society of Motor Manufacturers and Traders.

[17] Department for Transport (2007). Table 1: Motor vehicles licensed by body type: 1998-2007. Vehicle licensing statistics: 2007. London, Department for Transport. 8th May. http://www.dft.gov.uk/pgr/statistics/datatablespublications/vehicles/licensing/vehiclelicensingstatistics2007.

[18] Department for Transport (2007). Highways Economics note No 1. 2005 Valuation of the Benefits of Prevention of Road Accidents and Casualties. London, UK Department for Transport.

[19] Royal Society for the Prevention of Accidents (Rospa) (2008). Young Drivers. Birmingham, Royal Society for the Prevention of Accidents (RoSPA). http://www.rospa.com/roadsafety/info/youngdrivers.pdf.

[20] Clarke, D.D., Ward, P. and Truman, W. (2002). In-depth accident causation study of young drivers. Prepared for Road Safety Division, Department for Transport, Local Government and the Regions. Crowthorne, Transport Research Laboratory. TRL542.

[21] Evans, L. (1986). "Double paired comparison – a new method to determine how occupant characteristics affect fatality risk in traffic crashes." Crash Analysis and Prevention **18** (3):217–227.

[22] Department for Transport (2008). Table 7c All casualties: killed or seriously injured: by road user type and age: 1994-98 average, 2000 - 2007. Road Casualties Great Britain: 2007. London, Department for Transport. 25th September. http://www.dft.gov.uk/pgr/statistics/datatablespublications/accidents/casualtiesgbar/roadcasualtiesgreatbritain20071.

[23] Evans, L. (1998). Antilock Brake Systems and Risk of Different Types of Crashes in Traffic. 16th International Technical Conference on the Enhanced Safety of Vehicles (ESV), Windsor, Ontario, 98-S2-O-12.

[24] Broughton, J. and Baughan, C. (2002). "The effectiveness of antilock braking systems in reducing accidents in Great Britain." Accident Analysis and Prevention **34**:347-355.

[25] Kreiss, J.-P., Schüler, L. and Langwieder, K. (2005). The Effectiveness of Primary Safety Features in Passenger Cars in Germany. 19th International Technical Conference on the Enhanced Safety of Vehicles (ESV), Washington DC, 05-0145.

STUDTY OF BODY CONFIGURATION AND SUPERIOR OCCUPANT PROTECTION DURING ROLLOVER

Toshiaki Sakurai
Department of Mechanical Engineering, Iwaki Meisei University, Japan
ESV PaperNumber:09-0284

ABSTRACT

This paper describes reconstructions of rollovers involved in the initial velocity before accidents are very important and the body structures of automotive vehicles with some curved configurations that have the incontestable superiority for occupant protection in rollover accidents over plain square body structures. The oval configuration and the curved structure are recommended. Furthermore, in a rotational movement system, acceleration force, inertia force and rotational moment of the vehicle to dummy should be considered as input forces.

INTRIDUCTION

Researching the safer body structures for occupant protection during rollovers, main analyses are performed as indicated below:

1. Introducing the accident data reported by the Institute for Traffic Accident Research and Data Analysis in Japan regarding rollovers.
2. Discussing the deformation of body structures and the conditions of contact areas between the roof and the loading panel after testing according to the FMVSS No.216.
3. Considering occupant behavior in the cabin based on not only the equation of inertial motion but also the equation of motion including the Coriolis' force and the force of inertia.
4. Researching the influence of the initial distance between the occupant's heads and the roofs of vehicles before accidents, and the occupant survival space after accidents.

INTRODUCING ACCIDENTS DATA [1]

The accident data reported by the Institute for Traffic Accident Research and Data Analysis [ITARDA] in Japan regarding rollovers are introduced. The data was taken during 10 years from 1993 to 2003 in the Tsukuba area located north of Tokyo.

Results classified all the accidents into a single accident and a mutual accident of auto vehicles with four wheels.

The total numbers of accidents were 1965. Rollover accidents are about eleven (11) % among the total accidents. They also classified the trigger of rollover into three categories:

/From side slip to rollover
/Instability after riding on the banks
/Dropping

They reported on the velocity of vehicles before accidents of drivers that did not use the brakes. The rate of accidents in the higher velocity shows the high scores compared with the lower velocity. Also the rate of accidents of rollovers on highways is higher than that of standard roads.

The rate of rollover accidents of classified vehicles is shown in **Figure 1**. Light vehicles, sports utility vehicles (SUV) and cargo trucks occupied higher averages. The unbelted passengers face more danger compared with the belted passengers. Research was conducted to determine the impact point of the head to the car body of passengers not using seatbelts. They showed that the necks of passengers made contact with the roof interior during rollovers. There is no information of the relationship between roof strength and occupant injury.

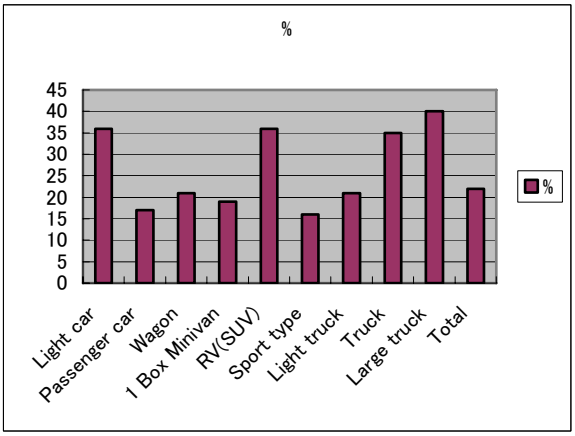

Figure 1. The relation of the rate of rollover accidents of classified vehicles

Investigation of the accident cases reconstructed with real accidents.

Case 1:

On a highway road, a belted driver turned the steering wheeled sharply when the vehicle encountered a strong side wind. The vehicle slipped to the side and after the vehicle rolled over with one turn. Two unbelted occupants seated in the rear seats were ejected and one suffered a fatal injury.

Recently, all passengers including rear occupants are required to fasten the seat belt in Japan and it is assumed that the ejections from vehicles will reduce during rollovers.

It is important in the actual accidents that the processes to rollover are clarified by considering the reconstruction.

FMVSS216, DROP TEST AND RAMP ROLLOVER TEST BY SAKURAI [2]

In 1991, T. Sakurai published a paper with tests results according to FMVSS 216, dummy drop test and ramp rollover test.

Figure 2 shows the schematic drawing of the body structures after tests carried out according to FMVSS216.

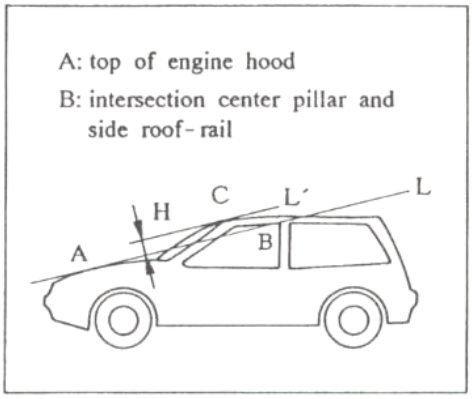

Figure 2. The schematic drawing of the body structures after tests according to FMVSS 216

In **Figure 2**, the line HL' shows the base line of the load plate and point C indicates the first contact point with the loading plate and the body structure before testing according to FMVSS 216. The line AL shows schematically the line of collapse of the body after testing. Point A indicates the position of the top of the engine hood and point B the intersection of the center pillar and the side roof rail.

We would like to design a body configuration along the Lines with the final body configuration after testing. Because of the curved roof configuration, contact areas are wider compared to the plain square ones as described later. As a result, the stress level becomes lower.

We performed the drop test with the inverted Hybrid Ⅲ dummy whole body drops and the ramp rollover tests. The relationship between the initial height of the drop tests and ramp rollover tests and the neck loads is shown in **Figure 3.**

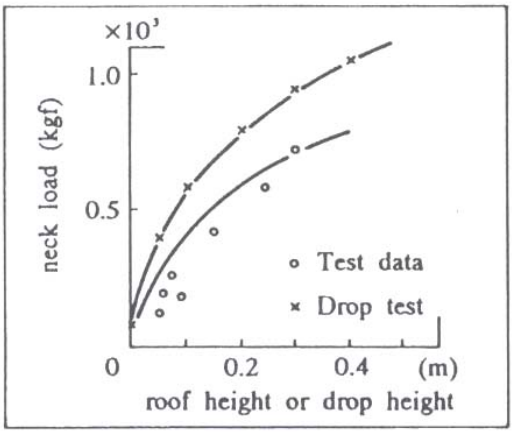

Figure 3. The relation between dummy neck load and the height of drop tests and the ramp rollover test.

As shown in **Figure 3**, the higher the height, the more the neck loads. Comparison of the loads, the loads of the ramp tests are lower to the drop test. The reasons why lower values are considered is that in the ramp rollover test dummy neck loads would be applied to not only the axial load but also bending load or twist loads.

The ramp rollover tests were performed.

Figure 4 shows the relationship between the neck load, roof deformation and time history.

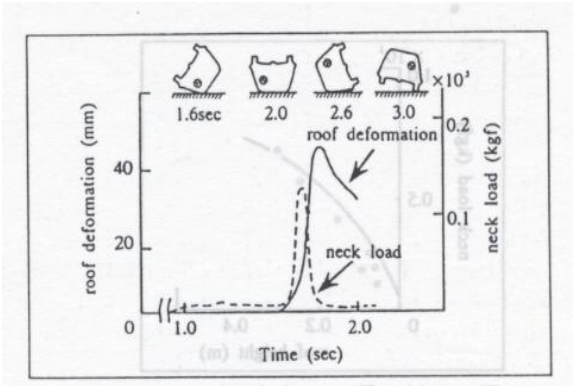

Figure 4 The relationship between the neck load, roof deformation and time history.

First, the neck would contact the side roof rail, and then the position of the roof located at the conjunction of the side and front roof rails and front pillar are formed and reaches the maximum roof deformation. When the maximum load of the dummy neck occurred, the roof deformation would still be deformed at the position less than 10mm. Important to note is that the dummy head and the deformed roof do not contact at the time of the roof's forming.

Here, summarized data referring the dolly test [3] is shown, **Figure 5** indicates the time, the neck load, and roof deformation.

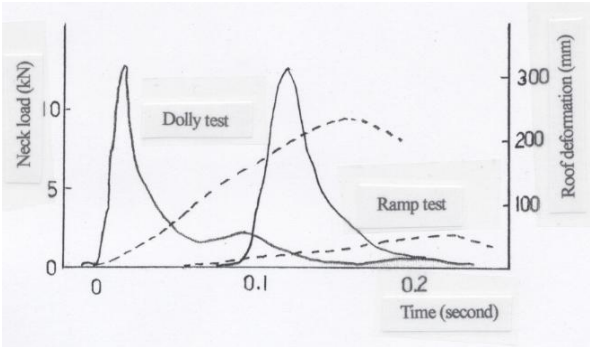

Figure 5. The time, dummy neck load, and the roof deformation

In ramp rollover tests, first, the dummy neck maximum load appears and next the maximum roof deformation occurs. The interval Δt of the two phenomena is about 0.1 second. By reading the maximum of neck load, the value shows about 1250N. The roof deformation at the point of maximum neck load is around 10mm. In dolly rollover tests, the same tendency occurs. The interval Δt is about 0.14 second. .

It is known that the human endurance is a higher value at the shorter duration time. By the reference of the Wayne State Tolerance Curve, the acceleration depends effectively on the duration times.

In the ramp test, duration time is very little and is very little in the dolly test.

BODY CONFIGURATION TO ROLLOVER

As shown in the previous **Figure 2**, we understand that bodies collapsed a certain configuration according to FMVSS216 test method. In the first design stage, a body configuration should be considered to be superior to rollover.

It is necessary to consider kinematics and plastic deformation of the body. There are many textbooks teaching these principles in the nature. We selected an egg. The egg has a dimension that the long axis is 46mm and short axis is 40mm, and thickness is 0.5 mm. One of the typical characteristics is that it transfers toward direction during rotation. We can explain the mechanism by using a formula and schematic figure.

Figure 6 shows the schematic feature of rotation and its kinematics formula (2). The configuration having a deviative elliptical oval configuration can change the direction in rotation.

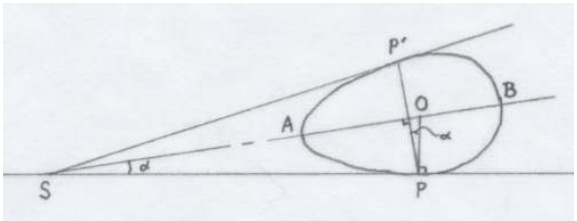

Figure 6. Rotation of egg feature

$$OP = SP \tan\alpha \qquad (1)$$

We try to make a deviative elliptical oval configuration by using the mathematical formula. It is found that the oval of Cassini curve is suitable for the mathematical expression in many formulae as shown in the formula.

$$r_1 r_2 = b^2 \qquad (2)$$

Figure 7 indicates Cassini Curves of oval configuration.

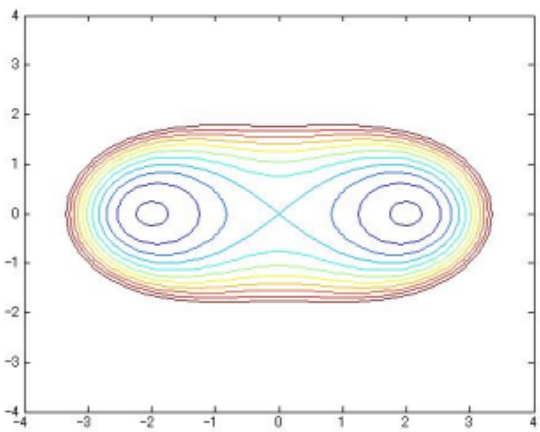

Figure 7. Cassini curves of oval configuration

By using the Computer Aided Design (CAD), we can identify an elliptical oval configuration of an egg as shown in **Figure 8**[4].

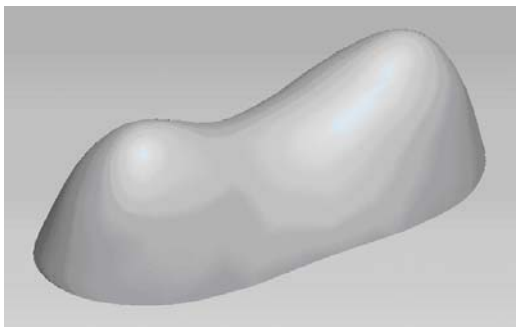

Figure 8. An expression according to Cassini curves shown in Figure 7 by using CAD

Figure 9 shows an identification of an elliptical oval configuration using CAD, not using free curves like B-spline function.

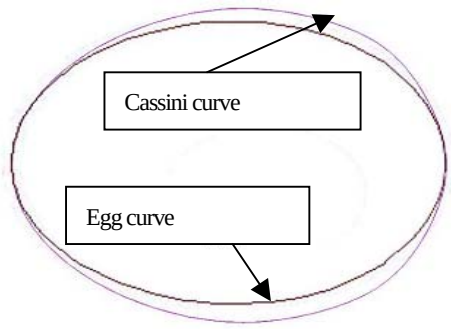

Figure 9. Identification of an elliptical oval configuration using CAD

As an example, by using the Finite Element Method (FEM), we try to calculate stress analysis of frames that are constructed from the box and oval configurations. Calculation results shown in **Figure 10** are the same as mechanical conditions like dimensions, materials, and restraint conditions. As shown in **Figure 10**, the feature having an elliptical oval configuration has a constant stress distribution compared with the box type configuration.

The strength of the oval type frame is superior to that of the box type frame if the same mechanical conditions are used. From the point of contact fields, occupants contact with the body structures having curvatures to be a lower stress level.

The oval body structure as satisfied with the above effects will make it possible to decrease occupant injuries. But we have not yet confirmed these characteristics by using actual vehicles.

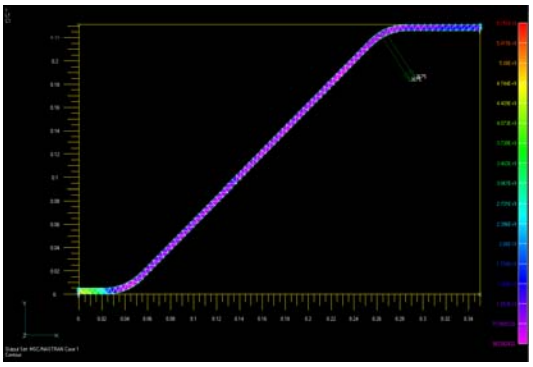

(A) Box type frame

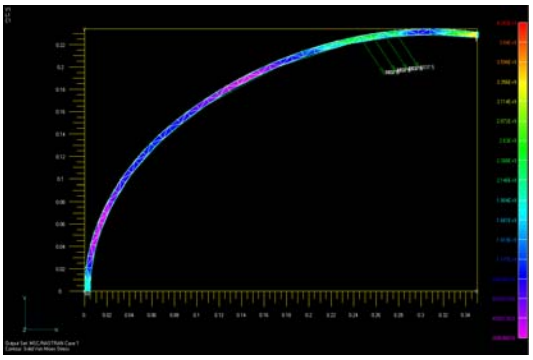

(B) Oval type frame

Figure 10. Calculation results of box and oval type frames by using FEM

CONSIDERING OCCUPANT BEHAVIOR

As rollover phenomena of the occupant movements in the cabin are complicated, we must consider not only the deformation and the configuration of body but also kinematics motion. In rotational motion, the equation of motion (3) should be introduced into the accident analysis to correctly seek the precise solutions.

$$\frac{f}{m} = \frac{dV}{dt} + \left(\frac{dv'}{dt}\right)' + \left[\frac{d\omega}{dt} \times r'\right] + 2\left[\omega \times v'\right] + \left[\omega \times \left[\omega \times r'\right]\right] \qquad (3)$$

Here, $\frac{dV}{dt}, \left(\frac{dv'}{dt}\right)'$: Acceleration,

$\frac{d\omega}{dt} \times r'$: Inertia,

$2\left[\omega \times v'\right]$: Coriolis acceleration,

$\left[\omega \times \left[\omega \times r'\right]\right]$: Centripetal acceleration.,

(non-prime): the motion from the fixed coordinate systems,

(‘: prime): the motion from the motion coordinate systems.

In case of $d\omega/dt = 0$, $\left[\frac{d\omega}{dt} \times r'\right]$ is equal to zero and $2\left[\omega \times v'\right]$ is precisely called Coriolis Acceleration.

The motion as shown in formula (3) is considered as relative motion in the rotational system. We must assume the coordinate systems during rollover.

Again we think the occupant movement during rollover as shown in **Figure 5**. Here, a coordinate is defined as Cartesian coordinate system (x, y, z). X-axis is a direction of processing of vehicle by the right hand system clockwise.

In the ramp rollover test, the test vehicle goes to the ramp. When the right wheel of the vehicle reaches the ramp, the vehicle leans slightly toward the left side y-axis. The direction of both vehicle and dummy faces straight. The vehicle leans to the left direction and also the torso of dummy when the front wheel is swiftly compelled to turn to left in the center of x-axis (rolling). On the other hand, the head (neck) on the torso of dummy keeps moving straight ahead. The phenomenon raises the relative motion between the vehicle and the head (neck) of dummy. When the vehicle touches down on the ground rolling, head (neck) relatively rotating to the vehicle hits the side roof rail and soon the neck load reveals the maximum load. When the head hits these parts of the vehicle, the roof deformation reveals about 10mm and does not yet reach the maximum deformation when the neck reaches a maximum load. Progressively, 0.01second after, the roof deformation shows the maximum deformation, about 20mm far from the neck hit to the roof position. As for these phenomena, it does not seem that the strong relationship between the neck load and the roof deformation exists. By these phenomena, the relative motion of the dummy and the first impact to the vehicle body might become fatal injuries of the dummy.

From the point of relative motion, if the motion of the head (neck) of dummy is considered to be the fixed coordinate system, the motion of roof deformation is the motion from the motion system. On the contrary, if the roof deformation is looked upon as the fixed coordinate system, the head (neck) of dummy is the motion. It moves toward the roof and contacts the body structures. It looks like diving movements relatively.

PROPOSE RESEARCH AND TEST METHOD

In reports regarding real world rollover accidents, the relation between roof strength and injuries of the occupants is studied. When they inspected the body deformation collapse after rollover accidents, the roofs showed severer collapses and there were no survival spaces in the cabins. They proposed designing a stronger roof.

According to consideration of the ramp rollover test, we must investigate the phenomena of actual rollover accidents.

First, what is the initial velocity of vehicles before rolling?

Why happened to the rollover, and what triggers is it to roll?

The relative motion of occupants to the vehicle like acceleration force, inertia force, rotational moment occurs and the first impact of the head to the vehicle body occurs before producing larger collapses of roof and these factors might become fatal injuries of occupants.

When ultimately fatal injuries occur during rollover, where is its position in the vehicle body?

By considering these papers, we have to find evidence in order to request car makers to make countermeasures of body structures to prevent fatal injuries as follows:

1. Reconstructions of rollover accidents involved in the initial velocity
2. Considering roof configuration, deformation and rotational movement with the dummy
3. To make the dummy for rollover with the neck having measurements of axel force and bending load (tort ional load)
4. To make test procedure and methods reflecting the actual rollover accidents [5]
5. To evaluate not only the strength and intrusion of the roof but also deformation situations of the roof like sharp edges, folding patterns, etc.
6. To evaluate the survival space areas after collapse

CONCLUSIONS

Some results of our researches are summarized as follows:

1. It is very important to study reconstructions of rollover accidents involved in the initial velocity before accidents occur
2. The body configuration should be considered from point contact fields.
3. In rotational movements, acceleration force, inertia force, rotational moment should be considered as input forces.
4. In order to reduce fatal injuries in rollover accidents, some proposal items are recommended.

REFERENCES

[1] The Institute for Traffic Accident Research and Data Analysis (ITARDA), Vehicle Rollover Accident, No.65, 2006 (Japanese)

[2] T. Sakurai, Y. Takigawa, H. Ikeno, Study on Passenger Car Rollover Simulation, The 13th International Technical Conference on Experimental Safety Vehicles, 11-1991

[3] G. S. Bahling, R. T. Bundorf, G. S. Kaspzyk, E. A. Moffatt, K. F. Orlowski, J. E. Stocke, Rollover and Drop Tests – The Influence of Roof Strength on Injury Mechanics Using Belted Dummies, 1990 SAE International Congress and Exposition, SAE 902314, 11-1990

[4] T. Sakurai, K. Inoue, Study on the configuration of vehicle and Cassini Curve represented oval curves, Proceedings of the Japan Society for Graphic Science, 2008 (Japanese)

[5] T. Chen, E.C. Chirwa, M. Mao, J. Latchford, Rollover far side strength test and simulation, Icrash 2006

CAR ROLLOVER MECHANISMS AND INJURY OUTCOME

Richard Cuerden
Rebecca Cookson
David Richards
TRL
United Kingdom
Paper Number 09-0481

ABSTRACT

The study focused on the mechanisms which result in passenger cars over turning. Approximately 21% of the car occupant fatalities examined in the UK's Co-operative Crash Injury Study (CCIS) experienced a rollover. However rollovers are shown to be complex events, which can occur with or without impact(s) and are not always the principal cause of the resulting occupant injuries.

The study differentiates the different types of rollovers and presents the influencing factors which precede them. Rollover events are divided into three categories: simple rollovers which don't involve a significant impact; rollovers followed by impact(s); and impacts followed by rollovers.

The research correlated the cars' dynamic motion immediately prior to the initiation of the roll, the mechanisms which caused the car to roll and the consequences with respect to occupant injury. A significant proportion of the cars were identified as 'sliding' laterally to some degree prior to the roll and off-road soft surfaces such as grass or earth were the most frequent roll initiators. Cars were also described as skidding or having lost control prior to leaving the road or striking a kerb or other roadside object or other vehicle. For this reason Electronic Stability Control (ESC) systems were identified as an important countermeasure with respect to potentially preventing a proportion of future rollover accidents.

Occupants, who were either fully or partially ejected from their cars, were strongly linked to severe injury outcome. Seat belts (ideally used in conjunction with other restraint devices designed to prevent either all or part of the occupants' body leaving the car through window apertures during the rollover) were shown to be effective.

INTRODUCTION

The data source for this paper is the UK's Co-operative Crash Injury Study (CCIS), which is one of Europe's largest car occupant injury causation studies (www.ukccis.org).

The programme of research started in 1983 and continues to investigate real-life car accidents. Multi-disciplinary teams examine crashed vehicles and correlate their findings with the injuries the victims suffered to determine how car occupants are injured. The objective of the study is to improve car crash performance by continuing to develop a scientific knowledge base, which is used to identify the future priorities for vehicle safety design as changes take place.

CCIS investigates and interprets real-world car occupant injury crashes retrospectively. Police reported injury road traffic crashes from defined geographical areas of England are reviewed to establish if they meet the CCIS sample criteria. The basic selection criteria used for the accidents presented in this analysis were:

- The accident must have occurred within the investigating teams geographical area
- The vehicle must be a car or car derivative
- The vehicle must have been less than 7 years old at the time of the accident
- The vehicle must have at least one occupant who is injured (according to the police)
- The vehicle must have been towed from the scene of the accident.

Accidents were investigated according to a stratified sampling procedure, which favoured cars that met the age criteria and contained a fatal or seriously injured occupant as defined by the British Government definitions of fatal, serious and slight. Where possible all crashes that met the criteria and involved a CCIS classified fatal or seriously injured occupant were investigated. Random selections of accidents involving slight injury were also investigated, up to a target maximum.

Vehicle examinations were undertaken at recovery garages several days after the collision. An extensive investigation of the cars' residual damage and structural loading along with detailed descriptions of the restraint system characteristics and any occupant contact evidence was recorded using the CCIS data collection protocols. This process allows the nature and severity of the impact(s) and/ or rollover damage to be precisely documented so different crash types can be compared.

Where practical the investigation teams visit the scenes of rollover crashes a day or two after the crash and gather evidence with respect to the highway and environmental factors.

Car occupant injury information was collected from hospital records, coroners' reports and questionnaires sent to survivors. The casualties' injuries were coded using the Abbreviated Injury Scale [1]. AIS is a threat-to-life scale and every injury is assigned a score, ranging from 1 (minor, e.g. bruise) to 6 (currently untreatable). The Maximum AIS injury a casualty sustains is termed MAIS. The scale is not linear; for example, an AIS 4 is much more severe than two AIS scores of 2.

The casualties' characteristics (age, gender, seat belt use) and injury information were correlated with the vehicle investigation evidence. This methodology allows the causes and mechanisms of the injuries to be documented.

Accidents investigated between December 2002 and September 2008 were included in the analysis (CCIS Phases 7 and 8 – to data release 8h).

RESULTS AND DISCUSSION

The relationship between impact type and injury severity for the car occupants in CCIS is shown in Table 1. In total, of the 8,526 occupants recorded in CCIS with known MAIS, 1,341 (16 %) were in cars which rolled over.

Table 1.
Impact types and injury severity for car occupants in CCIS

Type of Collision	Survivors (MAIS)			Killed	Total
	0	1	2+		
Single impact					
Frontal	642	1840	740	137	3359
Right side	204	601	172	61	1038
Left side	128	334	142	84	688
Rear	49	204	18	8	279
Multiple impact	256	856	303	112	1527
Rollover	176	776	284	105	1341
Other	9	7	4	4	24
Total	**1464**	**4618**	**1663**	**511**	**8256**

Rollovers are over-represented for occupants with higher injury severities, especially for occupants who were killed: of the 511 fatally injured occupants, 105 (21 %) were in rollovers.

Single vehicle accidents made up 38% of all accidents which resulted in serious or fatal injury (MAIS 2+) in the CCIS dataset. Rollovers occurred in 7% of multi-vehicle and 41% of single vehicle accidents. Of all the rollover accidents, 73% were single vehicle accidents.

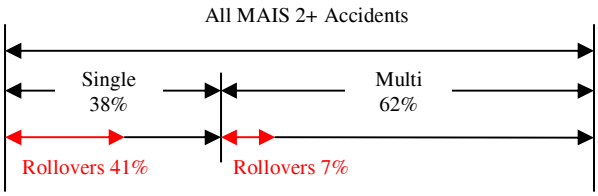

Figure 1. Proportion of single and multi vehicle accidents that result in rollovers

CCIS examines cars and car derivatives (light goods/commercial vans). Comparing the proportions of different vehicle types involved in CCIS accidents showed that 31% of off-road vehicles rolled over compared to 9% of estate cars.

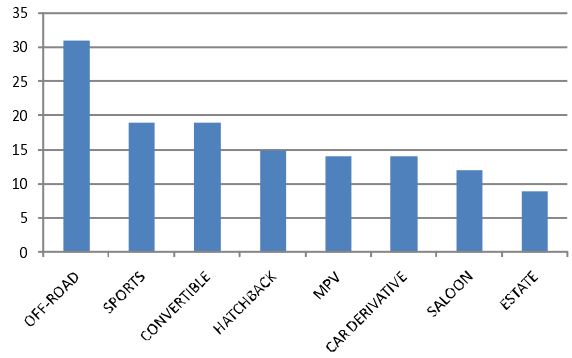

Figure 2. Percentage of vehicles by type which rolled over

Table 2 categorises the occupants involved in rollovers into four distinct groups, depending on whether there was a significant impact as well as the rollover, and whether that impact occurred before or after the roll. Fay et al. [2] presented similar results and also commented that:

'In practice, the characteristics of vehicle rollover can be more complicated than such analysis suggest because of the large number of vehicles which experience multiple events in crash sequences, including combinations of impacts and rollover events.'

Table 2.
Categories of rollover

Type of Rollover	Survivors (MAIS)			Killed	Total
	0	1	2+		
Rolled before 1st impact	15	79	31	20	145
Rolled after last impact	96	390	149	54	689
Rolled without any impacts*	59	289	92	25	465
Rolled between impacts	6	17	11	6	40
Other	-	1	1	-	2
Total	**176**	**776**	**284**	**105**	**1341**

* Significant impacts

Depending on exactly what caused them to roll, the groups where a rollover occurred before an impact are the groups of casualties for whom the rollover may have been prevented if an active safety system, such as ESC, was fitted to the vehicle [3]. A limitation of this analysis was that the fitment of ESC systems was not correlated with the pre-roll vehicle dynamics. Future work is planned to account for these systems and to quantify their real world effects and potential limitations.

The following diagrams (Figure 3 and Figure 4) show how the data was grouped for the analysis from this point on. The occupants were split by severity, with the "non-injured" and "slight" casualties (MAIS 0-1) separated from the "serious and killed" (MAIS 2-6) casualties. It should be noted that there was one occupant who had a MAIS of 1, who was killed; this occupant has been included in the "serious and killed" group of casualties.

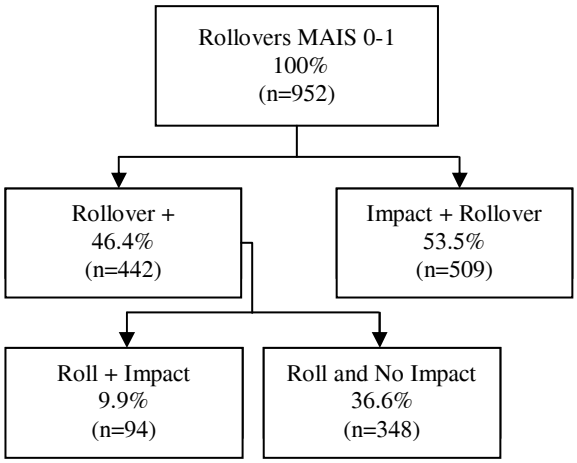

Figure 3. Distribution of rollover types for occupants with no or slight injuries

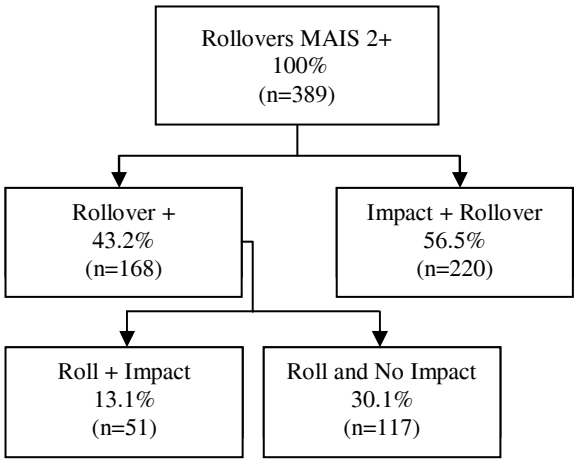

Figure 4. Distribution of rollover types for occupants with serious or fatal injuries

Occupants who had a roll then an impact, and a roll but no impact, are subsets of the "Rollover +" group – occupants where the rollover occurred first. This was the first group of occupants studied to see which factors influenced or caused their cars to roll. The characteristics of the pre-roll events were then compared with the respective injury outcomes. The occupants in the two subsets of roll this group encompasses were also analysed.

Following this, the occupants in vehicles which had an impact first, then rolled over, were investigated.

Rolled first

This section investigates the characteristics of the rollovers where the rollover occurred before an impact, or where there was no impact. Table 3 shows how the cars' attempted manoeuvres related to the direction of travel of the cars immediately before the rollover, for the occupants whose car rolled before any impact (or rolled and did not have an impact).

A large number of these vehicles were travelling on left and right bends, and were sliding (they had lost control). These vehicles accounted for 204 (33 %) of the occupants in cars which rolled over first. These are occupants where it is possible that ESC may have prevented the rollover and resultant injuries, by preventing the initial loss of control. A further 136 (22%) casualties were in cars described as attempting to proceed 'Forwards', but were also known to be sliding or have lost control prior to rolling. The precise reasons for these vehicles having lost control

were not always known, but included poor manoeuvres and avoidance actions such as swerving to negotiate obstacles/ other vehicles. It is reasonable to assume that a proportion of these incidents could have been prevented if ESC was fitted to all the cars.

Table 3.
Manoeuvre prior to event versus direction of travel at start of event – rolled first

Cars' direction of travel at the start of event	Manoeuvre prior to event				Total
	Forwards	Left bend	Right bend	Other/ unknown	
Forwards	107	37	31	24	199
Forwards & sliding to R	67	60	19	9	155
Forwards & sliding to L	49	8	63	3	123
Rearwards	-	4	-	-	4
Rearwards & sliding to R	2	4	6	-	12
Rearwards & sliding to L	3	1	-	-	4
Purely sideways to R	9	11	12	1	33
Purely sideways to L	6	3	17	-	26
Unknown	42	1	-	11	54
Total	**285**	**129**	**148**	**48**	**610**

Table 4 shows the initiating factor of the rollovers. The most frequent initiation of the rollovers for all injury severities was grass/earth or some other soft surface.

Table 4.
Roll initiation – rolled first

Roll initiation influence	Survivors (MAIS)			Killed	Total
	0	1	2+		
Kerb	14	62	24	7	107
Gradient up	2	11	12	3	28
Gradient down	8	31	11	3	53
Grass/ earth or soft surface	30	158	47	23	258
Tarmac/ hard surface	14	67	15	4	100
Other vehicle	1	7	2	1	11
Safety barrier/ low structure	-	8	3	-	11
Fence/ high structure	-	3	1	2	6
Sharp turning or spinning	3	11	5	2	21
Not known	2	10	3	-	15
Total	**74**	**368**	**123**	**45**	**610**

With the exception of "tarmac / hard surface", "other vehicle" and "sharp turning or spinning", the initiating factors all indicate that the vehicle left the carriageway, or struck something on the edge of the carriageway.

Table 5 shows the direction of roll of the vehicle, and the seating position and injury severity of the occupants.

Table 5.
Direction of roll by seating position and injury severity – rolled first

Direction of roll	Survivors (MAIS)			Killed	Total
	0	1	2+		
Roll to Right					
Driver	21	122	40	19	202
Front passenger	9	46	11	3	69
Rear passenger	9	30	15	2	56
Not known	-	1	-	-	1
	39	***199***	***66***	***24***	***328***
Roll to Left					
Driver	10	89	39	15	153
Front passenger	8	40	8	3	59
Rear passenger	14	26	3	2	45
Not known	1	1	-	-	2
	33	***156***	***50***	***20***	***259***
Rear over front					
Driver	-	7	4	-	11
Front passenger	1	2	1	-	4
Rear passenger	-	2	-	-	2
Not known	-	-	-	-	0
	1	***11***	***5***	***-***	***17***
Front over rear					
Driver	1	1	-	1	3
Front passenger	-	-	-	-	0
Rear passenger	-	-	-	-	0
Not known	-	-	-	-	0
	1	***1***		***1***	***3***
Not known	***0***	***1***	***2***	***0***	***3***
Total	**74**	**368**	**123**	**45**	**610**

The majority of the casualties (96 %) either rolled right to left or left to right. In order to simplify the analysis of roll direction and seating position in the car, the offside occupants in cars which rolled to the right were combined with the nearside occupants in cars which rolled to the left, and vice versa, to create two groups. Only seat belted occupants were selected. The injury severity of these groups is shown in Table 6.

Table 6.
Roll direction and seating position – rolled first

Roll direction and seating position	MAIS 0&1	MAIS 2-6	Total
Seated on side adjacent to direction of roll	133 78.7%	36 21.3%	169
Seated on opposite side to direction of roll	115 72.3%	44 27.7%	159
Total	248	80	328

This shows that occupants seated on the opposite side to the direction of roll (for example, drivers whose cars rolled from right to left) tend to be more severely injured. This may be related to the kinematics of the occupants at the moment the roof makes contact with the ground – the occupant seated on the opposite side

to the roll will accelerate towards the roof more than the occupant seated on the same side to the roll.

Figure 5 shows the direction of the force which initiated the roll, and also shows whether the vehicle rolled to the left or rolled to the right.

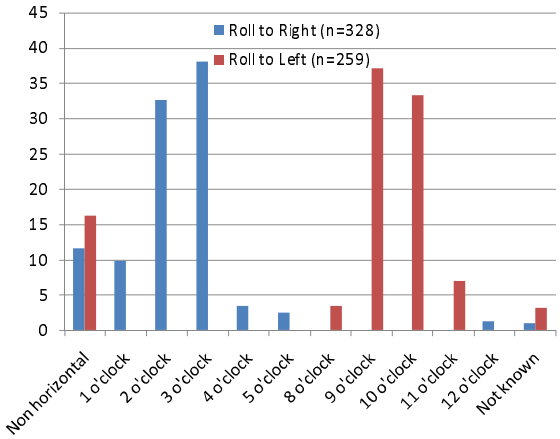

Figure 5. Direction of roll initiation force – rolled first

The majority of the rolls to the right had an initiation direction of force of 2 or 3 o'clock. The majority of rolls to the left had an initiation direction of force of 9 or 10 o'clock.

Figure 6 shows the point of action of the initiation forces, with two thirds of the initiation forces of rolls to the right and left applied to both the respective wheels.

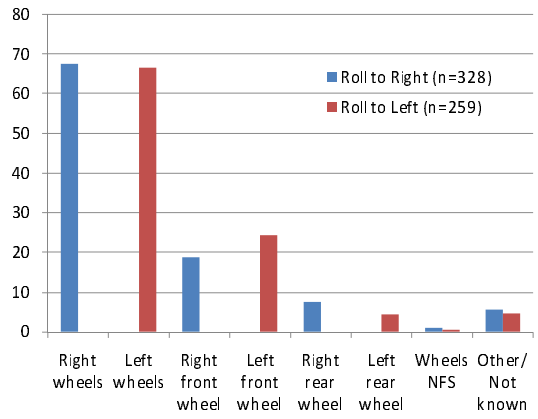

Figure 6. Point of action of initiation force – rolled first

Figure 7 shows the surface on which the vehicles that rolled over landed. There is virtually no difference between the landing surface and the direction of roll, implying cars leave the carriageway to the left and right evenly.

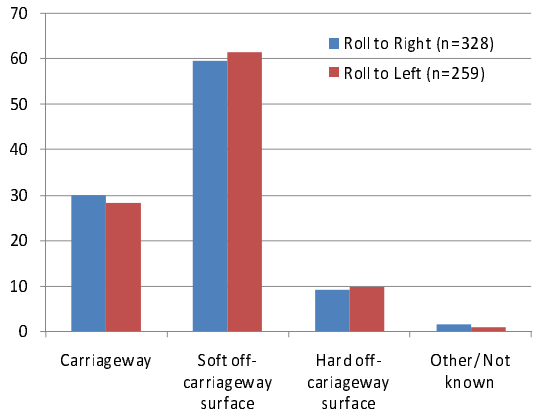

Figure 7. Landing surface – rolled first

Roll and no impact

The "roll and no impact" group is a subsection of the "rolled first" group. This section analyses the characteristics and consequences of rolls where there was no impact.

Figure 8 shows the relationship between the number of rolls and the injury severity of the occupants. The number of rolls is recorded as multiples of 0.25, where 0.25 rolls would be a roll onto the side, 0.5 rolls would be a roll onto the roof, etc.

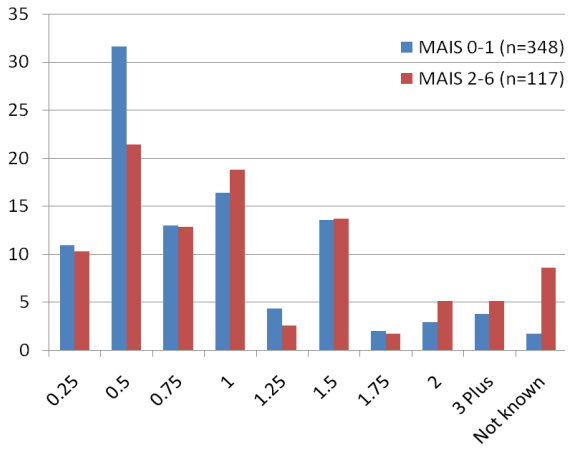

Figure 8. Number of rolls by severity – roll and no impact

Occupants in vehicles which rolled two or more times tend to be more severely injured, although there were relatively few vehicles that rolled this often. Slightly injured occupants are over-represented in vehicles which rolled 0.5 times.

Figure 9 shows the relationship between injury severity of the occupants, and whether their vehicle was airborne during the rollover.

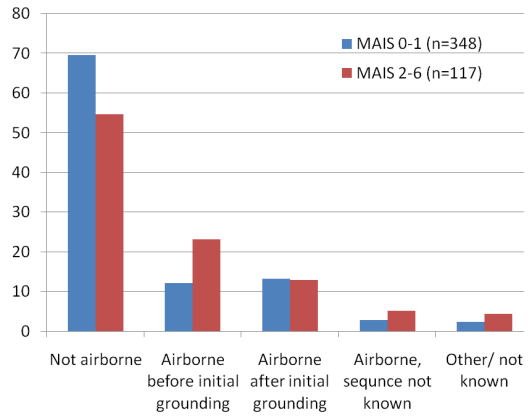

Figure 9. Severity of occupants and whether vehicle was airborne – roll and no impact

The relationship between injury severity and whether the vehicle was airborne is clearer than the relationship between the number of rolls. Of the occupants with MAIS 0-1, the vehicle was not airborne for almost 70 % of the occupants. For occupants with MAIS 2-6, the vehicle was not airborne for 55 % of the occupants.

For the vehicles which rolled, the most frequent area of most significant damage was the roof (47 % in total, 47 % of MAIS 0-1 occupants, and 45 % of MAIS 2-6 occupants). Table 7 explores the relationship between ejection and seat belt use for the occupants in a vehicle which rolled but had no other impact.

Table 7.
Ejection and seat belt use – roll and no impact

Ejection	**Seat belt use**			**Total**
	Used	Not used	Not known	
None				
MAIS 0-1	231	31	82	344
MAIS 2-6	42	16	15	73
	273	***47***	***97***	***417***
Full				
MAIS 0-1	1	1	-	2
MAIS 2-6	1	17	-	18
	2	***18***	***-***	***20***
Partial				
MAIS 0-1	3	-	-	3
MAIS 2-6	17	4	4	25
	20	***4***	***4***	***28***
Total				
MAIS 0-1	235	32	82	349
MAIS 2-6	60	37	19	116
	295	**69**	**101**	**465**

It is clear that seat belt use and full ejection in rollovers are strongly related. 75 % of occupants who were not ejected were wearing a seat belt, compared to only 10 % of occupants who were fully ejected. Occupants who were fully ejected were also much more likely to have severe injuries; 18 % of occupants who were not ejected had MAIS 2-6, compared to 90 % of occupants who were fully ejected.

Severe injury was also common among occupants who were partially ejected, with 89 % having MAIS 2-6. However the seat belt use of these occupants was relatively high, at 83 % which implies that seat belts prevent full ejection, but other systems (e.g. curtain airbags) are also required in order to prevent partial ejection.

Table 8 and Table 9 show the AIS 2+ and AIS 3+ injuries received by the occupants in cars which rolled over with no other impact.

Table 8.
Proportion of occupants with AIS 2+ injuries, by seat belt use and body region – roll and no impact

Injured ISS body region Percentage AIS 2+	Seat belt used	Seat belt not used	Seat belt use not known
MAIS 2+ (n)	60	37	19
Head AIS 2+	45%	56.8%	36.8%
Face AIS 2+	1.7%	2.7%	10.5%
Thorax AIS 2+	25%	59.5%	36.8%
Abdomen AIS 2+	13.3%	21.6%	21.1%
Limbs AIS 2+	51.7%	67.6%	47.4%
External AIS 2+	8.3%	-	5.3%

Table 9.
Proportion of occupants with AIS 3+ injuries, by seat belt use and body region – roll and no impact

Injured ISS body region Percentage AIS 3+	Seat belt used	Seat belt not used	Seat belt use not known
MAIS 2+ (n)	60	37	19
Head AIS 3+	23.3%	48.6%	26.3%
Face AIS 3+	-	2.7%	-
Thorax AIS 3+	15%	48.6%	26.3%
Abdomen AIS 3+	5%	10.8%	10.5%
Limbs AIS 3+	15%	24.3%	31.6%
External AIS 3+	1.7%	-	-

For seat belted occupants, the most frequent AIS 2+ and AIS 3 + injuries were to the head and the limbs. For non-belted occupants, the most frequent AIS 2+ injuries were to the head, thorax and limbs, and the most frequent AIS 3+ injuries were to the head and thorax. Occupants not wearing a seat belt generally had more injuries to more body regions, and the

proportion of thorax injuries especially increased for occupants not wearing a seat belt.

Table 10 shows how the injury severity of front seat occupants depended on the direction of the roll. Only occupants wearing a seat belt were selected for this table.

Table 10.
Roll direction and seating position – roll and no impact

Roll direction and seating position	MAIS 0&1	MAIS 2-6	Total
Seated on side adjacent to direction of roll	105 80.8%	25 19.2%	130
Seated on opposite side to direction of roll	83 72.8%	31 27.2%	114
Total	188	56	244

This shows that occupants seated on the opposite side to the direction of roll (for example, drivers whose cars rolled from right to left) tend to be more severely injured.

For seat belted occupants only, no statistical relationship was found with respect to the number of rolls, surface rolled onto, initiation influence or initiation type when comparing MAIS 0-1 and MAIS 2-6 occupants. However, the proportion of occupants in airborne vehicles was greater for MAIS 2-6.

Roll followed by impact

The group of occupants whose vehicle rolled before having an impact is also a subset of the occupants who rolled first. However, this group of 145 occupants is relatively small compared to the number who rolled over without an impact, so less detail is presented. Also, because these vehicles had an impact following the rollover, it is difficult to distinguish the injurious effects of the rollover from those of the impact.

Figure 10 shows the relationship between the number of rolls of the vehicle and the injury severity of the occupants. This shows no clear relationship between the two variables, but the vehicles as expected rolled fewer times than those which rolled without subsequent impact(s).

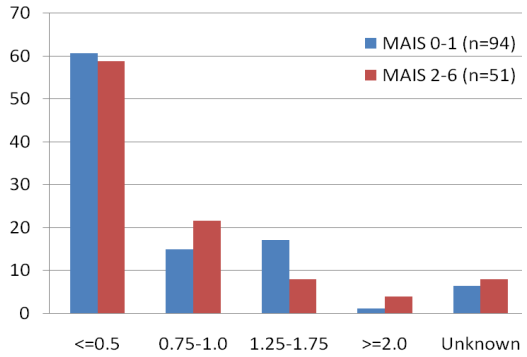

Figure 10. Number of rolls by severity – roll followed by impact

Figure 11 compares the injury severity of the occupants to whether their vehicle was airborne.

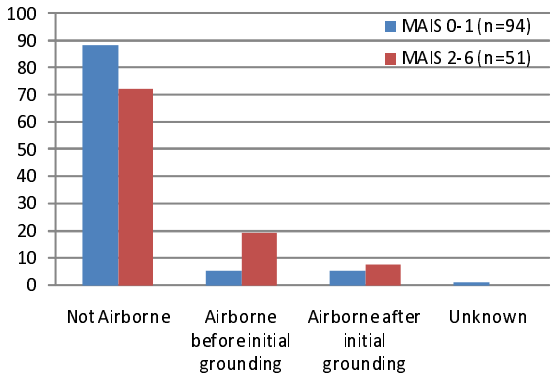

Figure 11. Severity of occupants and whether vehicle was airborne – roll followed by impact

As for rollovers with no impact, the severity is greater in rollovers where the vehicle has become airborne.

For the occupants in vehicles which rolled over then had an impact, the principal damage was to the roof of the car (61 cases, 16 MAIS 2+); the left (20 cases, 5 MAIS 2+) and right (18 cases, 6 MAIS 2+). This shows that principal damage is less often to the roof when the vehicle has an impact as well as a roll.

Table 11 shows the relationship between seat belt use, ejection, and injury severity for the occupants in rollovers followed by an impact.

Table 11.
Ejection and seat belt use – roll followed by impact

Ejection	Seat belt use			Total
	Used	Not used	Not known	
None				
MAIS 0-1	71	5	17	93
MAIS 2-6	22	6	4	32
	93	***11***	***21***	***125***
Full				
MAIS 0-1	-	-	-	0
MAIS 2-6	-	9	1	10
	-	***9***	***1***	***10***
Partial				
MAIS 0-1	1	-	-	1
MAIS 2-6	5	3	1	9
	6	***3***	***1***	***10***
Total				
MAIS 0-1	72	5	17	94
MAIS 2-6	27	18	6	51
	99	***23***	***23***	***145***

All of the occupants who were fully ejected, and for whom seat belt use was known, were not wearing a seat belt. These occupants were all seriously injured or killed.

Table 12 and Table 13 show the proportion of AIS 2+ and AIS 3+ injuries received by the occupants by body region and seat belt use.

Table 12.
Proportion of occupants with AIS 2+ injuries, by seat belt use and body region – roll followed by impact

Injured ISS body region Percentage AIS 2+	Seat belt used	Seat belt not used	Seat belt use not known
MAIS 2+ (n)	27	18	6
Head AIS 2+	52%	72%	50%
Face AIS 2+	11%	6%	-
Thorax AIS 2+	59%	72%	67%
Abdomen AIS 2+	19%	33%	17%
Limbs AIS 2+	56%	50%	50%
External AIS 2+	4%	-	17%

Similarly to rollovers without impacts, the injuries were dominated by head, thorax and head injuries. Occupants who were not wearing a seat belt had more injuries to more body regions, especially head and thorax injuries.

Table 13.
Proportion of occupants with AIS 3+ injuries, by seat belt use and body region – roll followed by impact

Injured ISS body region Percentage AIS 3+	Seat belt used	Seat belt not used	Seat belt use not known
MAIS 3+ (n)	27	18	6
Head AIS 3+	48%	61%	50%
Face AIS 3+	-	6%	-
Thorax AIS 3+	44%	61%	67%
Abdomen AIS 3+	4%	28%	-
Limbs AIS 3+	15%	17%	-
External AIS 3+	-	6%	33%

Impact followed by roll

Rollovers which occurred after an impact are likely to be different to rollovers which occurred before an impact or with no impact. Because this paper concentrates on the causes and consequences of rollovers, factors which are likely to be affected by the initial impact as well as the rollover, and where the effects of each cannot be distinguished (for example, roll direction and injury severity by seating position) have not been analysed here.

Table 14 shows the relationship between the manoeuvre prior to the impact, and the car's direction of travel at the start of the event. Compared to rollovers which occurred before / without an impact, a smaller proportion were sliding and travelling around a bend (16 % compared to 33 %). This suggests that the prevention of loss of control by ESC would have a relatively smaller effect of reducing rollover for these occupants. Similarly, the casualties described as in cars travelling 'Forwards' and sliding laterally to some degree represent about 28% of the "Impact followed by roll" group. These crashes often involved the car striking another vehicle or object and losing control or spinning before rolling over. ESC is likely to offer less benefits in these situations compared with the rolled first group.

Table 14.
Manoeuvre prior to event versus direction of travel at start of event – impact followed by roll

Cars' direction of travel at the start of event	Manoeuvre prior to event				Total
	Forwards	Left bend	Right bend	Other/ unknown	
Forwards	178	46	27	34	285
Forwards & sliding to R	74	15	11	18	118
Forwards & sliding to L	58	11	30	14	113
Rearwards	4	2	2	4	12
Rearwards & sliding to R	5	-	-	-	5
Rearwards & sliding to L	2	9	-	-	11
Purely sideways to R	39	16	3	11	69
Purely sideways to L	19	5	19	3	46
Unknown	42	2	2	24	70
Total	421	106	94	108	729

Table 15 shows the initiating factor of the rollovers by the injury severity of the occupants.

Table 15.
Roll initiation – impact followed by roll

Roll initiation influence	**Survivors (MAIS)**			**Killed**	**Total**
	0	**1**	**2+**		
Kerb	10	43	12	2	67
Gradient up	2	15	6	3	26
Gradient down	8	30	16	4	58
Grass/ earth or soft surface	24	86	33	16	159
Tarmac/ hard surface	13	78	15	2	108
Other vehicle	14	62	15	10	101
Safety barrier/ low structure	12	43	28	9	92
Fence/ high structure	5	19	18	8	50
Sharp turning or spinning	9	14	11	1	35
Other	-	6	-	2	8
Not known	5	11	6	3	25
Total	102	407	160	60	729

Compared to rollovers which occurred before / without an impact, the proportion of rollovers initiated by impact with another vehicle was much greater. However, grass/earth or soft surface was still the most frequent initiating factor.

Figure 12 and Figure 13 show the direction of the initiation force and the point of action of this force respectively.

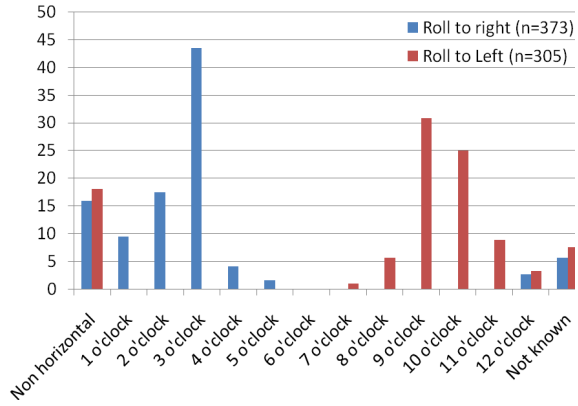

Figure 12. Direction of roll initiation force – impact followed by roll

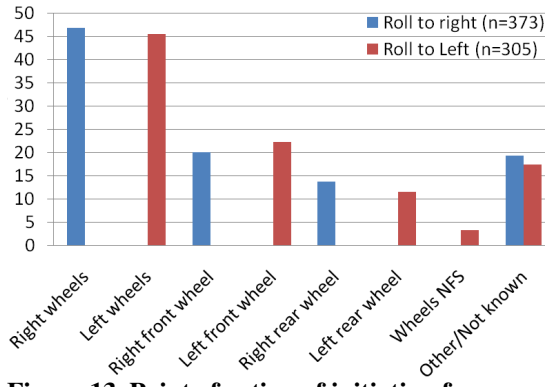

Figure 13. Point of action of initiation force – impact followed by roll

The majority of rolls to the right and left are still caused by initiation forces to the left and right wheels respectively.

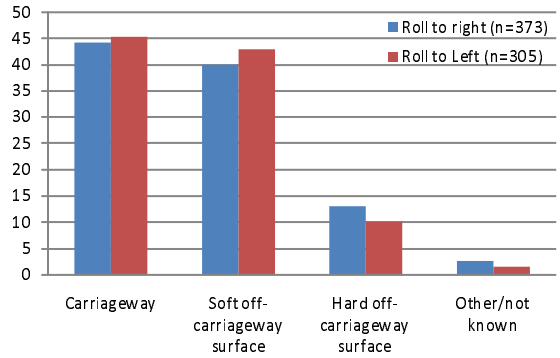

Figure 14. Landing surface – impact followed by roll

Figure 14 shows that the surface the vehicles landed on was not related to the direction of the roll, but the carriageway or road surface was proportionally much

more common (~ 45%) compared to roll first incidents (~ 30%).

Figure 15 shows the relationship between the number of rolls and the MAIS of the occupants.

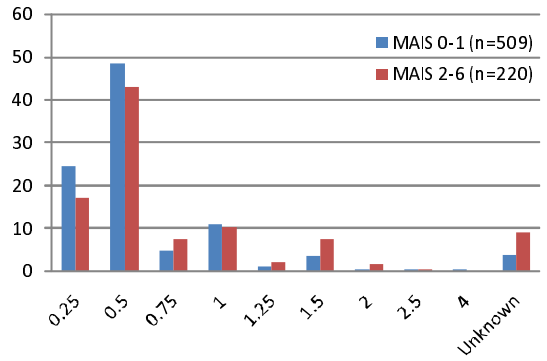

Figure 15. Number of rolls by severity – impact followed by roll

Occupants in a vehicle which rolled 0.25 times and 0.5 times tended to have a lower injury severity compared to these occupants in vehicles with more rolls. However, there is a much clearer relationship between injury severity and whether the vehicle became airborne, which is shown in Figure 16.

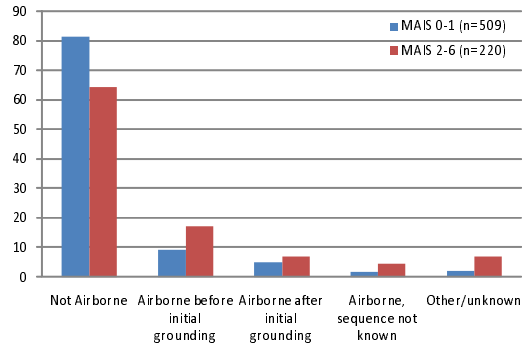

Figure 16. Severity of occupants and whether vehicle was airborne – impact followed by a roll

This figure shows that just over 60 % of the MAIS 2-6 occupants were in a vehicle which did not become airborne, compared to about 80 % of MAIS 0-1 occupants.

Table 16 explores the relationship between seat belt use, ejection and injury severity.

Table 16.
Ejection and seat belt use – impact followed by roll

Ejection	Seat belt use			Total
	Used	Not used	Not known	
None				
MAIS 0-1	310	61	124	495
MAIS 2-6	100	36	31	167
	410	***97***	***155***	***662***
Full				
MAIS 0-1	-	4	-	4
MAIS 2-6	4	20	2	26
	4	***24***	***2***	***30***
Partial				
MAIS 0-1	5	2	3	10
MAIS 2-6	10	9	6	25
	15	***11***	***9***	***35***
Unknown				
MAIS 0-1	-	-	-	0
MAIS 2-6	-	2	-	2
	-	***2***	***-***	***2***
Total				
MAIS 0-1	315	67	127	509
MAIS 2-6	114	67	39	220
	429	***134***	***166***	***729***

As seen for all other types of rollover impact, the risk of ejection was much greater for occupants who were not wearing a seat belt, and the injury severity of all ejected occupants tended to be higher than for occupants who were not ejected.

Table 17 and Table 18 show the AIS 2+ and AIS 3+ injuries received by the occupants in cars that rolled following an impact.

Table 17.
Proportion of occupants with AIS 2+ injuries, by seat belt use and body region – impact followed by roll

Injured ISS body region Percentage AIS 2+	Seat belt used	Seat belt not used	Seat belt use not known
MAIS 2+ (n)	114	67	39
Head AIS 2+	42.1%	61.2%	43.6%
Face AIS 2+	10.5%	6.0%	5.1%
Thorax AIS 2+	45.6%	46.3%	41.0%
Abdomen AIS 2+	26.3%	25.4%	17.9%
Limbs AIS 2+	50.0%	49.3%	48.7%
External AIS 2+	1.8%	1.5%	7.7%

Table 18.
Proportion of occupants with AIS3+ injuries, by seat belt use and body region – impact followed by roll

Injured ISS body region Percentage AIS 3+	Seat belt used	Seat belt not used	Seat belt use not known
MAIS 3+ (n)	114	67	39
Head AIS 3+	26.3%	41.8%	28.2%
Face AIS 3+	-	1.5%	2.6%
Thorax AIS 3+	36.8%	37.3%	35.9%
Abdomen AIS 3+	9.6%	9.0%	7.7%
Limbs AIS 3+	11.4%	22.4%	12.8%
External AIS 3+	-	1.5%	5.1%

Like occupants in other rollovers, the injuries were dominated by injuries to the head, limbs and thorax. However, unlike occupants in the other types of rollover, the proportion of unrestrained occupants receiving thorax, abdomen, or limb AIS 2+ injuries, and thorax or abdomen AIS 3+ injuries, was very similar to the proportion received by occupants wearing a seat belt. This was due in part to the nature of these accidents, where, for example some casualties experienced significant side impacts involving direct loading of their torso before their car rolled over.

CONCLUSIONS

Approximately 21% of the car occupant fatalities examined in the UK's Co-operative Crash Injury Study (CCIS) experienced a rollover. However rollovers are shown to be complex events, which can occur with or without impact(s) and are not always the principal cause of the resulting occupant injuries.

The study differentiates the different types of rollovers for MAIS 2+ occupants:

- Rollovers which do not involve a significant impact (30.1%);
- Rollovers followed by impact(s) (13.1%) and
- Impacts followed by rollovers (56.5%).

For cars which rolled first, 33% were described as travelling on bends (turning) and 'sliding' laterally and 22% were described as originally intending to proceed 'Forwards', but had also 'lost control'. ESC was identified as an important countermeasure with respect to potentially preventing a proportion of these rollover accidents. For cars which had an impact before rollover, the potential effectiveness of ESC is likely to be less.

The most common roll initiation influence was off-road soft ground (grass or earth) applying force to both wheels (right or left).

Casualties in cars which became airborne during the roll suffered proportionally more serious injuries.

Occupants, who were either fully or partially ejected from their cars, were strongly linked to severe injury outcome. Seat belts (ideally used in conjunction with other restraint devices designed to prevent either all or part of the occupants' body leaving the car through window apertures during the rollover) were shown to be effective.

ACKNOWLEDGEMENTS

This paper uses accident data from the United Kingdom's Co-operative Crash Injury Study (CCIS) collected during the period 2002 to 2008 (Phases 7s and 8h). Currently CCIS is managed by the Transport Research Laboratory (TRL Limited), on behalf of the United Kingdom's Department for Transport (DfT) (Transport Technology and Standards Division) who fund the project along with Autoliv, Fiat, Ford Motor Company, Nissan Motor Company and Toyota Motor Europe. Previous sponsors include Daimler Chrysler, LAB, Rover Group Ltd, Visteon, Volvo Car Corporation, Daewoo Motor Company Ltd and Honda R&D Europe (UK) Ltd. Data was collected by teams from the Birmingham Automotive Safety Centre of the University of Birmingham; the Vehicle Safety Research Centre at Loughborough University; TRL Limited and the Vehicle & Operator Services Agency (VOSA) of the DfT
Further information on CCIS can be found at http://www.ukccis.org

REFERENCES

[1] AAAM, (1990). The Abbreviated Injury Scale. 1990 Revision. Des Plaines, Illinois 60018, U.S.A: Association for the Advancement of Automotive Medicine (AAAM).

[2] Fay, P., Sferco, R. and Frampton, R. (2003). Vehicle Rollover – An important element in multiple impact crashes. Proceedings of 18th International Technical Conference on ESV.

[3] Erke, A. (2008). Effects of electronic stability control (ESC) on accidents: A review of empirical evidence. Accident Analysis & Prevention 40 (2008) 167-173.

SUMMARY TABLES

Table A 1. Severity of injury related to seating position and sex

Seating Position + Sex	Survivors (MAIS) 0	1	2+	Killed	Total
Driver					
Male	64	297	142	62	565
Female	27	174	48	14	263
Not known	1	2	-	-	3
	92	***473***	***190***	***76***	***831***
Front passenger					
Male	20	89	27	10	146
Female	16	84	31	8	139
Not known	6	-	-	-	6
	42	***173***	***58***	***18***	***291***
Rear passenger					
Male	21	60	18	6	105
Female	13	65	18	5	101
Not known	4	2	-	-	6
	38	***127***	***36***	***11***	***212***
Not known	***4***	***3***	***0***	***0***	***7***
Total	**176**	**776**	**284**	**105**	**1341**

Table A 2. Severity of injuries related to seating position and belt use

Seating Position + Belt	Survivors (MAIS) 0	1	2+	Killed	Total
Driver					
Belted	53	359	110	36	558
Unbelted	9	34	44	27	114
Not known	30	80	36	13	159
	92	***473***	***190***	***76***	***831***
Front passenger					
Belted	30	109	37	12	188
Unbelted	2	18	13	5	38
Not known	10	46	8	1	65
	42	***173***	***58***	***18***	***291***
Rear passenger					
Belted	14	54	7	1	76
Unbelted	7	33	25	8	73
Not known	17	40	4	2	63
	38	***127***	***36***	***11***	***212***
Not known	***4***	***3***	***0***	***0***	***7***
Total	**176**	**776**	**284**	**105**	**1341**

Table A 3. Severity of injury related to seating position and age

Seating Position + Age	Survivors (MAIS) 0	1	2+	Killed	Total
Driver					
< 17	1	1	-	-	2
17 – 24	28	172	63	17	280
25 – 39	21	156	66	31	274
40 – 59	21	87	39	20	167
60 +	12	37	20	8	77
Not known	9	20	2	-	31
	92	***473***	***190***	***76***	***831***
Front passenger					
< 17	4	18	4	-	26
17 – 24	5	73	28	9	115
25 – 39	3	25	14	3	45
40 – 59	3	17	7	3	30
60 +	6	17	4	3	30
Not known	21	23	1	-	45
	42	***173***	***58***	***18***	***291***
Rear passenger					
< 17	16	47	9	-	72
17 – 24	9	55	22	6	92
25 – 39	1	8	3	3	15
40 – 59	1	4	1	-	6
60 +	-	7	-	2	9
Not known	11	6	1	-	18
	38	***127***	***36***	***11***	***212***
Not known	***4***	***3***	***0***	***0***	***7***
Total	**176**	**776**	**284**	**105**	**1341**

NHTSA's Class 8 Truck-Tractor Stability Control Test Track Effectiveness

Frank S. Barickman and Devin H. Elsasser
National Highway Traffic Safety Administration
Heath Albrecht, Jason Church, and Guogang Xu
Transportation Research Center Inc.
United States of America

Paper Number 09-0552

ABSTRACT

Statistical analyses of crash data in the United States show that a large percentage of heavy truck crashes are rollover related. To evaluate roll stability for truck tractors, the National Highway Traffic Safety Administration (NHTSA) has performed test maneuvers with several Class 8 combination truck tractor/trailers on a test track. Stability Control interventions have been observed with all test track maneuvers conducted on dry pavement. Rollover events have been observed to be mitigated by stability control interventions in tests conducted with the truck tractor/trailer combinations loaded with a High Center of Gravity (CG) load.

This paper discusses the initial test track observations and test maneuvers NHTSA evaluated. Test maneuvers included constant radius increasing velocity tests, J-turn tests, and double lane change maneuvers. These tests were conducted with and without tractor and trailer stability control systems enabled. Tests were conducted under different loading conditions and on high coefficient of friction surface.

INTRODUCTION

According to the Large Truck Crash Facts 2006, there were 4,321 large trucks involved in fatal crashes during 2006. A total of 221 fatal crashes attributed rollover as the first harmful event [1]. Depending on the effectiveness of a stability control system, some number of these may possibly have be prevented.

Electronic stability control (ESC) systems have been available on light vehicles for the past decade. Over this time, NHTSA and others have estimated that this technology has the potential to prevent over 8,000 fatal crashes per year [2]. Recognizing the safety potential of this technology, NHTSA has mandated that all vehicles less than 10,000 lbs. be equipped with ESC by model year 2012 [3].

More recently, heavy vehicle manufacturers and suppliers have begun offering stability control systems in the North American market on late model truck tractors and trailers. Some manufacturers have made these systems standard equipment. Unlike passenger cars, heavy vehicle stability systems are available in different configurations with different levels of performance. Depending on the application, it can be installed as a tractor based system or a trailer based system. Tractor based systems are available that can mitigate roll only (Roll Stability Control, RSC) or are available that can mitigate roll and yaw instability (ESC). In addition, trailer based systems are available that can mitigate rollover only.

Since 2006, NHTSA has been conducting heavy truck stability control research on a test track to understand the performance benefits of this technology. For this study two truck tractor stability systems and a trailer based stability system were tested to understand how stability control modified the base vehicle's performance. A variety of test maneuvers were used to conduct this testing.

TRUCK TRACTOR STABILTY

Truck tractors that pull a semi-trailer in service are subject to many different loading conditions. Often these loads can dramatically change the handling characteristics of combination units. A combination vehicle can be loaded so that the CG is raised significantly. In these conditions the vehicle is more prone to roll instability. Tank trailers carrying fuel or liquids have been measured to have CG heights of over 193 centimeters from the ground where as a conventional flat bed trailer may have CG of just over half that. Since the same truck tractor may be in service pulling either type of trailer, a safety beneficial stability system must be able to adapt to either condition.

Heavy vehicle stability systems are being sold in North America in three different configurations. These include:

- Trailer-based Roll Stability Control (RSC).
- Tractor-based RSC.
- Tractor based Electronic Stability Control (ESC).

Trailer-based RSC is capable of generating torque at the trailer axle brakes only. These systems generally do not have as much stability margin as the tractor based systems. Stability margin is defined as the ratio between the vehicles performance with the technology compared to its performance without.

Tractor based RSC is capable of applying brake torque to the wheels on the tractor drive axles and trailer axles. Tractor based RSC systems generally have a larger stability margin than the trailer based systems. This is because they are able to electronically reduce engine torque on the tractor in addition to the trailer and therefore apply more braking torque than trailer-based systems. Temporally the tractor will experience lateral forces before the trailer. With a proper understanding of the combination vehicle's dynamics, the stability system can intervene earlier during the event since the stability system is sensing tractor lateral acceleration. The stability system can reduce engine torque by electronically removing the drivers throttle input and by activating engine or exhaust braking. Having the ability to control the tractor's drive axle wheels in addition to the trailer axle wheels allows the combination vehicle to decelerate more rapidly. These contributing factors have been observed to increase the platform's stability margin when compared to a combination vehicle with just trailer based RSC.

Tractor based ESC has the same functionality as tractor based RSC, with additional performance capabilities. Tractor based ESC adds the capability to brake the steer axle wheels, sense the steering wheel position, and measure the tractor's angular yaw rate. With the additions of these capabilities, the ESC system can not only assist drivers in mitigating roll events but also yaw instability events.

TEST TRACK PERFORMANCE STUDY

To gain a better understanding about the performance of heavy vehicle stability systems, a test track study was conducted. The study evaluated stability control performance of two truck tractors pulling a semi-trailer under a variety of different loading conditions and test maneuvers.

Tests were conducted with a 2006 Freightliner Century Class 6x4, a 2006 Volvo VNL64T630, and 1999 Fruehauf 53 ft. (16m) van trailer. Both of the 6x4 tractors were modified with an external roll bar for the driver's protection. The van trailer was modified to support outriggers and a load frame so that the trailer could be ballasted safely. These structures are included in the base weight and CG measurements for each vehicle. Table 1 describes the basic platform characteristics for each test vehicle:

Table 1. Base vehicle parameters.

	Freightliner	**Volvo**	**Fruehauf**
Configuration	6x4 Tractor	6x4 Tractor	53 ft' Van
Wheel Base	546 cm	536 cm	n/a
Base Weight	8,854 kg	8,763 kg	7,820 kg
Vertical CG	91 cm	100 cm	120 cm
Length	810 cm	803 cm	1,605 cm
Width	231 cm	234 cm	257 cm
Height	292 cm	381 cm	409 cm
Brake Type	Air Disc	S-Cam	S-Cam
Stability System	ESC	ESC	RSC

All tests were conducted with a tractor pulling the Fruehauf 53 ft. van trailer under three different loading conditions. These conditions included, a lightly loaded vehicle weight (LLVW), a low CG gross vehicle weight rating (GVWR), and a high CG GVWR. LLVW was defined as the base vehicle weight that included outriggers, roll bar, instrumentation, etc. without adding any ballast to the trailer. The low and high GVWR conditions were setup to achieve close to a 5,443 kg (12K lb) steer axle, 15,422 kg (34K lb) drive axle, and 15,422 kg (34K lb) trailer axle combined weight. The low CG condition was limited by placing blocks directly on the floor of the trailer while the high CG was created by raising the ballast.

Ballasting the trailer was accomplished by using cement blocks that were fastened by chains and binders to the floor of the trailer. Each cement block weighed approximately 1,900 kg, and was 61 cm x 61 cm x 183 cm. Blocks were placed directly over the kingpin and trailer axles to achieve desired axle weight ratings. To elevate the vertical CG of the trailer, loading tables that accept the cement blocks were used. The ballast blocks and tables can be used in various configurations to achieve different loading conditions. Table 2 documents the loading conditions used to perform this testing.

Tests were conducted on the vehicle dynamics area (VDA) at the Transportation Research Center, Inc. Although the coefficient of friction does change over time on the VDA, the average peak and slide

coefficients of friction were measured at 0.97 and 0.86 for this time period.

Table 2. Trailer loading for different test conditions.

LLVW		Trailer Vertical CG = 154 cm from ground.	
	Steer (kg)	Drive (kg)	Trailer (kg)
Freightliner	4984	6586	5443
Volvo	5025	6309	5279
Low CG		Trailer Vertical CG = 152 cm from ground	
	Steer (kg)	Drive (kg)	Trailer (kg)
Freightliner	5316	15159	15295
Volvo	5384	15140	15299
High CG		Trailer Vertical CG = 219 cm from ground	
	Steer (kg)	Drive (kg)	Trailer (kg)
Freightliner	5302	15413	15345
Volvo	5307	15118	15404

For each vehicle and loading combination, three handling maneuvers were performed. The matrix displayed in Table 3 was completed for each of the three maneuvers. This matrix was designed to allow a performance comparison of the combinations with and without stability control at the three different load conditions. This methodology also allowed the observance of interactions between the tractor and trailer stability control systems.

Table 3. Test matrix conducted for each test maneuver.

	Speed (KM/H) at Critical Event					
	LLVW		**~GVWR**			
			Low CG		**High CG**	
	Trailer RSC		**Trailer RSC**		**Trailer RSC**	
	OFF	**ON**	**OFF**	**ON**	**OFF**	**ON**
Freightliner						
ESC OFF						
ESC ON						
Volvo						
ESC OFF						
ESC ON						

Based on the experience from previous NHTSA light vehicle research, several maneuvers were chosen to evaluate combination unit truck stability control performance on a high coefficient of friction surface [4]. These maneuvers included the following:

- Constant radius circle with increasing velocity
- J- turn with constant radius
- Double Lane Change Maneuver

Testing was conducted both clockwise and counter-clockwise for each maneuver. Very minor asymmetries were observed. For purposes of this paper, direction will not explicitly be discussed. Results will be combined showing both clockwise and counterclockwise maneuvers, unless otherwise noted.

Constant radius circles with increasing velocity tests were conducted on the 45 m and 61 m radius circles located on the center of the VDA. For both of these maneuvers, the test driver followed the radius with either the passenger side steer tire (clockwise) or the driver side steer tire (counter-clockwise) while slowly increasing the vehicle's speed. As speed increased, the driver steered the vehicle to maintain the radius as the vehicle tended to understeer. The test was complete when the driver was no longer able to follow the radius (vehicle plows out), no longer increase velocity (drive axles lose traction), and/or the trailer wheels lifted more than 5 cm off the ground (outriggers making contact with the test surface).

J-turn tests with a constant radius were conducted using a 45 m and 61 m radius located on the center of the VDA. For purposes of this paper, only the 45 m data will be discussed.

To conduct this maneuver, the driver entered a start gate delineated by pylons and then followed the radius with either the passenger side steer tire (clockwise) or the driver side steer tire (counter-clockwise) at a given test entrance speed. When the driver entered the start gate (cones at the point tangent to the radius), they were instructed to drop-throttle, and complete the maneuver following the radius as best they were able. Test entrance speeds started at 32 km/h and were incremented by 3 km/h to increase severity until the test termination condition was met. The test termination condition was satisfied when either the outriggers made contact with the ground, the combination vehicle was noticeably under-steering, stability control brake activation was observed, or when the test entrance speed of 80 km/h was achieved. 80 km/h was chosen for a maximum test entrance speed based on available test area and design of the safety support equipment (outriggers, roll bar, etc.)

Double lane change tests were performed on the VDA. Gates were setup as detailed in Figure 1. The test driver was instructed to enter the starting gate a given test entrance speed, drop throttle, and then to steer the combination vehicle through the gates, as

best they were able without hitting any of the pylons delineating the course. Test entrance speeds started at 32 km/h and were incremented by 3 km/h to increase severity until the test termination condition was met. The test termination condition was satisfied when either the outriggers made contact with the ground, the combination vehicle was grossly under or over-steering, stability control brake activation was observed, or when the test entrance speed of 80 km/h was achieved.

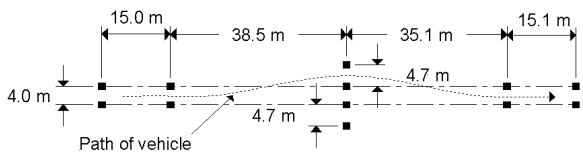

Figure 1. Double lane change maneuver.

MEASURES

Each tractor and the trailer were instrumented with a variety of sensors to measure the vehicles' dynamics and state of stability control system. Table 4 and 5 list the measures that were collected on the tractors and trailer respectively.

Table 4. Tractor based measures.

Measure	Units
Lateral Acceleration	G's
Longitudinal Acceleration	G's
Vertical Acceleration	G's
Yaw Angular Rate	Deg/sec
Roll Angular Rate	Deg/sec
Pitch Angular Rate	Deg/sec
Throttle Position	% displaced
Brake Treadle Switch	On/Off
Steering Wheel Angle	Deg.
Frame Rail Height @ approx long. CG	L/R cm
Rear Drive Axle Height	L/R cm
Brake Chamber Pressures (6)	kPa
Glad Hand Pressure	kPa
Wheel Speeds (6)	KM/H
Tractor Ground Speed	KM/H
J1939 VDC1 CAN MSG	RSC/ESC Status

Table 5. Trailer based measures.

Measure	Units
Lateral Acceleration	G's
Longitudinal Acceleration	G's
Yaw Angular Rate	Deg/sec
Roll Angular Rate	Deg/sec
Outrigger Height (Left and Right)	cm
Rear Trailer Axle Height (Left and Right)	cm
Brake Chamber Pressures (4)	kPa
Wheel Speeds (4)	KM/H

While most of the measures collected are self-explanatory, a short discussion about how wheel lift was calculated and how stability control activation was determined is described.

Rear drive axle height on the tractor and rear axle height on the trailer are both measured with sensors mounted on the left and right of the relevant axles. Data are processed and analyzed for determining if wheel lift has occurred. It should be noted for purposes of this study, wheel lift is considered to be greater than 5 cm. The value of 5 cm is used because it has been demonstrated that at this height, it can be visually confirmed.

The brake treadle switch, glad hand pressure, and brake chamber pressures were all measured to determine the source of brake activation. Under the given test protocol, the driver should not be braking during a maneuver. If this does occur the test is invalid. Monitoring the trailer brakes and glad hand pressure, confirms if the trailer RSC activated. If there was no glad hand pressure (trailer air brake command) and pressure was observed at the chambers, then Trailer RSC intervention was inferred. Tractor ESC braking was confirmed by observing pressures build in the tractor brake chambers while their treadle pressure was at zero. In cases where both the tractor and trailer based systems were enabled, the tractor system dominated the trailer system because it activated earlier and mitigated the instability before the trailer based system could activate. In the rare event that both systems engaged simultaneously, a difference between the glad hand pressure and trailer chamber pressures could be observed.

Using the SAE J1939 VDC1 CAN message available on both tractors, several status bits were observed to help determine the source of tractor stability activation. This message contains four bits that indicate the state of the stability system. These bits indicate if one of the following occurs:

- Engine torque reduction ESC
- Engine torque reduction RSC
- Brake activation ESC
- Brake activation RSC

RESULTS

Data from each test series was processed and analyzed. For purposes of this paper, results will be discussed in terms of the ground speed of the tractor at the start of the maneuver and the maximum lateral acceleration experienced at the CG of the tractor

during the test maneuver. Results will also be discussed in terms of tests that resulted in trailer wheel lift greater than 5 cm and if the stability system activated during the maneuver.

Constant Radius Circle

Table 6 summarizes the results in terms of speed at the critical event during the maneuver. The speed was representative of all runs in a series including both left and right conditions. The critical event occurred when the stability system activated or for the case where stability control was disabled, the speed that wheel lift occurred. In some cases, the vehicle may not have had a critical event. The trailer RSC condition was tested with only the Volvo tractor.

Test results show that tractor ESC as well as trailer based RSC were capable of mitigating wheel lift in this maneuver. When any of the stability systems were enabled, wheel lift was no longer observed.

With ESC completely disabled, both the LLVW and low CG conditions resulted in the vehicles severely under-steering before wheel lift occurred. The speeds where this occurred were very similar for each of the truck tractor combinations tested. For the high CG load condition, each test resulted in wheel lift.

Table 6. Constant Radius maneuver speed at critical event test results.

	Speed (km/h) at Critical Event					
	LLVW		~GVWR			
			Low CG		High CG	
	Trailer RSC		Trailer RSC		Trailer RSC	
	OFF	ON	OFF	ON	OFF	ON
Freightliner						
ESC OFF	64^	X	56^	X	47*	42
ESC ON	48	49	43	42	41	40
Volvo						
ESC OFF	65^	49	55^	48	46*	42
ESC ON	58	49	38	39	36	37

* - Denotes wheel lift.
^ - Denotes no critical event.
X - Denotes not tested.

The effects of stability control can be observed by comparing maximum lateral acceleration vs. speed for each load and stability condition. Maximum lateral acceleration (Ay) vs. critical event speed data for the constant radius test are displayed in Figures 2 and 3, for the Freightliner and Volvo. In each figure there are three subplots. Each subplot represents one of the loading conditions, they are labeled LLVW, Low and High.

All test runs with trailer wheel lift occurred without stability control active. No cases of wheel lift were observed under the LLVW or low CG condition. Under these load conditions, both tractors would understeer and did not reach a velocity much greater than 65 and 55 km/h for their respective loading conditions. When loaded in the high CG condition, wheel lift occurs in every test that results in a lateral acceleration greater than 0.45G.

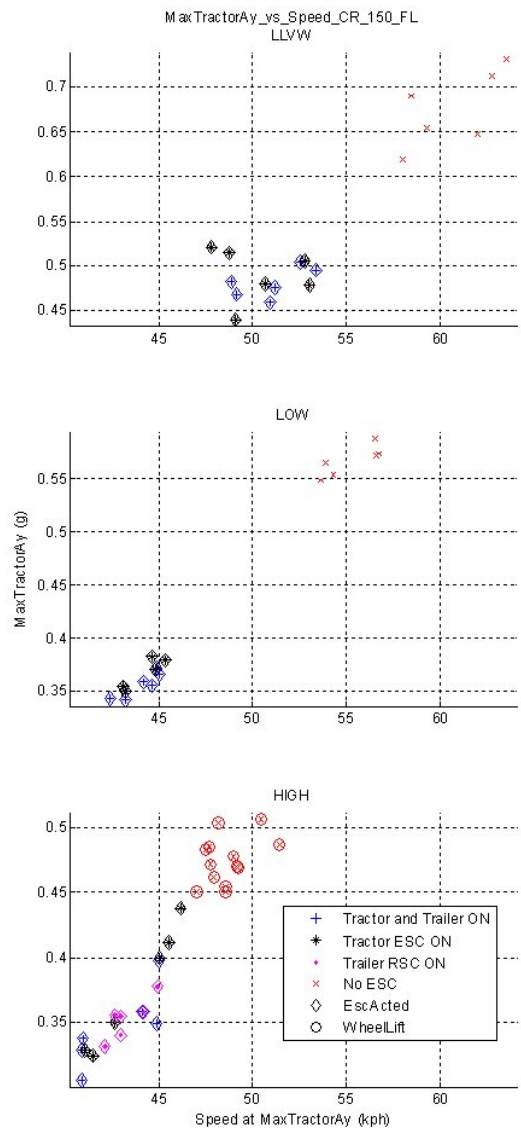

Figure 2. Freightliner maximum tractor Ay vs. speed during the 45 m constant radius test.

Truck tractor based stability control limited the maximum lateral acceleration of the tractor and prevented wheel lift for the different loads tested. Both tractors function in a similar manner, allowing higher maximum lateral accelerations for the LLVW

as compared to the low and high CG conditions. There was little difference in peak lateral acceleration under the low and high CG conditions.

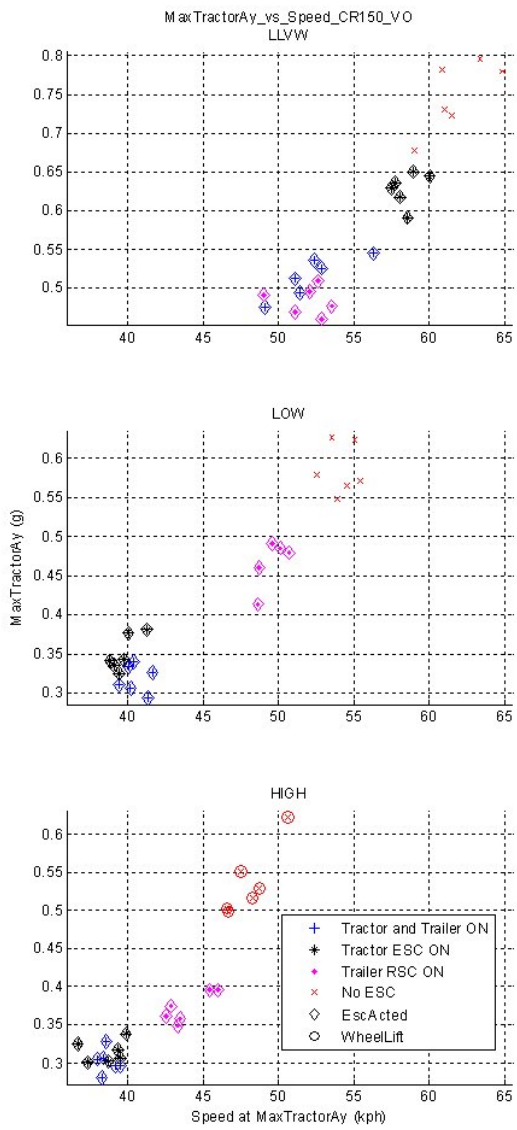

Figure 3. Volvo maximum tractor Ay vs. speed during the 45 m constant radius test.

Trailer based RSC was observed to limit maximum lateral acceleration and mitigate wheel lift with the different loads tested. Tractor maximum lateral acceleration was limited by the trailer to under 0.5 G for LLVW, 0.4 G to 0.5 G for Low CG, and 0.35 to 0.4 G for the high CG condition.

When both truck tractor and trailer based stability control were enabled, results were similar to the tractor based stability control system for the low and high CG conditions and closer to the trailer only RSC condition under the LLVW load. This might be expected as the trailer based system has a more conservative approach to adjust the allowable maximum lateral acceleration based on loading condition. In comparison, the truck tractor based systems were observed to be more adaptive as the load increases.

45 m J-turn

Table 7 summarizes the test results for the 45 m J-turn maneuver in terms of maneuver entrance speed at which a critical event was observed. Both left and right maneuvers were performed. Although results were observed to be similar for both directions only results from tests performed to the left are shown. The critical event occurred when the stability control system activates, or for the cases where stability control was disabled, the speed that wheel lift occurred. In some cases, the vehicle may not have encountered a critical event. The trailer RSC condition was tested with only the Volvo tractor.

For all tests with tractor based ESC, no cases of trailer wheel lift were observed for the J-turn maneuver. For both tractors in the low and high CG loading conditions, tractor based ESC intervened with braking at a speed well before the speed observed to produce trailer wheel lift. In the LLVW conditions the Freightliner's ESC system activated braking approximately 12 km/h sooner than the Volvo's.

Table 7. 45 m J-turn maneuver speed at critical event test results.

	Speed (km/h) at Critical Event					
	LLVW		~GVWR			
			Low CG		High CG	
	Trailer RSC		Trailer RSC		Trailer RSC	
	OFF	ON	OFF	ON	OFF	ON
Freightliner						
ESC OFF	81^	X	61*	X	49*	X
ESC ON	49	49	44	43	44	43
Volvo						
ESC OFF	77*	60	60*	45	50*	45
ESC ON	61	60	40	40	40	40

* - Denotes wheel lift.
^ - Denotes no critical event.
X – Denotes not tested.

Trailer based RSC was also observed to improve the base combination vehicle's roll propensity. From Table 7, the trailer system was observed to activate at similar speeds as the tractor based system for the LLVW load condition. When the Low and High CG load conditions were tested at GVWR the tractor

based system was observed to activate at approximately 5 km/h sooner. For this maneuver, when both systems were enabled, the tractor based system was observed to dominate the trailer system.

The effects of stability control can be observed by comparing maximum Ay vs. maneuver entrance speed for each load and stability condition. This data for the J-turn maneuver are displayed in Figures 4 and 5 for the Freightliner and Volvo. As previously mentioned each subplot represents one of the three loading conditions, they are labeled LLVW, Low and High.

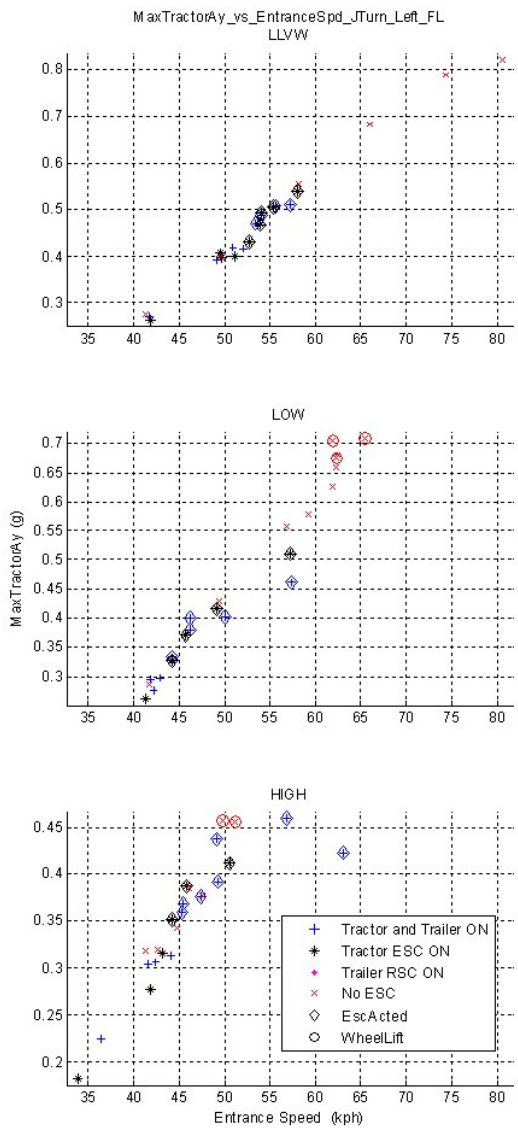

Figure 4. Freightliner maximum tractor Ay vs. speed during the J-turn drop throttle maneuver.

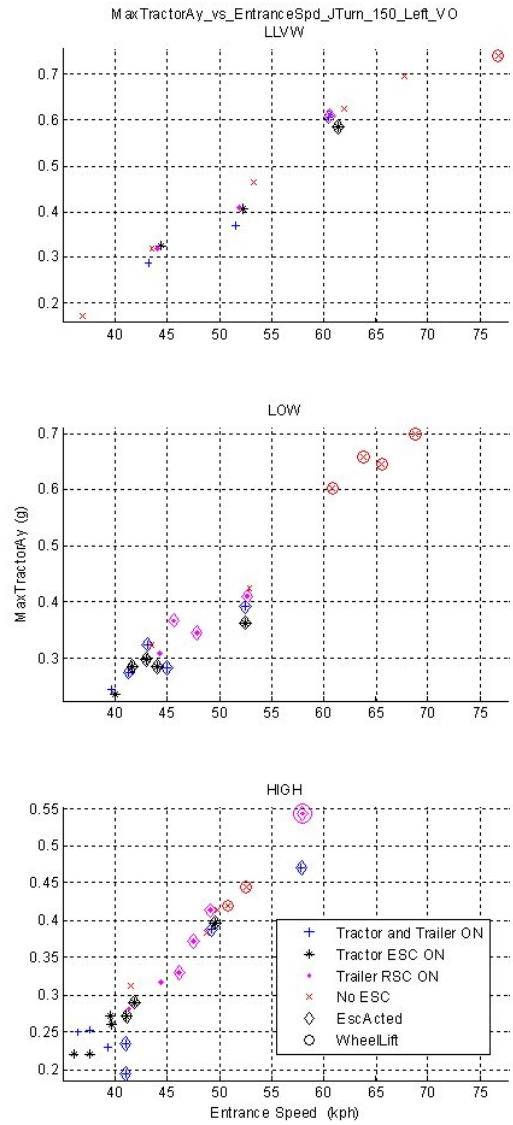

Figure 5. Volvo maximum tractor Ay vs. speed during the J-turn drop throttle maneuver.

For both tractors, in the base configuration with stability control disabled, wheel lift occurred in all load combinations except for the Freightliner in the LLVW condition. For the Volvo and LLVW load condition, wheel lift of the trailer was observed when the tractors' maximum lateral acceleration exceeded 0.75 G.

With stability control disabled and Low CG load condition, wheel lift was observed for tractor maximum lateral accelerations greater than 0.67 G for the Freightliner and 0.6 G for the Volvo. For the High CG condition wheel lift was observed for tractor maximum lateral accelerations that achieved

approximately 0.45 G with the Freightliner and 0.42 G for the Volvo.

Enabling tractor ESC limited the maximum lateral acceleration for both the truck tractor and the trailer. As a result wheel lift was no longer observed for the range of speeds evaluated. When loaded in the LLVW load condition tractor maximum lateral accelerations were limited to approximately 0.6 G in the Freightliner and the Volvo did not appear to be limited. When loaded in the Low or High CG condition, tractor lateral accelerations were limited to 0.5 and 0.4 for the Freightliner and Volvo respectively.

Trailer RSC was able to mitigate trailer wheel lift in both the LLVW and Low CG conditions. In the High CG condition, several instances of trailer wheel lift were observed with the trailer stability system enabled. The trailer system was overdriven when maximum lateral acceleration exceeded 0.5 g with entry speeds above 57 km/h. Though wheel lift was observed at speeds above 57 km/h the trailer system improved roll stability from the base condition. Without any type of stability control enabled, trailer wheel lift was observed at speeds of 50-53 km/h.

Double Lane Change (DLC)

Table 8 summarizes the results in terms of maneuver entrance speed at which a critical event was observed during the DLC maneuver. The critical event was when the stability control system activated or for the cases where stability control was disabled, the speed that wheel lift occurred. In several cases both critical events were observed, and in such cases both speeds are reported. Results for both the LLVW and Low CG conditions are not reported since all tests, including ESC disabled on both the tractor and trailer, were completed without wheel lift up to the termination speed of 80 km/h. Only results for only the High CG condition are reported.

As shown in Table 8, instances of wheel lift were observed for the test conditions conducted with tractor stability control systems disabled and also when the systems were enabled. With both systems disabled, instances of wheel lift were observed at 66 KM/H with the Freightliner and 73 KM/H with the Volvo.

When the trailer system was enabled (tractor system disabled), two critical events were observed. First the trailer system was observed to activate at maneuver entrance speeds of 49 and 53 KM/H for the Freightliner and Volvo. Then wheel lift was observed at maneuver entrance speeds of 66 and 80 KM/H when the trailer was connected with the Freightliner and Volvo respectively.

With only the tractor based stability control systems enabled, two critical events were observed with the Freightliner and one event was observed with the Volvo. As shown in Table 8, the Freightliner's stability control system activated at 45 KM/H and then was overdriven at 82 KM/H (trailer wheel lift observed.) The Volvo's stability control system activated at 45 KM/H with no instances of trailer wheel lift at the subsequent higher test speeds.

When both truck-tractor and trailer stability control systems were enabled the tractor based stability control systems were observed to dominate the trailer systems. Two critical events were observed with the Freightliner combination. Stability control activation was first observed at 52 KM/H and then was overdriven at 82 KM/H (trailer wheel lift observed.) Stability control activation was observed at 46 KM/H with the Volvo. Trailer wheel lift was not observed for the range of speeds evaluated in this combination and maneuver.

Table 8. DLC maneuver speed at critical event test results.

	Entrance Speed (KM/H) at Critical Event	
	~GVWR High CG	
	Trailer RSC	
	OFF	ON
Freightliner		
ESC OFF	66*	49 66*
ESC ON	45 82*	52 82*
Volvo		
ESC OFF	73*	53 80*
ESC ON	45	46

* - Denotes wheel lift.

When the truck tractor based ESC systems were active, instances of wheel lift were no longer observed for test speeds less than 80 KM/H. The minimum speed observed to activate the truck tractor systems in the DLC maneuver was 45 KM/H for both truck tractor systems. The truck stability systems were observed to be activating at speeds 4 to 8 KM/H lower than the trailer based stability control system.

The effects of stability control can be observed by comparing maximum truck tractor lateral acceleration (Ay) vs. maneuver entrance speed for each testing

condition. These data for the DLC maneuver are displayed in Figures 6 and 7 for the Freightliner and Volvo.

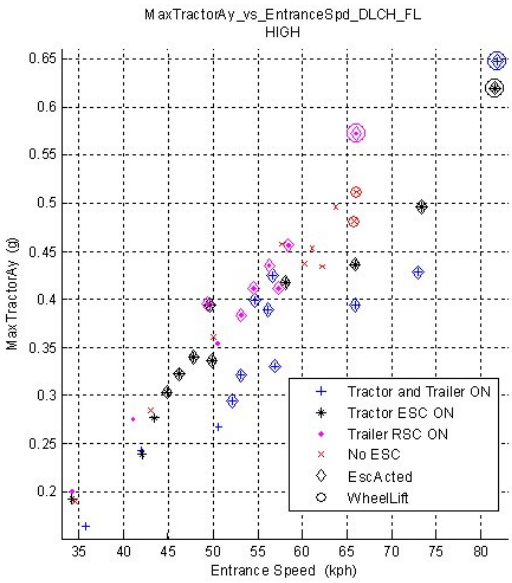

Figure 6. Freightliner maximum tractor Ay vs. speed during the DLC maneuver.

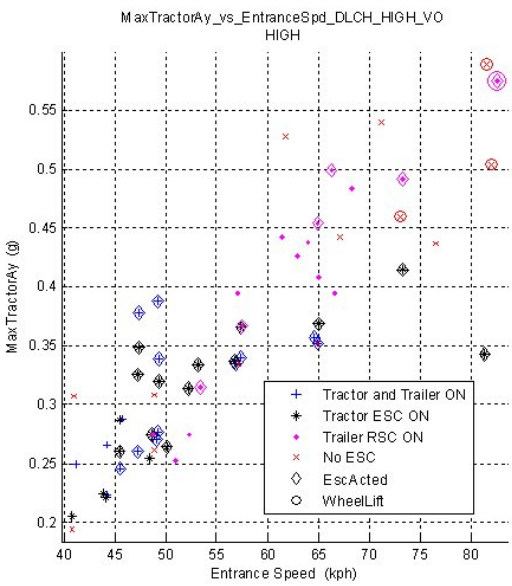

Figure 7. Volvo maximum tractor Ay vs. speed during the DLC maneuver.

As shown in Figure 6, the stability control activation in the Freightliner was first observed for a DLC maneuver that produced a maximum lateral acceleration of 0.3 G. The figure shows that when the systems were disabled wheel lift was not observed until a maximum tractor lateral acceleration of 0.45 G. The Freightliner's stability control system was observed to limit peak lateral acceleration to approximately 0.50 G, which, mitigated wheel lift at the trailer for tests performed under 80 km/h. Tests performed at speeds greater than 80 km/h resulted in maximum lateral accelerations that exceeded 0.6 G. Then trailer wheel lift was observed regardless of interventions by the tractors stability control system.

Figure 7 shows that the stability control system in the Volvo activated in a DLC maneuver at a tractor maximum lateral acceleration of 0.22 G. The Volvo's stability control system was then observed to limit tractor maximum lateral acceleration to approximately 0.40 G and mitigate wheel lift for all speeds evaluated in the DLC maneuver. When stability control systems were disabled with the Volvo, trailer wheel lift was observed when tractor maximum lateral acceleration reached 0.41 G.

For test series completed with only the trailer's stability control system enabled, the trailer system was observed to activate when maximum tractor lateral acceleration reached 0.38 G with the Freightliner (Figure 6) and 0.28 G with the Volvo (Figure 7). Trailer wheel lift was observed when a maximum tractor lateral acceleration of 0.57 G was reached with the Freightliner and 0.47 G with the Volvo. When all systems were disabled trailer wheel lift was observed at 0.45 G with the Freightliner and 0.41 G with the Volvo.

Maximum lateral acceleration from test series conducted with both tractor and trailer stability control systems enabled were similar to those test series conducted with the tractor stability control system enabled. For the Freightliner, activation was observed when the maximum tractor lateral acceleration first reached 0.3 G (tractor stability system enabled activated when maximum lateral acceleration reached 0.3 G). For the Volvo combination, activation was observed when the maximum tractor lateral acceleration first reached 0.20 G (tractor stability system enabled activated when maximum lateral acceleration reached 0.22 G)

Discussion

For both tractor based stability systems, changes in the tractor lateral acceleration when the stability systems activated were observed between the LLVW and GVWR loads. Maximum lateral accelerations were very similar between the low and high CG conditions. The trailer based system exhibited similar changes in tractor lateral acceleration when the stability system intervened but with less range.

This suggests that the heavy vehicle stability systems tested were capable of sensing or estimating load but are not estimating the CG of the load.

For the constant radius circle, increasing velocity tests both tractor and trailer systems were capable of mitigating trailer wheel lift and limiting maximum tractor lateral acceleration. This maneuver increased lateral acceleration at a moderate rate proportionately with the square of velocity. The maneuver did not produce a large amount of dynamic overshoot in lateral acceleration. The maneuver demonstrated differences between tests with and without stability control enabled, but was not very effective in demonstrating the differences between a tractor and trailer based system.

For the J-turn tests, tractor based systems were able to mitigate trailer wheel lift in all test series conducted. The trailer based RSC system provided some improvement in stability but was overdriven before 80 km/h was reached. For the J-turn, lateral acceleration increased at a faster rate than for the constant radius maneuver. At higher speeds, the maneuver generated dynamic overshoot in lateral acceleration making this a challenging maneuver. The maneuver was able to distinguish between tests with and without stability systems enabled, and demonstrated performance differences between tractor and trailer based systems.

Unfortunately, not all J-turn tests with the tractor based system enabled were conducted to the point of test termination speed or to the point where trailer wheel lift was observed. At higher speeds there was the potential to overdrive the tractor systems as well.

During DLC testing, tractor based systems were able to mitigate trailer wheel lift in most test series. In all completed tests, two instances of wheel lift were observed with the tractor based ESC system enabled on the Freightliner. In both of these cases, maneuver speed was just over 80 km/h and tests were conducted with the same driver. In further review of the data, it was determined that the system was not functioning properly for those test series. Regardless, the system performance was better than the base vehicle's.

The trailer based system provided some improvement in stability but was able to be overdriven at a lower speed than the tractor based systems. Again, its performance was still better than the base vehicle's performance.

The DLC maneuver was able to demonstrate differences between tests with and without a stability system enabled and between tractor and trailer based systems; however these results were not as clear when compared to the other maneuvers. The DLC is a very dynamic maneuver and can generate rapid rates of lateral acceleration, however, results varied by driver. Since the goal of the maneuver is to navigate the lane change gates, drivers can steer the tractor semi-trailer unit in a variety of ways to successfully complete the maneuver.

One strategy observed entailed the driver smoothly steering the vehicle over time to follow the path marked out for the maneuver. In some cases the driver was observed steering before the gate to anticipate tractor response time. The second observed strategy entailed the driver waiting until the last possible second to abruptly steer, then hold the steering wheel angle and wait for the truck to respond. This type of input was then repeated to make truck navigate the lane change successfully.

Because of these distinct strategies, the outputs from this maneuver can result in very different lateral accelerations for any test entrance speed. This potentially suggests why the data are not as clean in determining the differences between system performances. The repeatability of the test may suffer from driver influences.

Conclusions

Overall, both tractor and trailer stability control systems improved the roll stability of the base tractor semi-trailer. For a given maneuver, tractor-based stability systems were able to mitigate trailer wheel lift at the same or higher entrance speeds than trailer only based systems. Trailer-based stability systems were able to mitigate trailer wheel lift at the same or higher maneuver entrance speeds than the base tractor semi-trailer vehicle. For all test maneuvers and conditions performed on the test track, enabling stability control was not observed to degrade the stability of the tractor.

Based on the results of this study, a performance test based on the J-turn appears to be a suitable to evaluate tractor and trailer stability control systems. However, further study of this type of maneuver is necessary to understand how stability control technology and other factors influence the dynamic response of heavy vehicles.

References

[1] *Large Truck Crash Facts 2006.* Federal Motor Carrier Safety Administration. FMCSA-RI-08-001. January 2008.

[2] *FMVSS No. 126 Electronic Stability Control Systems; Final Regulatory Impact Analysis.* Docket: NHTSA-2007-27662-0002. 3/2007.

[3] *Electronic Stability Control Systems; Controls and Displays - Final Rule*. Docket: NHTSA-2007-27662-0001-0001. 4/6/2007.

[4] Forkenbrock, G. J., Garrott, W. R., Hietz, M., O'Harra, B. C., *A comprehensive Experimental Examination of Test Maneuvers That May Induce On-Road, Untripped, Light Vehicle Rollover – Phase IV of NHTSA Light Vehicle Rollover Research Program.* DOT HS 809 513. October 2002.